Development of Novel Soft-Core Embedded Architecture for Total Haemoglobin Estimation using Multivariate System

A THESIS SUBMITTED IN PARTIAL FULFILLMENT FOR THE DEGREE OF

DOCTOR OF PHILOSOPHY

IN THE SCHOOL OF PHYSICAL AND APPLIED SCIENCES
GOA UNIVERSITY

By

Caje Francis Pinto

Electronics Programme, School of Physical and Applied Sciences,

Goa University,

Goa

August 2021

DECLARATION

I, **Caje Francis Pinto** hereby declare that this thesis represents work which has been carried out by me and that it has not been submitted, either in part or full, to any other University or Institution for the award of any research degree.

Place: Taleigao Plateau.
Date: 05-08-2021

Caje Francis Pinto

CERTIFICATE

I hereby certify that the above Declaration of the candidate, **Caje Francis Pinto** is true and the work was carried out under my supervision.

Dr. Jivan S. Parab
Associate Professor Electronics, SPAS
Goa University

Acknowledgement

First and foremost, I would like to thank the Almighty GOD for showering upon me countless blessings and graces required by me during these years. I would like to express my deepest gratitude to my research guide, Dr. Jivan S. Parab, for his constant support and motivation throughout my research work. I will treasure the invaluable guidance that he gave me during these years. He has always been patient with me and inspired me to take up challenges during my research work. I consider myself privileged to have worked under his guidance.

I would like to convey my gratitude to Dr. M. Kunhanandan, Assistant professor, Department of Mathematics, School of Physical and Applied Sciences, Goa University, for his feedback and suggestions during the Department Research Committee (DRC) meetings which enabled me to improve in various facets of my research work.

I extend a big thank you to, Prof. R. S. Gad, Vice Dean of School of Physical and Applied Sciences, Goa University, for his insightful comments and encouragement throughout. I am sincerely grateful to my former professor, Dr. G. M. Naik, School of Physical and Applied Sciences, Goa University, who has been kind and gave constant source of encouragement and inspiration to me.

My many thanks and appreciation goes to Dr. N. G. Tavares, Dr. M. Sequeira, Dr. B. Lawrence, Mrs. Vilma M.T. Fernandes and Dr. N. Lobo for their valuable contribution and help rendered during my research work. I would like to thank Dr. N. T. Vetrekar, Mr. D. Gonsalves, Mrs. Y. Prabhu, Dr. C. Panem, Mr. A. Prabhu Dr. I. Nazareth, Mr. A. Gaonkar Dr S. R. Vernekar, Dr. V. R. Gad, Dr. U. V. Rane, Dr. S. R. Ghanti, Dr. N. Marchon, Dr. S. A. Patil, Mr. S. M. Patil, Mr. G. Abhyankar, and Mr. D. Chodankar for the valuable scientific discussions we have had during my research work.

I am grateful to the supporting staff of the Department of Electronics, School of Physical and Applied Sciences, Goa University, Mr. W. D'Souza, Mr. V. Malik, Mrs. A. Velip, Mrs. P. Andrade, who have always extended their helping hand whenever needed. I also thank Mr. M. Lanjewar, Technical Officer, and Mr. A. Lopes, USIC, Goa University, for their wise and encouraging words shared from time to time.

I would like to thank my parents, Michael V.M. Pinto and Rosy A. Antonio for supporting me throughout my academic career. This accomplishment wouldn’t be possible without the support of my beloved wife, Eustargia Rodricks, for her unwavering support and for believing in me and for always encouraging me to push myself and never to quit.

I would like to thank my brother Carmin Pinto and his wife Hazel Pereira who have been always there to support me in good and bad times. Finally, I would like to thank my colleagues in St. Xavier's College and all my friends who participated as subjects in my research work during the pandemic times. Besides this, several people have knowingly and unknowingly helped me, in the successful completion of this thesis. It has been a fruitful and enjoyable experience and the cooperation of all, meant a lot to me.

Dedicated with love to my family

Mr. Michael Vincent Mathew Pinto

Mrs. Rosy Antonia Pinto

Mrs. Eustargia Vila Nova Rodricks e Pinto

Ms. Louiselle Vincenza Pinto

Mr. Antonio Fernando Domenico Pinto

Contents

List of Tables

List of Figures

LIST OF ABBREVIATIONS

AC: signal Alternating Current signal

ADC: Analog to Digital Converter

ANN: Artificial Neural Network

ASCII: American Standard Code for Information Interchange

ASIC: Application Specific Integrated Circuit

BSP: Board Support Packages

CBC: Complete Blood Cell Count

CI: Confidence Interval

CLB: Configurable Logic Block

CLS: Classical Least Squares

DC: Direct Current signal

FPGA: Field Programmable Gate Array

FPS : Fitzpatrick scale

GPIO: General Purpose Input Output

GUI: Graphical User Interface

HAL: Hardware Abstraction Layer

Hb: Deoxyhaemoglobin

HbO2: Oxyhaemoglobin

HDL: Hardware Description Language

HIV: Human immunodeficiency virus

HRV: Heart Rate Variability

I2C: Inter Integrated Circuit

IDE: Integrated Development Environments

ILS: Inverse Least-Squares

IP: Intellectual Property

I/O: Input/output

IR: Infrared

LB: Logic Block

LC: Logic Cell

LE: Logic Element

LED: Light Emitting Diode

LUT: Look-Up Table

MIPS: Million Instructions Per Second

MLR: Multiple Linear Regression

NIPALS: Non-linear Iterative Partial Least Squares

NIR: Near-Infrared

PCA: Principal Component Analysis

PCR: Principal Component Regression

PLSR: Partial Least Squares Regression

PPG: Photoplethysmography

RBC: Red Blood Cell

RISC: Reduced Instruction Set Computer

RMSE: Root Mean Square Error

SBT: Software Build Tools

SDRAM: Synchronous Dynamic Random Access Memory

SIMPLS: Statistical Inspired Modification of PLS

SCD: Sickle cell Anaemia

SD: Standard deviation

SNR: Signal to Noise Ratio

SOC: System On Chip

SOPC: System on programmable chip

SPI: Serial Peripheral Interface

SVD: Singular Value Decomposition

UART: Universal Asynchronous Receiver Transmitter

UV: Ultraviolet

VHDL: Very High Speed Integrated Circuit Hardware Description Language

VIS: Visible

VLCS: Luschan chromatic scale

WBC: White Blood Cell

WHO: World Health Organization

PREFACE

This thesis is about the "Development of Novel Soft-Core Embedded Architecture for Total Haemoglobin Estimation using Multivariate System". This architecture is developed using Altera NIOS II soft-core platform on DE0 board having target as CYCLONE IV. The multivariate (PLSR) algorithm is developed in C++ language and ported on the NIOS II platform to estimate non-invasive haemoglobin concentration in human blood using five LED wavelengths in the range of 670 nm to 950 nm.

Chapters 1 contain an introduction to the thesis along with overview of anaemia and prevalence of anemia globally. It focuses on the problems associated with the invasive method and the mentions the importance in developing a non-invasive haemoglobin device.

Chapter 2 describes a literature review on various invasive and non-invasive methods in measuring haemoglobin. It also reviewed on the development of non-invasive haemoglobin devices by several researchers.

Chapter 3 discusses on optical absorption of skin tissue and blood. It also discusses the estimation of haemoglobin using visible and near-infrared light to estimate haemoglobin using the PPG features along with the mathematical empirical formula.

Chapter 4 discusses the methodology in designing an embedded platform for estimating non-invasive haemoglobin. It also focused on the selection of LED wavelengths, photodetector, and the importance of standardizing LEDs power to estimate non-invasive haemoglobin.

Chapter 5 elaborates on the various multivariate methods. It also discusses the multivariate Partial Least Square Regression (PLSR) model that was implemented in ParLes software for preliminary analysis.

Chapter 6 describes the design of an Altera NIOS II soft-core system for non-invasive haemoglobin estimation. It contains a survey of soft-core processors, DE0 Nano board to configure the NIOS II soft-core. Also, it describes the multivariate (PLSR) model implemented in the designed system to test and verify different validation cases.

Chapter 7 gives us a review on the results obtained for two different cases. Also, different performances measures such as Root Mean Square Error (RMSE), R^2 (Coefficient of determination), and r (Correlation coefficient) was used for comparisons. The designed system was also validated with Bland-Altman plot and analysis.

Journal Publications

1. **Caje Pinto**, Jivan Parab, Gourish Naik, **Non-invasive hemoglobin measurement using embedded platform** in Sensing and Bio-Sensing Research, Volume 29, Elsevier, 2020, 100370, ISSN 2214-1804, pp 1-6, doi: 10.1016/j.sbsr.2020.100370. (Scopus)
2. Jivan Parab, Marlon Sequeira, Madhusudan Lanjewar, **Caje Pinto**, Gourish Naik, **Backpropagation Neural Network-Based Machine Learning Model for prediction of Blood Urea and Glucose in CKD Patients,** in IEEE Journal of Translational Engineering in Health and Medicine, vol. 9, pp. 1-8, 2021, Art no. 4900608., doi: 10.1109/JTEHM.2021.3079714.
3. **Caje Pinto**, Jivan Parab, Marlon Sequeira, Gourish Naik, **Improving Hemoglobin Estimation accuracy through Standardizing of LED Power** in International Journal of Electrical and Computer Engineering (IJECE), Vol. 12, No. 1, February 2022, pp. 219-228 ISSN: 2088-8708, doi: 10.11591/ijece.v12i1.pp219-228 (Scopus)
4. Jivan Parab, M. Sequeira, M. Lanjewar, **C. Pinto**, G. M. Naik, **Blood Glucose Prediction Using Machine Learning on Jetson Nano Platform** in "Handbook of Intelligent Computing and Optimization for Sustainable Development" published by Wiley-Scrivener Publishing. (Scopus)(Accepted)
5. **C. F. Pinto**, G. M. Naik, J. S. Parab, **NIOS II Soft-Core Processor Based Wireless Notice Board** in International Journal of Advanced Research in Electrical, Electronics and Instrumentation Engineering, Vol. 4, Issue 10, October 2015, pp 8144-8149. (UGC Approved)

Conference Publications

1. **C F Pinto**, J S Parab, M D Sequeira, G M Naik, **Development of Altera NIOS II Soft-core system to predict total Hemoglobin using Multivariate Analysis** for International Conference on Advances in Smart Sensor, Signal Processing & Communication Technologies (ICASSCT 2021) on 19th & 20th March 2021and published a paper in IOP Publishing, Journal of Physics: Conference Series **1921** (2021) 012039, doi:10.1088/1742-6596/1921/1/012039
2. **C F Pinto**, J S Parab, M D Sequeira, G M Naik, **Testing the efficacy of various Artificial Neural Network for total haemoglobin estimation,** In: Chen J.IZ., Tavares J.M.R.S., Iliyasu A.M., Du KL. (eds) Second International Conference on Image Processing and Capsule Networks and published in Lecture Notes in

Networks and Systems, vol 300. Springer, Cham. https://doi.org/10.1007/978-3-030-84760-9_28 (Scopus)

3. M D Sequeira, J S Parab, **C F Pinto**, G M Naik, **Enhanced Accuracy for Glucose Prediction using Neural Network,** In: Chen J.IZ., Tavares J.M.R.S., Iliyasu A.M., Du KL. (eds) Second International Conference on Image Processing and Capsule Networks and published in Lecture Notes in Networks and Systems, vol 300. Springer, Cham. https://doi.org/10.1007/978-3-030-84760-9_33 (Scopus)
4. **Caje Francis Pinto,** Jivan S. Parab, G. M. Naik, **Development of the Soft-core System for Estimation of Blood Haemoglobin** for IEEE's 3rd International Conference for Convergence in Technology PUNE on 6th April 2018.
5. **Caje Francis Pinto,** J. S. Parab, G. M. Naik, **Filtering of PPG signal to Estimate Heart rate and Oxygen Saturation using the soft-core processor** for11th Annual Symposium on Deep Digitization, organized by Goa University, Department of Electronics, Goa University on 23rd March 2018.
6. **Caje F. Pinto,** Jivan S. Parab, Gourish M. Naik, **Development of Soft-core processor for Heart Rate and Oxygen** for 20th International Conference on Bioinformatics, Computational Biology and Biomedical Engineering, Mumbai, India, organized by World Academy of Science, Engineering and Technology, 22nd February 2018, pp 2019-2023.

Chapter 1

Introduction

1.1 Anaemia Overview

In the present scenario, it is very important to monitor the total haemoglobin count of patients during surgeries, deliveries, blood donations, dialysis in hospitals and also for monitoring patients in intensive care units, etc. Anaemia is a condition in which the blood has less than the required number of healthy Red Blood Cells (RBC) or when the haemoglobin level in the blood drops below the normal level. Anaemia can occur due to various causes like blood loss, decreased or faulty RBC production, destruction of RBC. Further on, it can also originate from a variety of factors that include nutritional deficiencies (e.g. iron deficiency and other nutritional deficiencies like vitamin B12, vitamin A, and folate), infections (e.g., malaria, hookworm disease, Human immunodeficiency virus (HIV)) [1, 2], chronic medical conditions (e.g., chronic kidney disease, inflammatory/autoimmune disorders)[1, 2], haemoglobin or RBC disorders (e.g., sickle cell disease (SCD), thalassemia, myelodysplastic syndromes), and pharmaceutical drug treatment (e.g., cancer chemotherapy) [3, 4].

Iron deficiency anaemia occurs due to low dietary iron consumption, chronic blood loss, blood loss due to hookworm infection, and iron mal-absorption, all of which are more common in low- and middle-income countries [5]. In endemic regions, malaria is a leading cause of anaemia. Malaria causes anaemia, especially in young children, in high-transmission areas. Malaria has been linked to maternal anaemia during pregnancy as well as poor birth outcomes at all levels of transmission [6]. SCD and thalassemia are inherited haemoglobin diseases that induce hemolysis of RBCs and severe, persistent anaemia [7, 8]. Haemoglobin levels are also decreased in patients due to blood loss in traumatic hemorrhages, cardiac surgery [9]. Early detection and treatment of anaemia can help to reduce the severity of the condition [10]. Misdiagnosis of the cause of anaemia will result in the wrong treatment, which can result in serious clinical consequences [11]. As a result, a quick and correct diagnosis of anaemia, as well as the identification of the underlying illness etiology, are critical. Before blood donation, the donor's eligibility must be identified and reviewed by a physical examination, a health history determination, and a

haemoglobin measurement. The haemoglobin levels for donor eligibility are more than 13.5 g/dL for males and more than 12.5 g/dL for females [12, 13]. Polycythemia vera is a condition in which the number of RBCs in the blood is abnormally high. In this condition, the blood becomes too thick and makes clotting easier. This increases the risk of heart attacks and strokes. The condition may be caused by several health-related factors including smoking, congenital heart disease, dehydration (decreased water), and hypoxia (low blood oxygen levels).

1.2 Worldwide Anaemia Breakdown

According to World Health Organization (WHO), anaemia is one of the world's most common health issues affecting pregnant women, preschool children, and adolescents [14, 15]. In milder situations, anaemia produces weakness, tiredness, and dizziness; in more severe cases, anaemia causes life-threatening cardiovascular collapse [3, 4]. Globally, anaemia affects 1.62 billion people, which corresponds to 24.8% of the population. The highest prevalence is in preschool-age children (47.4%) and the lowest prevalence is in men (12.7%). However, the population group with the greatest number of individuals affected is non-pregnant women which are around 468 million as shown in Table 1.1 [16, 17].

Table 1.1: Prevalence of anaemia globally.

Population Group	Prevalence of anaemia (percent)	Population affected number (million)
Preschool-age children	47.4	293
School age children	25.4	305
Pregnant Women	41.8	56
Non-Pregnant Women	30.2	468
Men	12.7	260
Elderly	23.9	164
Total Population	24.8	1620

WHO regional estimates generated for preschool-age children and pregnant and non-pregnant women indicate that the highest proportion of individuals affected are in Africa (47.5–67.6%), while the greatest number affected are in South-East Asia where 315 million individuals in these three population groups are affected. The prevalence of

anaemia in each WHO region is listed in Table 1.2 [16, 17]. In the global burden of disease (GBD) study done in 2013, the Institute for Health Metrics and Evaluation found that anaemia affected 27.0 % of the world's population (i.e. 1.93 billion people) [7]. Anaemia affected 41.8 % of pregnant women, 30.2% of non-pregnant women, 47.4% of preschool children, and 25.4% of school-aged children based on the data collected between 1993 and 2005 [16].

Table 1.2: Prevalence of anaemia in each WHO region.

WHO region	Preschool-age children	Pregnant women	Non-pregnant women
Africa	67.6	57.1	47.5
Americas	29.3	24.1	17.8
South-East Asia	65.5	48.2	45.7
Europe	21.7	25.1	19.0
Eastern Mediterranean	46.7	44.2	32.4
Western Pacific	23.1	30.7	21.5
Global	47.4	41.8	30.2

In 2021, WHO estimated that 29.6 % of non-pregnant women, 36.5 % of pregnant women, and 39.8 % of preschool children are anaemic globally, according to data gathered upto 2019 [17]. When compared to other developing nations, India has a high prevalence of anaemia, as seen in Table 1.3 [17].

Table 1.3: Prevalence of anaemia in various countries.

Country	Preschool-age children	Pregnant Women	Non-pregnant women
Brazil	16.1	19.1	16
Australia	8.5	15.7	8.2
Afghanistan	42.6	36.5	43.2
Pakistan	41.3	44.0	41.1
India	53.0	50.1	53.1
Liberia	42.6	49.7	41.9
Yemen	61.5	57.5	61.8

The prevalence of anaemia in pregnant women and children is shown in Figures 1.1 and 1.2 respectively. Women in their childbearing years are more vulnerable to iron deficiency anaemia arising from blood loss from menstruation and the increased blood supply needs during pregnancy. Pregnant women that are anaemic have an increased rise in low birth weight and increased prenatal and maternal mortality. Also, women who are anaemic have severe problems during menstruation and pregnancy [18].

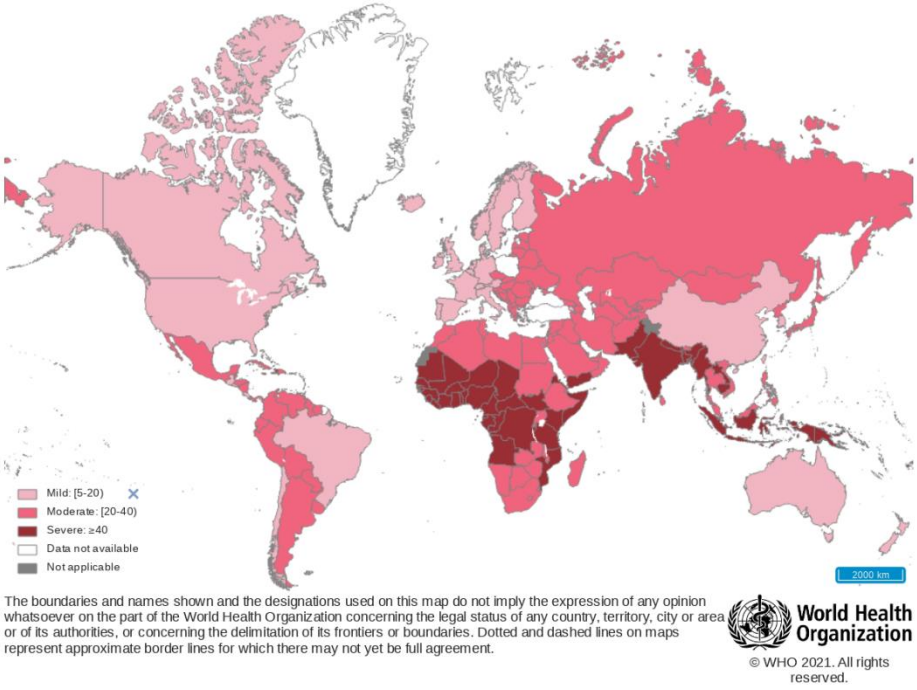

Figure 1.1: Prevalence of anaemia in pregnant women [17].

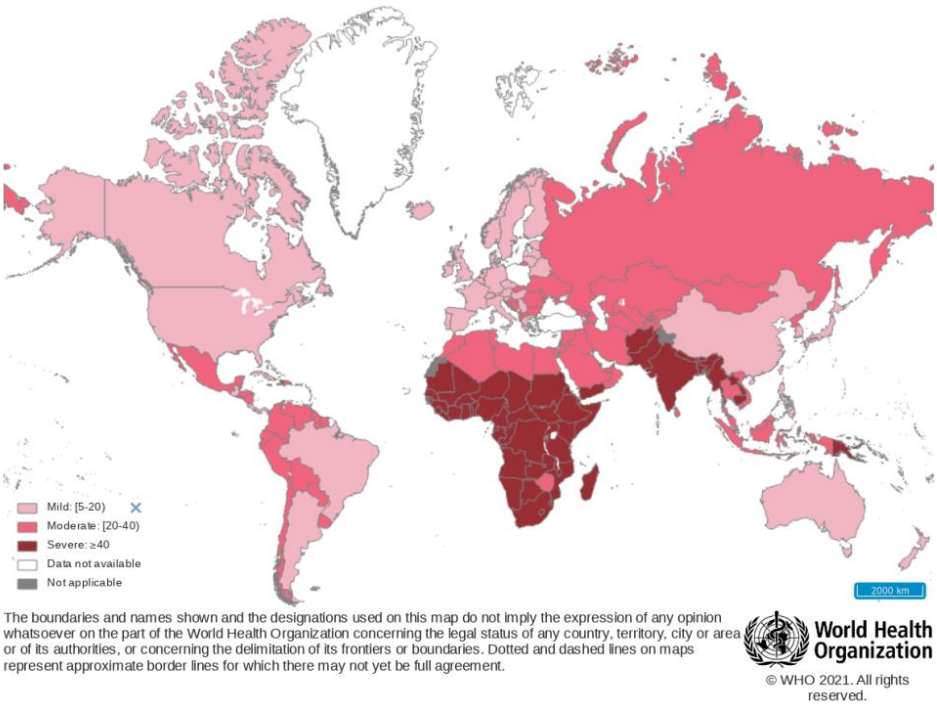

Figure 1.2: Prevalence of anaemia in preschool age children [17].

1.3 A brief history of monitoring haemoglobin in the blood

The haemoglobin molecule is made up of four protein chains with a central iron atom that binds an oxygen molecule. The structure of haemoglobin molecule is shown in Figure 1.3. When a haemoglobin molecule carries four oxygen molecules, it is referred to as oxyhemoglobin, and when it is not completely saturated with oxygen, it is referred to as reduced haemoglobin. Haemoglobin is an iron-containing oxygen-transport metalloprotein found in RBCs that delivers oxygen to tissues while returning carbon dioxide to the lungs [19].

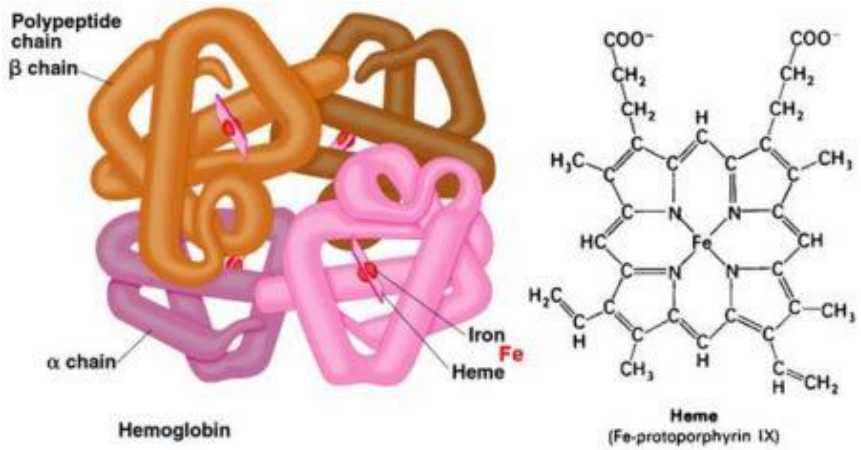

Figure 1.3: Structure of haemoglobin molecule [20].

The volumetric estimation of haemoglobin in red corpuscles in the blood is defined as hematocrit. Haemoglobin is typically tested using the whole blood count method and is represented in grams (g) per deciliter (dL) of whole blood. [21]. The normal haemoglobin concentration varies by gender, age, and altitude. The normal range of haemoglobin concentration in blood is from 14 to 18 g/dL for males and 12.0 to 16 g/dL for females [22]. The haemoglobin thresholds used to define anaemia are listed in Table 1.4 [16].

Table 1.4: Haemoglobin thresholds used to define anaemia.

Gender Group	Haemoglobin Threshold (g/dL)
Preschool age children	11
Pregnant Women	12
Non- pregnant Women	11
Men	13

The current diagnostic method for haemoglobin measurement, in a clinical laboratory, is a complete blood count using an automated hematology analyzer where blood is collected from a vein which includes the insertion of a needle, which causes minor discomfort to the individual. Also, it takes a lot of time to obtain the results from a pathology laboratory which does not allow real-time monitoring of the patient in critical situations. Hence, accurate, real-time, and non-invasive estimation of haemoglobin is very important. A non-invasive method allows on-the-spot or continuous monitoring of haemoglobin and provides safe management of subjects with minimal risk of infection and reduced pain [23, 24]. To address these challenges in estimating total haemoglobin, a real-time, non-invasive system was designed using an Altera NIOS II soft-core system with a finger probe consisting of five LED sources and OPT101 to detect the transmitted signal through the finger using the photoplethysmography (PPG) principle.

1.4 Composition of blood and its functions

Blood is a fluid that moves through the vessels of the circulatory system. The main components of blood are plasma, RBCs, white blood cells (WBCs), and platelets. Blood has, as its main function, the transportation of oxygen and nutrients to the lungs and tissues. Cells and platelets make up about 45% of human blood, while plasma makes up the other 55%.

Plasma

Plasma is the main component of blood which contains 90% water, with the remaining 10% consisting of proteins, ions, nutrients, and other wastes. Albumin is the main protein in plasma, and it helps in the prevention of fluid leakage from blood vessels into tissues. Antibodies, which actively protect the body against bacteria, viruses, fungi, and cancer cells are among the other proteins found in plasma.

Red Blood Cells

RBCs, also known as erythrocytes, account for 40% of the volume of blood. Haemoglobin is found in RBCs which is a protein that allows it to transport oxygen from the lungs to all body tissues. Cells use oxygen to generate energy for the body, leaving carbon dioxide as a waste product. Carbon dioxide is carried away from the tissues by RBCs and returned to the lungs. RBCs pick up oxygen in the lungs and release it to the

surrounding tissues as they circulate through the rest of the body. RBCs are also involved in the transport of carbon dioxide, a waste product, from tissues to the lungs. RBCs have a lifespan of 120 days on average. In the liver and spleen, old or weakened red blood cells are broken down, and new ones are formed in the bone marrow. The hormone erythropoietin, which is released by the kidneys in response to low oxygen levels, regulates RBC activity. The number of RBCs in the body remains relatively constant over time.

White Blood Cell

WBCs, also known as leukocytes, are fewer than RBCs and account for less than 1% of the cells in the blood. WBCs play a key role in the body's defense against infection.

Platelets

Platelets, also known as thrombocytes, are small and are lesser in number than red or white blood cells. Platelets aid in the clotting process by grouping together at a bleeding site to create a plug that closes the blood vessel; thrombocythemia occurs when the quantity of platelets in the blood is too high. In this condition, too much blood clotting occurs and blocks the blood vessels, causing problems such as a transient ischemic attack [25, 26].

References

1. A. Koukounari et al., “Relationships between anaemia and parasitic infections in Kenyan schoolchildren: A Bayesian hierarchical modelling approach,” Int. J. Parasitol., vol. 38, no. 14, pp. 1663–1671, 2008, doi: 10.1016/j.ijpara.2008.05.013.
2. M. Bechir, E. Schelling, M. A. Hamit, M. Tanner, and J. Zinsstag, “Parasitic Infections, Anemia and Malnutrition Among Rural Settled and Mobile Pastoralist Mothers and Their Children in Chad,” no. Chopra 2006, pp. 122–131, 2012, doi: 10.1007/s10393-011-0727-5.
3. C. Beghe, A. Wilson and W. B. Ershler, "Prevalence and outcomes of anemia in geriatrics: a systematic review of the literature", Am. J. Med., 116(Suppl 7A), 3s–10s, 2004 doi: 10.1016/j.amjmed.2003.12.009.
4. A. Calabrich and A. Katz, Management of anemia in cancer patients, Future Oncol., vol. 7, no. 4, pp. 507–517, 2011. doi: 10.2217/fon.11.24.
5. C. Camaschella, "Iron-Deficiency Anemia", N. Engl. J. Med.,vol. 372, no. 19, pp. 1832–1843, 2015, doi: 10.1056/NEJMra1401038.
6. N. J. White, "Anaemia and malaria", Malar. J.,vol. 17, no. 1, pp. 371, 2018, doi.org/10.1186/s12936-018-2509-9.
7. N. J. Kassebaum, et al., "A systematic analysis of global anemia burden from 1990 to 2010", Blood, vol. 123, no. 5,pp. 615–624, 2014, doi:10.1182/blood-2013-06-508325.
8. G. J. Kato et al., "Sickle cell disease", Nat. Rev. Dis. Primers, vol. 4, 18010, 2018. doi: 10.1038/nrdp.2018.10.
9. B. Joseph, A. Haider, and P. Rhee, “Non-invasive hemoglobin monitoring,” Int. J. Surg., vol. 33, no. Part B, pp. 254–257, 2016, doi: 10.1016/j.ijsu.2015.11.048.
10. J. P. Chalco, et al., "Accuracy of clinical pallor in the diagnosis of anaemia in children: a meta-analysis", BMC Pediatr., vol. 5,no. 46, 2005, doi.org/10.1186/1471-2431-5-46
11. M. W. Short and J. E. Domagalski, "Iron deficiency anemia: evaluation and management", Am. Fam. Physician, vol. 87, no.2, pp. 98–104, 2013.
12. S. T. Bateman et al., “Anemia, blood loss, and blood transfusions in North American children in the intensive care unit,” Am. J. Respir. Crit. Care Med., vol. 178, no. 1, pp. 26–33, 2008, doi: 10.1164/rccm.200711-1637OC.
13. "WHO, Haemoglobin concentrations for the diagnosis of anaemia and assessment of severity", Vitamin and Nutrition System, WHO/NMH/NHD/MNM/11.1, 2011.
14. Y. Balarajan, U. Ramakrishnan, E. Özaltin, A. H. Shankar, and S. V. Subramanian, “Anaemia in low-income and middle-income countries,” Lancet, vol. 378, no. 9809,

pp. 2123–2135, 2011, doi: 10.1016/S0140-6736(10)62304-5.

15. G. A. Stevens, et al., "Global, regional, and national trends in haemoglobin concentration and prevalence of total and severe anaemia in children and pregnant and non-pregnant women for 1995-2011: a systematic analysis of population-representative data", Lancet Glob. Health, vol. 1, no. 1, 2013, pp. e16–e25, doi: 10.1016/S2214-109X(13)70001-9.
16. E. McLean, M. Cogswell, I. Egli, D. Wojdyla, and B. De Benoist, "Worldwide prevalence of anaemia, WHO Vitamin and Mineral Nutrition Information System, 1993-2005," Public Health Nutr., vol. 12, no. 4, pp. 444–454, 2009, doi: 10.1017/S1368980008002401.
17. World Health Organization, https://www.who.int/health-topics/anaemia#tab=tab_1
18. C. Massot and J. Vanderpas, "A survey of iron deficiency anaemia during pregnancy in Belgium: Analysis of routine hospital laboratory data in Mons," Acta Clin. Belg., vol. 58, no. 3, pp. 169–177, 2003, doi: 10.1179/acb.2003.58.3.004.
19. C. S. Thom, et al., "Hemoglobin Variants: Biochemical Properties and Clinical Correlates", Cold Spring Harbor Perspect. Med., vol. 3, no. 3(a011858), 2013, doi:10.1101/cshperspect.a011858.
20. World of chemicals, [Online] Available at https://www.worldofchemicals.com/271/chemistry-articles/max-ferdinand-perutz-determined-hemoglobin-structure.html
21. Celia Henry Arnaud, "Paper device measures hematocrit", vol. 94, no. 37, 2016.
22. "Anemia Detection Methods in Low-Resource Settings: A Manual for Health Workers", 1997.
23. J. Kraitl, H. Ewald, and H. Gehring, "An optical device to measure blood components by a photoplethysmographic method," J. Opt. A Pure Appl. Opt., vol. 7, no. 6, pp. S318–S324, 2005, doi: 10.1088/1464-4258/7/6/010.
24. U. Timm, E. Lewis, G. Leen, D. McGrath, J. Kraitl, and H. Ewald, "Non-invasive continuous online hemoglobin monitoring system," in 2010 IEEE Sensors Applications Symposium (SAS), 2010, pp. 131–134, doi: 10.1109/SAS.2010.5439415.
25. Overview of Blood - Blood Disorders - MSD Manual Consumer [Online] Available at https://www.msdmanuals.com/en-in/home/blood-disorders/biology-of-blood/components-of-blood
26. Components of blood [Online] Available at https://www.khanacademy.org/science/biology/human-biology/circulatory-pulmonary/a/components-of-the-blood

Chapter 2

Literature Review

Haemoglobin test is very important to screen and diagnose conditions that affect the RBCs; for anaemia (low haemoglobin) or Polycythemia (high haemoglobin). Also, it's important to test for blood donations and major surgeries. Hence it becomes crucial to monitor the haemoglobin levels. Many different methods are used to monitor haemoglobin, these methods can be broadly classified into invasive and non-invasive. In this chapter, we provide an overview of the different invasive techniques like reagent-based and reagent-less methods and non-invasive methods.

2.1 Invasive methods

In Invasive methods, blood tests are done by pricking the finger or drawing blood from the arm under medical guidance.

2.1.1 Haemoglobincyanide method

Haemoglobin is converted to cyanmethemoglobin using this method, which involves adding ferricyanide and potassium cyanide to a standard solution. The erythrocytes are destroyed by a haemoglobin solution that is equally distributed. All types of haemoglobin found in blood are converted to a single cyanmethemoglobin, with the solution's absorbance measured at 540 nanometers in a spectrophotometer. At this wavelength, hemoglobincyanide exhibits a broad absorption peak. The availability of an internationally accepted reference standard calibrator is one of the advantages. It also provides accurate and precise results. The disadvantage is that it is time-consuming. The potassium cynaide is photosensitive and toxic. This technique is still employed in clinics, particularly in poor countries [1].

2.1.2 Vanzetti's Azide Methemoglobin method

Haemoglobin is converted to potassium ferricyanide to produce the coloured, stable azide methemoglobin form, which has an absorbance spectrum that is almost identical to Haemoglobincyanide. In this method, sodium azide is replaced with potassium cyanide as a reagent. First, the blood is extracted into a dry reagent cuvette by capillary action. The reagent then breaks down the RBC walls, releasing free haemoglobin, which is then oxidised to methemoglobin. Finally, it is converted into azide methemoglobin a stable colored complex. This complex is then photometrically measured at 570 nm and 880 nm for turbidity compensation; the measurement takes between 15 to 60 seconds, depending on the haemoglobin concentration. HemoCue 201 and EKF Hemo Control are shown in Figures 2.1 and 2.2 respectively [2]. It is quick and gives immediate result. The use of disposable cuvette makes it expensive.

Figure 2.1 : HemoCue 201[3].

Figure 2.2: Hemo Control [2].

2.1.3 Reagent-Less method

HemoCue301 was the first POC device to have reagent-based cuvettes as shown in Figure 2.3. This device measures the absorbance of oxyhaemoglobin and deoxyhaemoglobin, while the turbidity is measured and compensated at 880 nm. The DiaSpect technology measures haemoglobin concentration without a reagent. The optical sensor element calculates the absorbance of the blood for a wide wavelength range [4].

Figure 2.3: HemoCue 301[5].

2.1.4 Copper sulphate method

To ensure a certain haemoglobin level for blood donation, the copper sulphate method is utilized, which is based on the haemoglobin dependent gravity of blood. A blood droplet is allowed to fall into a copper sulphate solution with a specific gravity equal to blood having a cut-off haemoglobin level of 12.5 g/dL as shown in Figure 2.4. The donor qualifies if the drop of blood sinks to the bottom in a reasonable length of time. The donor is rejected if the drop of blood floats or takes too long to sink [6].

Figure 2.4: Specific gravity method [7].

2.1.5 Sahli's method

The haemoglobin meter is a device that has a haemoglobin tube, pipette, stirrer, and comparator as shown in Figure 2.5. Haemoglobin is converted to acid hematin using hydrochloric acid. This solution is then diluted until the colour matches the comparator block. The clinician utilizes the calibration tube to calculate the haemoglobin concentration. This method is simple, inexpensive and the results are not always precise. The produced colour is unstable, and it must be read after 10 minutes of standing. The other disadvantages are inter-observer unpredictability [8].

Figure 2.5: Sahli's method [9].

2.1.6 Hematology Analyzer

This is an automatic analyzer to provide high throughput to analyze haemoglobin levels from the blood sample as shown in Figure 2.6. This method has a higher precision value when compared with manual methods. The initial cost of setting up is high and it may not be suitable outside a laboratory environment. Also, regular maintenance and laboratory personnel are needed which increases the costs. In most instances, the sample needs to be sent to the laboratory causing longer turn-around times for the results [5,10].

Figure 2.6: 5-part Hematology Analyzer [10].

2.1.7 Blood Gas Analyzer

Blood gas analyzers (BGAS) analyze a mixture of blood gas, pH, electrolytes, metabolite parameters, and haemoglobin from whole blood samples, primarily arterial blood. They're typically seen in intensive care units, surgery rooms, delivery wards, and emergency rooms. This device is more robust and user-friendly, although it still requires maintenance [3,11]. In the clinical environment, BGAs such as the ABL 800 Flex is used as shown in Figure 2.7.

Figure 2.7: ABL800 Flex Blood Gas Analyzer [11].

2.2 Non-Invasive methods

In the non-invasive method, the tests do not require puncturing the skin. This technique offers several advantages such as avoiding finger pricking, no pain, and discomfort, as well no exposure to medical staff, and no biomedical waste.

2.2.1 Histogram-based image processing

The blood vessel imaging is based on infrared light absorption. In the reflection method, IR LEDs illuminate the target and the reflected light is filtered with an IR filter. The image is captured by a charge-coupled device camera. In the transmission method, IR light source is located on the opposite side of the target. Many blood constituent evaluation initiatives are based on image-based blood research, but most processing algorithms are difficult to implement and unable to handle large images. Histogram-based image processing has grown popular as a way to speed up image processing since it is simple to implement and understand [12, 13].

2.2.2 Smartphone-based non-invasive system

Smartphone-based non-invasive methods for determining haemoglobin levels have recently been used. Because of the visibility of conjunctival mucosa and underlying micro-vessels, some of these technologies employ images of the lower eyelid. To compute the haemoglobin level, eyelid-based images and a colour chart are combined. These technologies are currently unreliable for estimating haemoglobin levels. To improve access to haemoglobin testing and properly manage patients with hematologic diseases, a noninvasive, easy-to-use, and inexpensive assessment of haemoglobin levels is desired. A smartphone-based haemoglobin estimate tool may also assess crucial physiological parameters to provide a snapshot of a patient's state at home with a haemoglobin issue. In smartphone-based, the videos are captured using near-infrared light and are processed using image processing techniques and machine learning algorithms to estimate non-invasive haemoglobin concentration in blood [14].

2.2.3 Impedance Plethysmography

Impedance plethysmography (IPG) is a method of measuring blood volume changes by detecting changes in impedance. The blood volume in the arteries changes during the cardiac cycle. The change in blood volume in peripheral tissue can be measured by measuring the change in impedance in that tissue [15]. An alternating current is passed through a peripheral body part that has been identified, and differential voltage changes across it are recorded in IPG. These voltage changes are caused by changes in blood flow.

2.2.4 Optoacoustic

Optoacoustic uses short laser pulses which generate optoacoustic waves also known as ultrasonic waves in absorbing media. The depth of the signal determines the time resolution of the resultant signal, which is detected using an acoustic transducer. When compared to light waves, ultrasonic waves scatter and attenuate significantly less in tissues. Tissue characterization with submillimeter resolution can be achieved by detecting and analyzing the temporal features and amplitude of optoacoustic pressure waves [16].

2.2.5 Diffuse reflectance spectroscopy

Diffuse reflectance spectroscopy is a non-invasive technique for determining the characteristic reflectance spectrum generated when light passes through a substance. Absorption and scattering are the primary mechanisms involved, which always vary with wavelength to produce the reflectance spectrum, which is recorded and contains information about the optical properties and structure of the medium being studied [17].

2.2.6 Photoplethysmography

Photoplethysmography (PPG) is a low-cost, non-invasive optical method that measures changes in blood volume in a microvascular bed of tissue [18]. PPG uses different light sources to measure the transmission or reflection of light through the volume of blood-based on the light absorption characteristics of haemoglobin. It is low cost, portable, and easy to use.

Sensors

Optical sensors are photometric devices that capture an optical signal from an external source, which can be an LED, laser, or different spectra of light [19]. Photodiodes, which are made of InGaAs and Indium phosphor, are typically utilized as optical sensors. Also, there are optical sensors that contain an on-chip trans-amplifier that has a high spectral response from 500nm-1600nm. We will discuss several sensors using CMOS, CCD, InGaAs sensor, and a specialized PPG sensor which is routinely used for acquiring PPG signals.

CMOS sensor

Complementary Metal Oxide Semiconductor (CMOS) converts photons to electrons for digital processing. Photolithography-light-capturing cells in CMOS chips capture photons of various wavelengths and convert them to electrons. A digital-to-analog converter converts electrons into different-colored pixels [20]. The RGB camera collects three spectral images in three separate spectral ranges (600-700 nm, 500-600 nm, and 400-500 nm) and converts the intensity of red, green, and blue values into optical density variations and then used to map skin haemoglobin distribution.

CCD sensor

A CCD is a light-sensitive integrated circuit (IC) in which each pixel is turned into a color-related electrical charge. CCDs have a high sensitivity and can produce an image even in low-light situations. Even when the illumination level is low, the image quality is not significantly affected [21].

Photodetectors

Photodetectors are designed to detect photons. The reverse current flows through the photodiode when it is sensing light. If the photons excite carriers in a reverse biased PN junction, a very small current proportions to the light intensity flows. The sensitivity depends on the wavelength of light. Photons are converted to a measurable signal by a detector, which is employed in all spectroscopic studies. All the detectors are evaluated in terms of spectral response, quantum efficiency, and response time. The range of optical wavelengths or frequencies in which a photodetector has a high responsivity is known as its spectral response. Silicon photodiodes are used in the UltraViolet and visible regions of the spectrum and are not sensitive beyond 1100 nm. Photodiodes made of germanium are insensitive to Ultraviolet and can detect wavelengths up to 1800 nm. Responsitivity (R_λ) is defined as the ratio of radiant energy (in watts) P, incident on the photodiode to the photocurrent output in amperes (I_p). Quantum efficiency is a measure of how much a detector can convert photons into an electrical signal. Response time is the time taken by the detector output to respond to the changes in the light intensity [22, 23].

InGaAs photodetector and Si Photodetector

Indium Gallium Arsenide (InGaAs) is a gallium arsenide-indium arsenide alloy. InGaAs is utilized as an infrared light detector in photodiodes. An InGaAs photodiode's spectrum response is between 850 nm to 1800 nm [24]. The spectral response of Silicon (Si) Photodetector is between 400 nm to 1000 nm. The spectral response for a photodiode is amps per watt of incident radiation. The spectral response for several semiconductor photodiodes is shown in Figure 2.8.

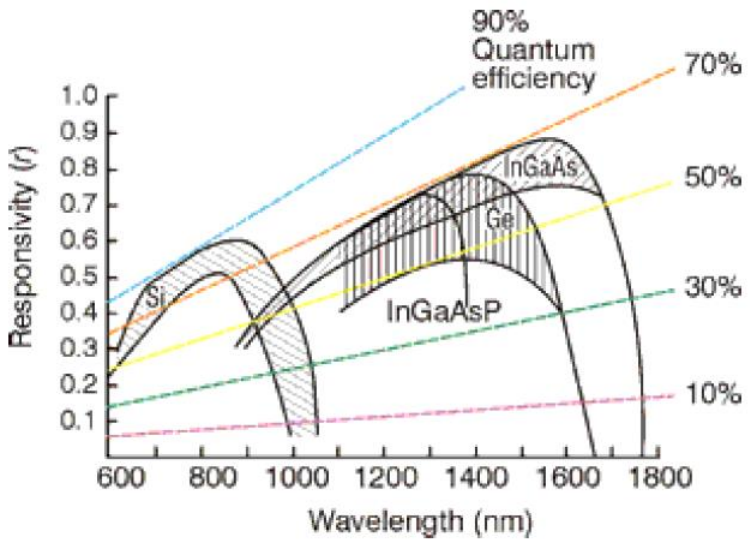

Figure 2.8: Spectral response for several semiconductor photodiodes [23].

With the rise in new technologies to estimate haemoglobin concentration, non-invasive methods are widely used. Some of the non-invasive devices use the principle of pulse oximetry while others capture the transmitted data using white light and calculate haemoglobin concentrations in the tissue capillaries. Recently, non-invasive methods have become commercially available using near-infrared spectroscopy to identify the spectral pattern of haemoglobin in an underlying blood vessel and derive a measurement of haemoglobin concentration. Given the advantage of obsolescence of finger-sticks and the option for more frequent measurements in clinical settings, the literature remains unclear about the precision and accuracy of the current non-invasive haemoglobin monitors. In practical use, patient movement, nail polish, skin color, or ambient light have been shown to influence the measurement. Recent technological advancements have made non-invasive methods for point-of-care anaemia screening a promising new option. These methods do not require a blood sample to produce results, reducing the risk of infection and eliminating patient pain involved in testing. Non-invasive devices also have an inherently different cost structure than invasive methods, since they do not require additional material inputs for each test administered. Instead of analyzing blood haemoglobin levels directly, noninvasive devices use spectrophotometry to estimate haemoglobin concentration based on light intensity.

2.2.7 Commercially available haemoglobin meters

Radical® Device

Masimo Corporation has developed Radical 7, a non-invasive device, which utilizes a sensor with various LEDs in the range of 500 nm to 1400 nm that passes light through a fingertip and measures the changes in light absorption during the blood pulsatile cycle using a photodetector. The maximum radiant power of the strongest light is rated at ≤ 25 mW**.** This can measure haemoglobin in the range of 8 g/dL to 17 g/dL with a precision of ±1 g/dL[25]. It estimates the haemoglobin levels in approximately between 30 to 45 seconds when the finger is placed.

NBM-200

The NBM 200 works on occlusion spectroscopy technology. It uses a ring-shaped sensor probe with LED wavelength range from 600 to 940 nm that fits on the subject's finger. The sensor temporarily occludes the blood flow and measures the intensity of multiwavelength light passing through the finger which is proportional to haemoglobin concentration. The average radiated power is ≤ 1 mW**.** This can measure haemoglobin in the range of 7 to 17 g/dl with a precision of less than 1g/dL [26]. It estimates the haemoglobin levels in approximately between 90 to 120 seconds when the finger is placed.

ASTRIM FIT

The ASTRIM FIT uses the principle of the Near-infrared spectroscopic image measurement method. Red or near-infrared light easily passes through the living body, and the transmitted light is detected using a CMOS camera located on the opposite side of the LED. The density of the blood vessel image obtained from the transmission image is determined by the degree of dimming of the blood, that is, the amount of haemoglobin in the blood. Astrim calculates the haemoglobin estimate per unit area based on the blood vessel image from multiple wavelength light sources and the blood vessel width. It estimates the haemoglobin levels in approximately 40 seconds when the finger is placed [27].

Haemospect®

The Haemospect® device (MBR Optical systems, Wuppertal, Germany) uses transcutaneous reflection spectroscopy to measure haemoglobin levels. The Haemospect works by placing a sensor on the palm side of the dominant hand immediately below the index finger, and as subsequent measurements are often necessary to obtain a reading, a second measurement can be taken by placing the sensor on the forearm of the same arm. The sensor projects white light into the underlying tissue, and some of this light is absorbed while the rest is reflected in the device to be broken down into separate wavelengths by a spectrometer and analyzed by an electronic evaluation unit connected to the system [28]. It estimates the haemoglobin levels in approximately between 20 to 30 seconds when the finger is placed.

ToucHb

ToucHb (Biosense, Irvine, California) is a non-invasive device that works on reflectance photometry. Instead of analyzing different wavelengths of light, it assesses overall light intensity as a way to quantitatively measure pallor and estimate haemoglobin concentration in the blood. This device captures an image of the patient's exposed conjunctiva, which is then used to measure pallor and predict blood haemoglobin concentration in grams per deciliter [29].

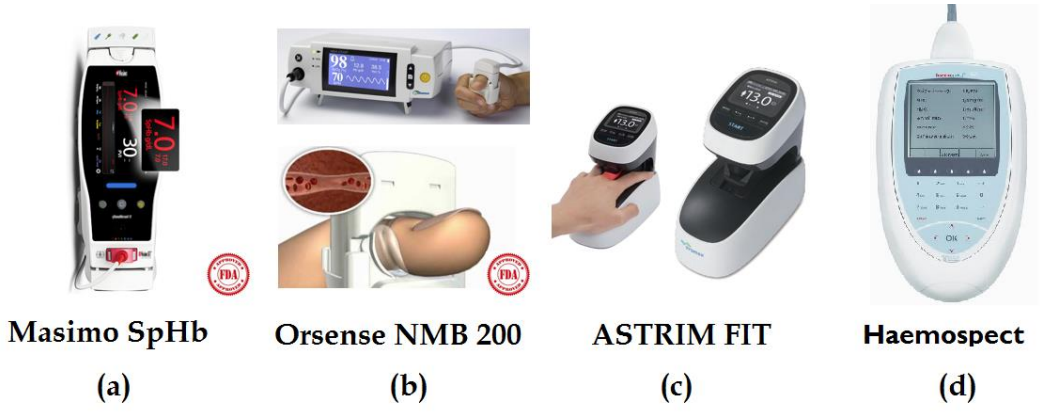

Figure 2.9: Commercially available non-invasive haemoglobin meters.

Apart from commercially available non-invasive devices as shown in Figure 2.9, several researchers are working to improve the prediction accuracy level. Edwards et al. [30] used NIRS to establish a non-invasive way of detecting haemoglobin flow across an organ. They assessed changes in deoxyhemoglobin and oxyhemoglobin concentrations by monitoring fluctuations in near-infrared light absorption in the organ. They captured the

spectral response using laser diodes with wavelengths of 797.5, 802.5, 831.2, 848.7, 866.5, and 907.8 nm in the forearms of six healthy young adults to assess haemoglobin flow using least-squares linear regression. R. Kumar et al. [31] worked on photons at two wavelengths (741 nm & 810 nm) which were pumped into the skin of the finger and the transmitted photons were received at a photodetector which is calibrated in terms of haemoglobin content in the blood. For each sample, the haemoglobin level was measured using a cyan-methemoglobin method and stored in the system. R. Doshi et al. [32] developed a device with two wavelengths 660 nm and 940 nm along with OPT101 to detect light transmitted through the subject's finger. The sensor probe was tested on 60 subjects from different age groups and it was observed that the AC signal was proportional to haemoglobin measure using a conventional method. Nirupa et al. [33] acquired PPG signals by illuminating the finger with monochromatic light at two different wavelengths (624 nm and 850 nm). To determine haemoglobin content in blood, an empirical equation was created utilizing a model for light attenuation via skin, bone, tissue, and blood, well-known extinction coefficients of haemoglobin, and clinical data. Two different empirical equations (one for the male population and the other for the female population) were implemented and the errors in the estimated haemoglobin concentration were reduced compared to having just one empirical equation that combines both genders for 69 subjects. Rochmanto et al. [34] developed non-invasive hemoglobin for anaemia diagnosis with spectroscopy methods with two LEDs at the wavelength of 670 nm and 940 nm and a photodiode to detect the transmitted light through the finger for 78 subjects of pregnant women. M.P. Mcewen et al. [35] used multiple wavelengths of high-power light sources with a focusing lens and two photo-detectors (BPW34B- 470 nm & PT611- 1200 nm) in conjunction with noise cancellation techniques to estimate haemoglobin. X. Li et al. [36], utilized spectroscopy methods for non-invasive haemoglobin measurement using eight laser diodes in the wavelength range from 600 nm to 1100 nm to record PPG signals in 220 subjects. However, their instrument setup was not portable for the non-invasive measurement of haemoglobin. Timm et al. [37] developed an optical-based sensor system with three LEDs (670 nm, 810 nm, and 1300 nm) and a single photodetector (InGaAs) to measure the intensity of the received wavelength. Later, it was processed using LabVIEW with an empirically derived partial least squares (PLS) calibration and statistical regression of the measurements to estimate the haemoglobin concentration. Ding et al. [38] developed a high-performance spectrophotometric system with a broadband light source consisting of 9 LEDs (600 to 1050 nm) with a grating spectrograph and Si photodiode array and

recorded the finger tip spectra of 109 volunteers. Konyukhov et al. [39] designed a finger probe to acquire PPG signal (LASER diodes with four wavelengths of 658 nm, 776 nm, 974 nm, and 1348 nm) to estimated haemoglobin level using computer-based software. Ulrich Timm et al. [40] developed a photometric device OxyTrue Hb® with four wavelength in the range of 600 nm to 1400 nm to measure the haemoglobin and methemoglobin concentration non-invasively and compared with the reference devices HemoCue® and a blood gas analyzer with 1008 measurements. H. Liu et al. [41] developed a system for non-invasive monitoring of haemoglobin concentration using eight LEDs in the wavelength range from 610 to 940 nm with a photodiode array. The system was a portable, continuous, and non-invasive haemoglobin monitoring system but utilized a lot of resources and power. With the advancement in technology, several non-invasive methods like transmission spectroscopy, reflection spectroscopy, imaging, video, and optoacoustic spectroscopy have been proposed for the estimation of concentration in blood.

In our study, Optical Photoplethysmography (PPG) method is used which is low-cost, easy to use, and portable is used for non-invasive estimation of haemoglobin. The finger probe was designed with Multichip LED's with 5 wavelengths and a photodetector to acquire good quality PPG signals and to implement preprocessing and quality assessment of the PPG signal to extract the main features of the PPG signal. The entire system was designed on an Altera NIOS II soft-core system to customize the core as per our requirements by minimizing the resources thereby decreasing power consumption. And also, to improve the prediction accuracy of estimating total haemoglobin present in blood with an error of less than 1g/dL. And finally to make the designed system portable and inexpensive.

References

1. V. B. Shah, B. S. Shah, G. V. Puranik, "Evaluation of non-cyanide methods for haemoglobin estimation", Indian J Pathol Microbiol, vol. 54, no. 4, pp.764-768, 2011.
2. G. Vanzetti, "An azide-methaemoglobin method for haemoglobin determination in blood", J Lab Clin Med, vol. 67,no 1, pp.116-126,1966.
3. Hemocue201, [Online] Available at https://medical.andonline.com/product/hemo-cue-hb-201/hc121720si
4. HemoControl, [Online] Available at https://www.medicalexpo.com/prod/hemocue/product-83757-565603.html
5. EKF Anemia Portal [Online] Available at https://www.ekfdiagnostics.com/methods-of-hemoglobin-testing.html
6. R. A. Phillips, D. D. Van Slyke, P. B. Hamilton, V.P. Dole, K. Emerson, R.M. Archibald, "Measurement of specific gravities of whole blood and plasma by standard copper sulfate solutions", J Biol Chem, vol. 183, no.1, pp. 305-330, 1950.
7. Specifc Gravity method, [Online] Available at https://www.bioscience.com.pk/topics/hemotology/item/779-specific-gravity-method-for-estimation-of-hemoglobin
8. T. Srivastava, H. Negandhi, S. B. Neogi, J. Sharma, R. Saxena, "Methods for Hemoglobin Estimation: A Review of What Works", J. Hematol Transfus, vol. 2, no.3, 1028, 2014.
9. Sahli's method, [Online] Available at https://www.biorays.com.pk/product/hemometer-1760/
10. Hematology Analyser, [Online] Available at https://www.mrclab.com/5part-hematology-analyzer
11. Blood Gas Analyser, [Online] Available at https://healthcare.omcbd.com/product/abl800-flex/
12. D. S. Kim, J.H. Choi, M.H. Nam, J. W. Yang, J. J. Pak, and S. Seo, "LED and CMOS Image sensor based hemoglobin concentration measurement technique", Sensors and Actuators B: Chemical, vol. 157, no. 1, pp.103–109, 2011, doi: 10.1016/j.snb.2011.03.032.
13. K. Ishihara, K. Asano, and Y. Maekawa, "Apparatus for measuring concentration of hemoglobin and method for the same" March 3 1998. US Patent 5,722,398.
14. P. Edwards, C. Zhang, B. Zhang, X. Hong, V. K. Nagarajan, B. Yu, and Z. Liu, "Smartphone based optical spectrometer for diffusive reflectance spectroscopic

measurement of hemoglobin", Scientific reports, vol. 7, no. 1, 12224, 2017, doi:10.1038/s41598-017-12482-5.

15. J. Nyboer, M. M. Kreider, and L. Hannapel, "Electrical Impedance Plethysmography A Physical and Physiologic Approach to Peripheral Vascular Study" Circulation, vol. 2, no 6, pp. 811-821, 1950, doi: 10.1161/01.cir.2.6.811
16. I. Y. Petrova, R. O. Esenaliev, Y. Y. Petrov, H. P. E. Brecht, C. H. Svensen, J. Olsson, "Optoacoustic monitoring of blood hemoglobin concentration: a pilot clinical study," OpticsLetters, Vol. 30, pp. 1677–1679, 2005, doi:10.1364/OL.30.001677.
17. J. E. Bender, A. B. Shang, E. W. Moretti, B. Yu, Lisa M. Richards, and N. Ramanujam, "Noninvasive monitoring of tissue hemoglobin using UV-VIS diffuse reflectance spectroscopy: a pilot study," Opt. Express 17, 23396-23409, 2009, doi:10.1364/OE.17.023396.
18. J. Allen, "Photoplethysmography and its application in clinical physiological measurement," Physiol. Meas., vol. 28, no. 3, 2007, doi: 10.1088/0967-3334/28/3/R01.
19. J. Kraitl, U. Timm, H. Ewald, and E. Lewis, "Non-invasive sensor for an in vivo hemoglobin measurement", In Sensors, 2011 IEEE, pages276–279. IEEE, 2011, doi: 10.1109/ICSENS.2011.6126982
20. CMOS Sensor, [Online] Available at https://whatis.techtarget.com/definition/CMOS-sensor.
21. Charge-coupled device, [Online] Available at https://searchstorage.techtarget.com/definition/charge-coupled-device.
22. Photodetectors, [Online] Available at https://chem.libretexts.org/Courses/BethuneCookman_University/BCU%3A_CH-346_Instrumental_Analysis/Spectrometer/Detectors/Detectors
23. Optical Detecors, [Online] Available at https://depts.washington.edu/mictech/optics/me557/detector.pdf
24. Indium gallium arsenide, [Online] Available at. https://en.wikipedia.org/wiki/Indium gallium arsenide.
25. Masimo Corporation. 2015, Continuous SpHb provides real-time visibility to changes, or lack of changes, in haemoglobin between invasive blood, http://www.masimo.com/technology/co-oximetry/sphb/.
26. The NBM 200 system, [Online] Available at http://www.orsense.com/product.php?ID=49
27. Press Releases Sysmex launches New ASTRIMFIT Product for Non-invasive

Measurement of Estimated Hemoglobin levels. https://www.sysmex.co.jp/en/news/2014/140115.html

28. Haemospect® [Online] Available at http://www.io.nihr.ac.uk/wp-content/uploads/migrated/1828.ff9b9ae47e0b41905767f204fa55b324.pdf
29. ToucHB, [Online] Available at https://www.biosense.in/touchb.php
30. A. D. Edwards, C. Richardson, P. V. D. Z., C. Elwell, J. S. Wyatt, M. Cope, D. T. Delpy, and E. O Reynolds, "Measurement of hemoglobin flow and blood flow by near-infrared spectroscopy", Journal of Applied Physiology, vol. 75, no 4, pp.1884–1889, 1993. doi: 10.1152/jappl.1993.75.4.1884
31. R. Kumar and H. Ranganathan, "Noninvasive Sensor Technology for Total Hemoglobin Measurement in Blood," J. Ind. Intell. Inf., vol. 1, no. 4, pp. 243–246, 2013, doi: 10.12720/jiii.1.4.243-246.
32. R. Doshi and A. Panditrao, "Non-Invasive Optical Sensor for Hemoglobin Determination," Int. J. Eng. Res. Appl., vol. 3, no. 2, pp. 559–562, 2013.
33. J. L. A. Nirupa and V. J. Kumar, "Non-invasive measurement of hemoglobin content in blood", 2014 IEEE International Symposium on Medical Measurements and Applications, pp. 1–5, 2014, doi: 10.1109/MeMeA.2014.6860140.
34. R. A. Rochmanto, H. Zakaria, R. D. Alviana and N. Shahib, "Non-invasive hemoglobin measurement for Anemia diagnosis," 2017 4th International Conference on Electrical Engineering, Computer Science and Informatics (EECSI), 2017, pp. 1-5, doi: 10.1109/EECSI.2017.8239096.
35. M. P. Mcewen and K. J. Reynolds, "Noninvasive monitoring with strongly absorbed light," Opt. Appl., vol. 44, no. 2, pp. 177–190, 2014, doi: 10.5277/oa140201.
36. X. Yi, G. Li, and L. Lin, "Noninvasive hemoglobin measurement using dynamic spectrum," Rev. Sci. Instrum., vol. 88, no. 8, 2017, doi: 10.1063/1.4998978.
37. U. Timm, G. Leen, E. Lewis, D. McGrath, J. Kraitl, and H. Ewald, "Non-invasive optical real-time measurement of total hemoglobin content," Procedia Eng., vol. 5, pp. 488–491, 2010, doi: 10.1016/j.proeng.2010.09.153.
38. H. Ding, Q. Lu, H. Gao, and Z. Peng, "Non-invasive prediction of hemoglobin levels by principal component and back propagation artificial neural network," Biomedical Optics Express, vol. 5, no. 4, pp. 1145–1152, 2014, doi:10.1364/BOE.5.001145
39. V. N. Konyukhov, V. P. Zakharov, I. L. Davydkin et al., "A system for non-invasive assessment of blood Haemoglobin level in screening tests," Biomedical Engineering, vol. 51, no. 2, pp. 93–96, 2017, http://doi.org/10.1007/s10527-017-9691-x

40. U. Timm, H. Gewiss, J. Kraitl, K. Stuepmann, M. Hinz, S. Koball, and H. Ewald, "Novel multi wavelength sensor concept to detect total hemoglobin concentration, methemoglobin and oxygen saturation", Proc. SPIE 9332, Optical Diagnostics and Sensing XV: Toward Point-of-Care Diagnostics, 93320J, 2015, doi: 10.1117/12.2080144.
41. H. Liu, F. Peng, M. Hu, J. Shi, G. Wang, H. Ai, W. Wang, “Development and Validation of a Photoplethysmography System for Noninvasive Monitoring of Hemoglobin Concentration,” J. Electr. Comput. Eng., vol. 2020, 3034260, 2020, doi: 10.1155/2020/3034260.

Chapter 3

Haemoglobin Estimation using Photoplethysmography

Spectroscopic measurements are mainly performed using three methods viz. Absorption, Scattering, and Emission. Scattering spectroscopy, e.g. Raman spectroscopy, analyses the quantity of light that a substance scatters at specific wavelengths, incidence angles, and polarisation angles in order to determine physical electromagnetic characteristics. Emission spectroscopy examines the light spectra emitted by a substance, whose energy is from a variety of sources such as temperature or chemical processes. Absorption spectroscopy uses the detection of transmitted or reflected photons with the same wavelength as the incident beam to quantify the quantities of compounds.

3.1 Optical properties of human tissue and blood

Light can penetrate deep enough into human tissues to permit spectral measurements. Optical imaging and non-invasive diagnosis of the human body depend largely on the optical and physical properties of the skin and blood. The skin's composition and morphology are extremely complex. Consequently, the composition and structure of the skin (finger) need to be investigated in order to build a suitable optical model.

3.1.1 Structure and composition of skin tissue

Various areas of the body have different skin structures and qualities. Figure 3.1 depicts the typical structure of the skin. The skin can be divided into three parts viz. epidermis, dermis, and subcutaneous fat. The thickness of the skin varies from 0.5 to 4.0 mm depending on the body site. The epidermis is made up of epithelial tissue, which comprises four major cell types: keratinocytes, melanocytes, Merkel cells and Langerhans cells. Keratinocytes create the protein keratin which protects the skin from heat, infections, and chemicals. Melanocytes are the pigment cells responsible for skin colour. They also protect the skin from UV rays. The Merkel cells act as touch sensors while Langerhans cells deal with immunological response. The stratum corneum is a thin, rough, and

protective top layer of dead and dry skin cells that covers the epidermis outermost layer. The dermis is made of cells, fibres, nerves, oil glands, sweat glands, blood vessels, and hair roots. The vascular network and sensory nerve endings are found in the papillary dermis, whereas the deeper reticular dermis is mostly made up of a loose connective structure and epithelial-derived structures like glands and follicles. Fat cells form subcutaneous fat, which acts as a cushion between the skin and the deeper muscles[1].

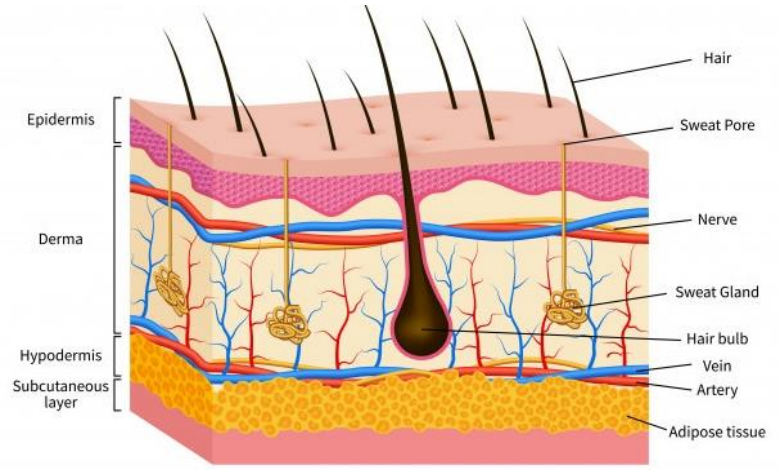

Figure 3.1: Structure of human skin [2].

Among the various possible body sites, the fingertip has several advantages. Fingertips are easily accessible, less sensitive to minor manipulations, and generally easy to control. In Figure 3.2, the different parts of a finger are depicted. The average adult male's fingernail is around 1 mm thick, the epidermis is 1.5 mm thick, the dermis is 3 mm thick, the finger bone is 6 mm thick, and the entire thickness of a finger from the dorsal to the ventral pad side is about 14 mm thick. The fingernail is made up of a translucent rigid protein called keratin [3].

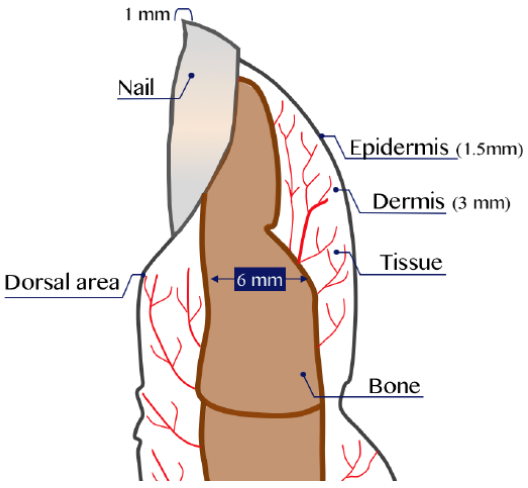

Figure 3.2: Different parts of the finger and it's thickness.

3.1.2. Optical absorption by skin tissue and blood

VIS-NIR spectroscopy uses the visible and near-IR regions of the electromagnetic spectrum. Melanin, lipids, proteins, and enzymes are among the chromophores found in tissues, in addition to haemoglobin and water. The varying concentrations of these essential components influence the tissue's overall absorption coefficient. The properties of VIS-NIR absorption change depending on the tissue constituents. Tissue is mostly made up of water, which absorbs light extremely well in the ultraviolet and long infrared wavelengths. Longer wavelengths in the visible and near-infrared regions may penetrate biological soft tissues rather deeply. Most of the biological soft tissues have low light absorption characteristics in the VIS-NIR spectral regions. This region is termed as optical window or therapeutic window and ranges from 600 nm to 1100 nm[4].Water and haemoglobin contained in the RBCs are the principal absorbers in the blood. There are various forms of haemoglobin such as methaemoglobin, carboxyhaemoglobin, deoxyhaemoglobin, and oxyhaemoglobin of which oxy and deoxyhaemoglobin are found in major concentrations. The absorption of oxyhaemoglobin (Hb) and deoxyhaemoglobin (HbO_2) associated with blood volume variations in peripheral and capillary arterial arteries is generally used in the estimation of illumination wavelength of PPG. Specifically, the light associated with particular wavelengths of skin having many peripheral blood arteries is preferred to illumination associated with surface skin layers with no arterial blood [5]. Figure 3.3 shows the extinction coefficient of haemoglobin species for a total haemoglobin concentration of 15 g/dL [6].

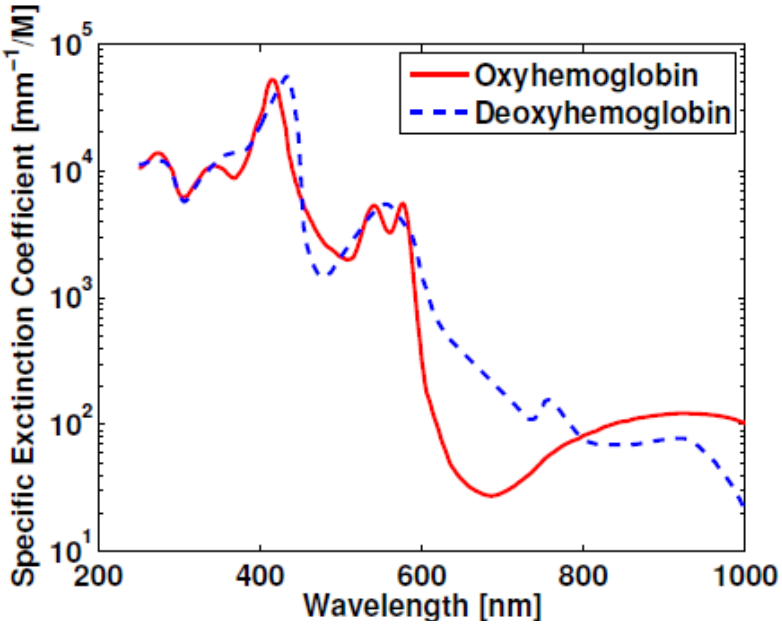

Figure 3.3: Extinction coefficient for two species of haemoglobin [6].

Figure 3.4 shows an optical window of the human tissue wherein the shorter wavelengths from 200 nm to 500 nm are significantly absorbed by melanin while water becomes dominant at wavelengths longer than 1,150 nm [7]. Fair skin possesses less melanin and a thinner dermis, allowing NIR radiation to penetrate deeper into human tissue as compared to dark skin that has more melanin and a thicker dermis. Water, in the surface layers of the skin, absorbs wavelengths between 1400 and 1500 nm, as well as wavelengths over 1850 nm, thereby causing heating and potentially painful sensations and burns[8].

VIS-NIR spectroscopy has several advantages which include reduced background interference due to water absorption, insignificant skin absorbance, and larger penetration depths at longer wavelengths, all of which are important for blood haemoglobin monitoring. Table 3.1 depicts the wavelengths of optical light that penetrate to a certain depth.

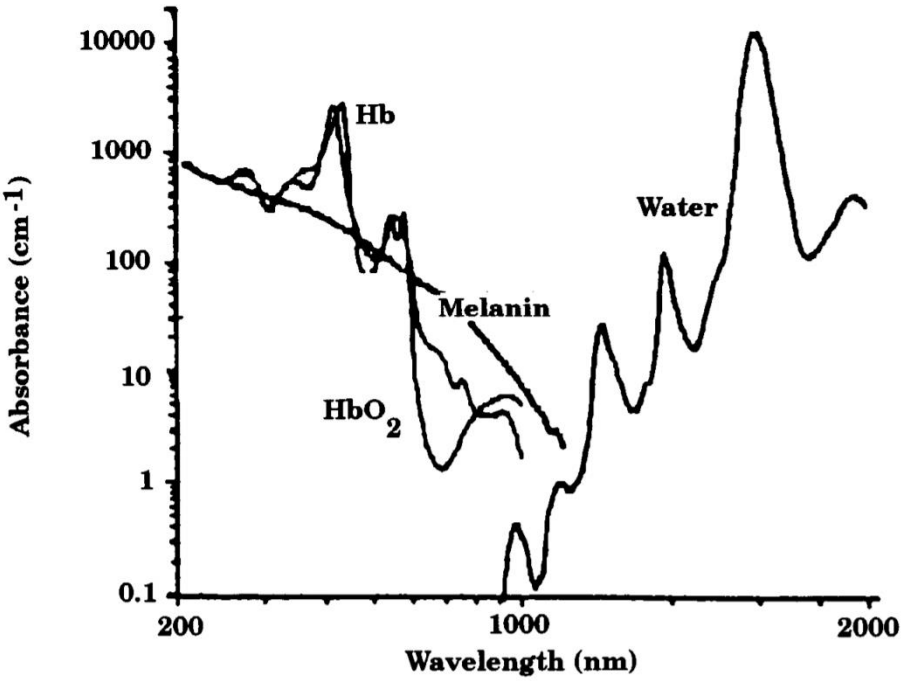

Figure 3.4: Skin tissue spectral window [7].

Table 3.1: Approximate penetration depth of optical radiation in skin tissue [3].

Wavelength (nm)	500	600	700	800	1000	1200
Depth (μm)	230	550	750	1200	1600	2200

Photoplethysmography (PPG) signal quality may be affected by pigments in different human skin types, and physiological measures may be invalidated as a result. The melanin content of skin and its associated pigments of skin types are attributable to the quality of PPG-based *in vivo* physiological monitoring [9]. As a result, incoming light with relevant wavelength illuminations is known to be substantially attenuated by melanin in human skin [10]. Furthermore, modeling and simulations have been carried out with inaccuracies owing to different pigments [11,12]. Measurement inaccuracies could be caused by ink on the skin or nail polish [13]. Melanin is responsible for a wide range of skin colour complexions and is solely necessary for skin colour. In skin categorization, the Von Luschan chromatic scale (VLCS) and the Fitzpatrick scale (FPS) are now used. VLCS [14] is often used to create racial categories for populations based on skin colour. FPS distinguishes several separate skin tones that typically come under white, or Caucasian, and does not provide an adequate difference on the darker side of the human skin colour gradient [15, 16]. Therefore, VLCS was utilized in the present study in order to better depict the true diversity of skin tones within various ethnic groups of people. Table 3.2 lists the most common skin types and their corresponding regions.

Table 3.2: Human skin types and associated region [14].

Type	Color/Description	VLCS	Area
I & II	Light/White	1-10	Europe
III	Medium, white to light brown	11-15	Asia
IV	Olive, moderate brown	16-21	Middle East
V	Brown, dark brown	22-28	Africa

3.2. PhotoPlethsmography

Photoplethysmography (PPG) is a low-cost, non-invasive optical method that measures changes in blood volume in a microvascular bed of tissue. The basic components of a PPG device are a light source and a photodetector. The light source should have a very narrow bandwidth and be as stable as possible at different temperatures, both in terms of average intensity and peak wavelength shift. It should also be small, have a long operational life, and be mechanically strong and dependable. The intensity should be strong enough to provide a meaningful signal while being low enough to avoid overheating the tissue. Light energy is converted into electrical energy by the photodetector which should be small, quick to respond, and sensitive to the wavelength produced by the LED. After the photodetector has detected the light, the signal is usually amplified and filtered using low-noise electrical circuitry[17]. PPG uses different light sources to measure the transmission or reflection of light through the blood volume based on the light absorption characteristics of haemoglobin. The most common PPG sensors utilize an IR-LED or red LED as the main light source. IR-LEDs and Red LED are most commonly used for measuring the flow of blood that is more deeply concentrated in certain parts of the body. PPG can operate in two modes: transmission and reflection, as illustrated in Figure 3.5. The photodetector and LED are on opposing sides of the tissue in transmission mode, and light is passed through it. The photodetector and LED are on the same side of the tissue in reflection mode, and the detected signal originates from backscattered light. The site of measurement is limited in transmission mode since the tissue has to be thin enough to transmit a detectable amount of light, whereas reflection mode measurements can be sited anywhere on the body [18]. In our approach, we will be using the transmission PPG principle to estimate total haemoglobin in the blood.

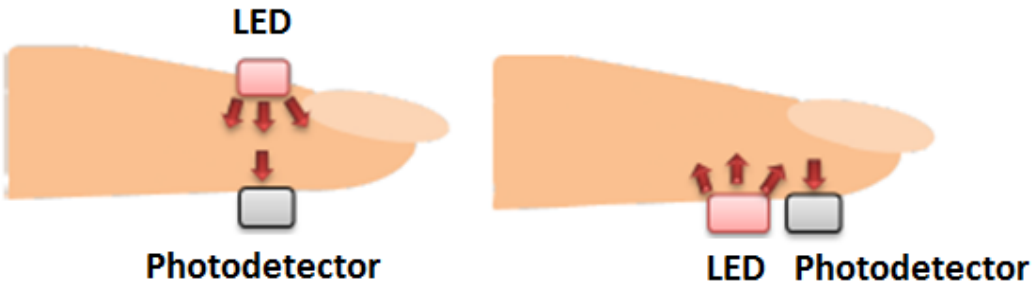

Figure 3.5: Two modes of PPG: transmission mode (left) and reflection mode (right).

3.2.1 Factors affecting PPG recordings

The measurement site (i.e. probe attachment site), the contact force, subject posture as well as respiration, all have an impact on PPG recordings. Some of these aspects are briefly discussed in the nextsection.

Measurement site of probe

The placement of the LED and Photodetector has a significant impact on signal quality. To optimize sensor performance, suitable measurement locations must be located. PPG sensors are commonly worn on the fingers due to the high signal amplitude that can be achieved in comparison with other sites [19]. Different measuring sites for PPG sensors have been intensively investigated in recent years, including the ring finger [20], wrist [21, 22], and earlobe [23-25]. The finger, earlobe, and forehead are routinely used in commercial clinical PPG sensors [26]. The perfusion values of 52 anatomical sites in healthy people revealed that the fingers, palm, face, and ears have significantly greater perfusion values as compared to other measurement sites [27], with the transmitted PPG signal amplitude from the earlobe having the highest perfusion value but has lesser variations in blood compared to the fingers.

Probe contact force

The contact force between the sensor and the measurement site may influence the PPG signal waveform. Depending on the PPG probe contact pressure, the waveform of the acquired PPG signal varies. The PPG waveform has been related to arterial stiffness and vascular reactivity in several investigations. According to various studies, the PPG signal can be improved by applying mild pressure on the sensor. Transmural pressure, defined as the differential in pressure between the interior and outside of a blood artery, is ideal for obtaining the best PPG signal (i.e., the pressure across the wall of the blood vessel). Also, insufficient pressure leads to inadequate contact and produces low AC signal amplitude. However, when the PPG signal is acquired with excessive pressure, the flow of blood is occluded and it produces low AC signal amplitude and distorted waveforms [18]. Therefore, subjects need to be requested to place their right-hand forefinger with slight pressure inside the finger probe in order to acquire good quality PPG signals.

3.2.2 PPG waveform

The light traveling through the biological tissue (e.g., the finger) is absorbed by different absorbing substances. The primary absorbers of light in the region from 600 to 1000 nm are arterial and venous blood and skin pigmentation. The measured PPG signal has two components: one alternating current (AC) and one direct current (DC). Because the AC component is dependent on pulsatile blood flow, it varies at the same rate as the pulse. The AC component may be used to assess blood perfusion asit is directly related to pulsatile blood. The DC component is quasi-constant, and it refers to the tissue's composition such as epidermis and skin other than pulsatile blood. Due to breathing, thermoregulation, and sympathetic nervous system activity, the DC component is not completely constant [28]. During the systolic cycle, the arteries increase in diameter and the volume of blood increases. During the diastolic cycle, the arteries decrease in diameter and the volume of blood also decreases. This change in volume of blood results in change of absorption of light in the tissues which produces time-varying transmitted signal called as Photoplethysmography signal. Figure 3.6 shows the variation in light attenuation by tissue. The intensity of light is attenuated as it passes through the finger due to the absorbance depending on the concentration of absorbers and optical path length of the medium according to the Beer-Lambert law which is discussed in detail in the next section.

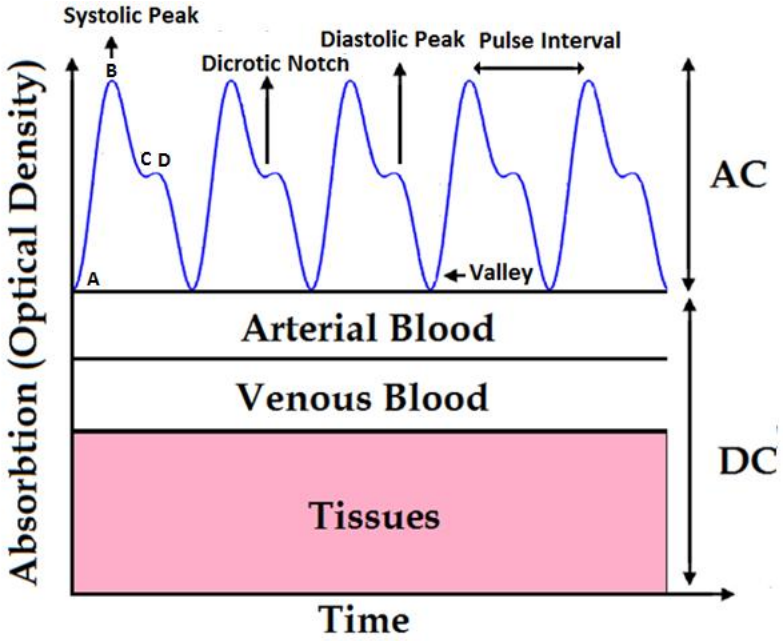

Figure 3.6: Variation in light attenuation by tissue and features of PPG signal.

PPG features

Any normal PPG signal consists of a systolic phase followed by a diastolic phase, both of which are separated by a dicrotic notch. In a typical PPG signal, the region from A to B point is the fast beating phase, and the region from B to C point is the delaying phase. B is the peak point of the PPG signal. At this point, the blood pressure has its maximum value in the entire period called the systolic peak. Another peak at point D is the artiole's dicrotic wave also known as the diastolic peak. The C point is called a dicrotic notch (small downward deflection). The shape and depth of the notch greatly vary from person to person depending upon his/her medical condition. In some cases, no deflection is seen while in some the deflection is significant and in varying contours. Thus the classification of notches could give us useful information about the condition of the patient. In pulse waveform analysis, Dawber et al. [29] defined four classes for the PPG signals as shown in Figure 3.7.

Class 1: A normal PPG signal with a prominent dicrotic notch.

Class 2: A PPG signal with no distinct dicrotic notch, but the downward slope becomes horizontal.

Class 3: A PPG signal with no obvious dicrotic notch, but a well-defined change in the angle of descent.

Class 4: A PPG signal with no evidence of a dicrotic notch.

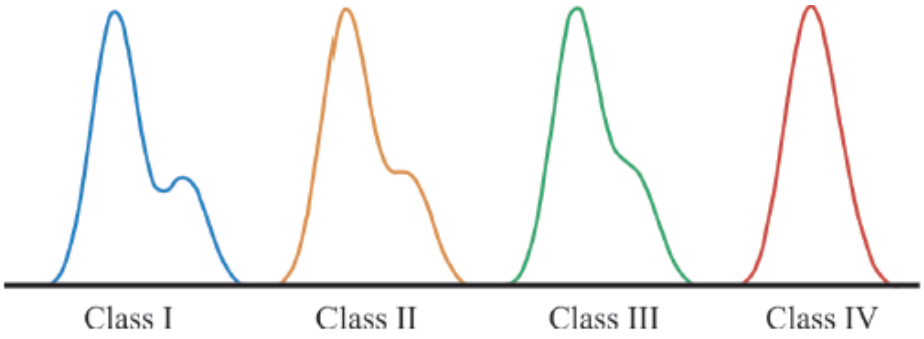

Figure 3.7: PPG classes as defined by Dawber et al. [29].

During the feature extraction from the PPG signal, time-domain features were extracted from the PPG signal after the pre-processing. Multiple features from the PPG signal including the systolic peak, diastolic peak, valley, rising time of PPG, falling time of PPG, etc are present [30] as shown in Figure 3.6.

Systolic peak (B): This is a measurement of arterial blood flow-induced pulsatile variations in blood volume.

Diastolic peak (D): The diastolic peak is observed as a result of pressure wave reflections in the lower body's arteries.

Valley (A): This is a measurement of the non-pulsatile changes in blood volume.

Dicrotic notch (C): This is a slight downward deflection in the PPG cycle between the systolic and diastolic points.

Pulse Interval: The distance between the beginning and end of the PPG waveform.

In our approach, we have used only two features of the PPG signal (Systolic peak and Valley) to estimate total haemoglobin in the blood in a non-invasive manner. This will be discussed in Chapter 6.

3.3 Beer-Lamberts law

Non-invasive haemoglobin measurement is based on the concepts of Beer-Lambert law which states that the attenuation of incident light (I_0) crossing a material is a function of the absorbing properties as shown in Figure 3.8 [31]. When an incident beam (I_0) enters the sample, the intensity of transmitted light (I) decreases exponentially as shown in Equation 3.1.

$$I = I_O e^{-\varepsilon^{\lambda}.C.L} \tag{3.1}$$

where:

I -----> intensity of transmission light

I_0 -----> intensity of incident light

ε -----> Molar extinction coefficient of the substance at a specific wavelength, mol-1 cm-1

c -----> concentration of absorbent, mol

L-----> optical path length in the medium, cm

The transmittance (*T*) of light passing through a medium containing an absorbing substance is the ratio of transmitted light (*I*) to the incident light (I_0), and absorbance is the negative natural logarithm of the transmittance, as shown in Equation 3.2 [31].

$$A = -log\, T = -log \frac{I}{I_O} = \varepsilon^{\lambda}.C.L \tag{3.2}$$

where:

A ---->absorbance, (absorbance unit)

T----> transmittance

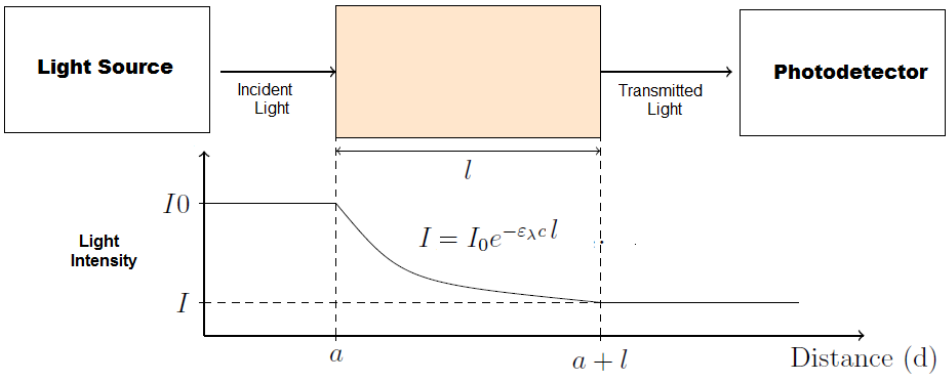

Figure 3.8: Beer-Lambert law.

When the finger is placed between the source and photodetector, it absorbs the light emitted by the LED source depending on its characteristics (tissue and blood). The transmitted light is measured by the photodetector and is recorded as a PPG signal. Beer-law Lambert's can also be used to compute the absorbance of a certain blood component at a specific wavelength using Equation 3.1

The total absorbance for n different components is represented as Equation 3.3.

$$A = \Sigma\, €(n)c(n)L \tag{3.3}$$

where €(n)= molar extinction coefficient of n^{th} solute, c(n)=concentration of n^{th} solute in the solution.

Thus, the concentration of the solute can be easily computed by knowing the values of path length L, absorbance A, and molar extinction coefficient € at a particular wavelength λ.

Absorbance is an additive function →Absorbance of a mixture is a sum of the absorbance's of the components: $A = \varepsilon_X[X]L + \varepsilon_Y[Y]L + \varepsilon_Z[Z]L$ where [X], [Y], [Z] are unknowns concentrations. Hence, we use different wavelengths to get different equations with different unknowns, which are the concentrations of haemoglobin like oxyhaemoglobin, and deoxyhaemoglobin. These equations can be solved to obtain the concentrations of these components [32].

3.4 Health parameters obtained from PPG signal

Heart Rate from PPG signal

Heart rate is the number of heartbeats in a minute. To calculate, Heart rate from the typical PPG signal shown in Figure 3.9, the time interval between adjacent peaks of the PPG signal is determined using Equation 3.4[33].

$$PP_{av} = \frac{PP_1+PP_2+PP_3}{3} \tag{3.4}$$

where PP_{av} is an average of three PPG intervals between successive peaks of the PPG signal and heart rate is calculated using Equation 3.5.

$$Heart\_Rate = 60 * \frac{1}{PP_{av}} \tag{3.5}$$

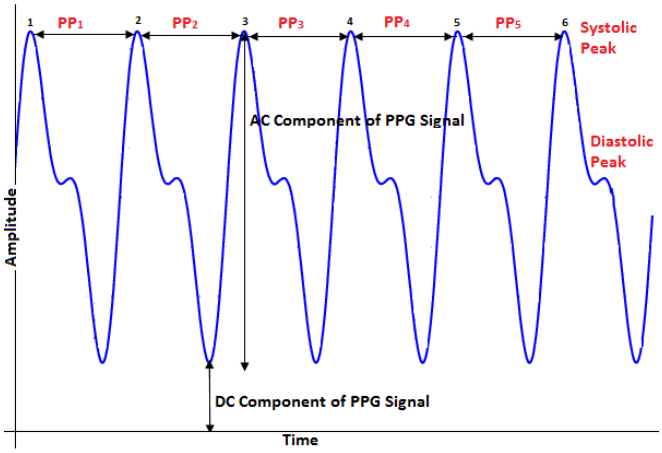

Figure 3.9: Typical PPG signal.

Heart Rate Variability from PPG signal

Heart Rate Variability (HRV) is an important parameter for the analysis of a patient's physiological conditions, as well as a method aiding the diagnosis of cardiopathies [34]. The analysis of HRV signals is important when studying the autonomic nervous system, as it supports the evaluation of the balance between the sympathetic and parasympathetic influences in the cardiac rhythm [35]. The HRV is a valuable vital signal, which reflects the physical condition of a patient [36]. An abnormal value between heartbeats is one of the first indicators of the existence of an anomaly in the patient's health. It can reveal diverse conditions, such as respiratory and cardiac arrest, systemic inflammatory response syndrome, renal insufficiency, cardiac insufficiency, systolic

arterial pressure, among others [37]. The changes in time intervals between adjacent heartbeats is simply the HRV. To calculate HRV from sample PPG Signal. Root Mean Square of Successive Differences (RMSSD) between normal heartbeats is found by first calculating the time difference between each successive heartbeats [38]. Then, all these values are squared and the average of the result is taken before taking the square root using Equation 3.6.

$$HRV = \sqrt{\frac{(\mathrm{PP}_2-\mathrm{PP}_1)^2+(\mathrm{PP}_3-\mathrm{PP}_{2)}{}^2+(\mathrm{PP}_4-\mathrm{PP}_3)^2}{3}} \tag{3.6}$$

The HRV value is calculated in terms of milliseconds.

Oxygen Saturation from PPG signal

The normalization technique is used where AC component is divided by the DC component. To calculate SpO_2, the AC and DC values of the pulsating RED (670 nm) and IR (950 nm) PPG are extracted and the ratio R is found. The Ratio of ratios 'R' is approximated in Equation 3.7 which is used to eliminate the time invariant absorbance due to the venous blood and surrounding tissues.

$$R = \frac{AC_{670}/DC_{670}}{AC_{950}/DC_{950}} \tag{3.7}$$

SpO_2 is computed based on the empirical calibration of the Ratio of ratios for the specific device using Equation 3.8 [39].

$$SpO_2\% = 115 - (15 \times R) \tag{3.8}$$

Total Haemoglobin Estimation, from PPG Signal using an empirical formula

The change in optical density or change in absorbance is calculated using Equation 3.9.

$$\Delta[A_\lambda] = -log\left[\frac{ACComponent\ of\ the\ PPG}{DCComponent\ of\ the\ PPG}\right] = \{\varepsilon Hb^\lambda(\Delta[Hb]) + \varepsilon HbO_2^\lambda(\Delta[HbO_2])L\} \tag{3.9}$$

ΔA_λ----->represents a change in absorbance for a PPG signal at a specific wavelength.

εHb^λ and $\varepsilon HbO_2^\lambda$ --> Molar extinction coefficient for deoxyhaemoglobin & oxyhaemoglobin at a specific wavelength.

ΔHb and ΔHbO_2 -->Change in concentration of deoxyhaemoglobin and oxyhaemoglobin in moles per liter.

L----->is the length of the light path through the finger.

where the AC Component of the PPG signal is the difference between the maximum and minimum of the PPG signal and the DC component of the PPG signal is the minimum of the PPG signal [40].

$$\begin{bmatrix} \Delta[Hb] \\ \Delta[HbO_2] \end{bmatrix} = \begin{bmatrix} \Delta[A_{670}] \\ \Delta[A_{770}] \\ \Delta[A_{810}] \\ \Delta[A_{850}] \\ \Delta[A_{950}] \end{bmatrix} \times \begin{bmatrix} \varepsilon Hb^{670} \varepsilon HbO_2^{670} \\ \varepsilon Hb^{770} \varepsilon HbO_2^{770} \\ \varepsilon Hb^{810} \varepsilon HbO_2^{810} \\ \varepsilon Hb^{850} \varepsilon HbO_2^{850} \\ \varepsilon Hb^{950} \varepsilon HbO_2^{950} \end{bmatrix}^{-1} \times [L]^{-1} \quad (3.10)$$

The concentrations of oxyhaemoglobin and deoxyhaemoglobin were calculated using the absorbances along with the well-known molar extinction coefficients of oxyhaemoglobin and deoxyhaemoglobin using Equation 3.10. The total haemoglobin is calculated by adding the concentrations of oxyhaemoglobin and deoxyhaemoglobin.

$$\Delta[Hb]_{total} = (\Delta[Hb] + \Delta[HbO_2]) \times 64500 \quad (3.11)$$

Equation 3.11 indicates the concentration of total haemoglobin in g/dL where 64500 is the molecular mass of haemoglobin.

Also, blood pressure and cardiovascular diseases can be estimated from the PPG signal with good processing algorithms. The entire algorithm for extracting PPG features and estimating total haemoglobin using a suitable empirical formula and with Multivariate (PLSR) model is implemented using C++, which is explained in Chapter 6.

References

1. A. N. Bashkatov, E. A. Genina, V. I. Kochubey, and V. V. Tuchin, “Optical properties of human skin, subcutaneous and mucous tissues in the wavelength range from 400 to 2000 nm,” J. Phys. D. Appl. Phys., vol. 38, no. 15, pp. 2543–2555, 2005, doi: 10.1088/0022-3727/38/15/004.
2. Human skin, [Online] Available at https://byjus.com/biology/skin-diagram/
3. Kenneth A Walters and Majella E Lane, "The human nail: Structure, properties, therapy and grooming", Cosmetic Formulation: Principles and Practice, pp. 77, 2019.
4. R. R. Anderson and J. A. Parrish, “The optics of human skin”, J. Invest. Dermatol., vol. 77, pp.13-19, 1981, doi: 10.1111/1523-1747.ep12479191.
5. K. Rogers, "Blood: Physiology and Circulation. Human body", Britannica Educational Pub., 2010.
6. S. Prahl, Optical properties spectra, [Online] Available at http://omlc.ogi.edu/spectra.
7. H.W. Lim, N.A.Soter, Clinical Photomedicine; CRC Press: New York, NY, USA, 1993.
8. Y. Tanaka Y, "Impact of near-infrared radiation in dermatology", World J Dermatol, vol. 1, no. 3, pp. 30-37, 2012, doi: 10.5314/wjd.v1.i3.30
9. C. Gertrude, J. Vincent, K. Hearing, "Human skin pigmentation: Melanocytes modulate skin color in response to stress, FASEB J. Rev., vol. 21, pp. 976–994, 2007, doi:10.1096/fj.06-6649rev
10. G. Zonios, J. Bykowski, N. Kollias, "Skin melanin, hemoglobin, and light scattering properties can be quantitatively assessed in vivo using diffuse reflectance spectroscopy", J. Investig. Dermatol., vol. 117, no. 6, pp. 1452–1457, 2001, doi:10.1046/j.0022-202x.2001.01577.x
11. A. Jubran, M. J. Tobin, "Reliability of pulse oximetry in titrating supplemental oxygen therapy in ventilator-dependent patients", Chest, vol. 97, no. 6, pp. 1420–1425, 1990, doi:10.1378/chest.97.6.1420
12. J.R. Emery, "Skin pigmentation as an influence on the accuracy of pulse oximetry", J. Perinatol. vol. 7,no.4, pp. 329–330, 1987.
13. A.C. Ralston, K. Webb, W. B. Runciman, "Potential errors in pulse oximetry. III: Effects of interferences, dyes, dyshaemoglobins and other pigments" Anaesthesia, vol. 46, no.4, pp. 291–295, 1991, doi:10.1111/j.1365-2044.1991.tb11501.x

14. D.K.Chanchal, "Swarnlata, S. Skin care assessment on the basis of skin hydration, melanin, erythema and sebum at various body sites", Int. J. Pharm. Pharm. Sci. vol. 3, pp. 209–213, 2011.
15. T.B. Fitzpatrick, "The Sun and the skin", J. Med. Esthet., vol. 2, pp. 33–34, 1975.
16. T.B. Fitzpatrick, "The validity and practicality of sun-reactive skin types I through VI", Arch. Dermatol. vol. 124, no. 6, pp. 869–871, 1988, doi:10.1001/archderm.124.6.869
17. J. Allen, "Photoplethysmography and its application in clinical physiological measurement," Physiol. Meas., vol. 28, no. 3, 2007, doi: 10.1088/0967-3334/28/3/R01.
18. T. Tamura, Y. Maeda, M. Sekine, and M. Yoshida, "Wearable Photoplethysmographic Sensors—Past and Present," Electronics, vol. 3, no. 2, pp. 282–302, 2014, doi: 10.3390/electronics3020282.
19. A.B. Hertzman, "The blood supply of various skin areas as estimated by the photoelectric plethysmograph", Amer. J. Physiol. vol. 124, pp. 328–340. 1938, doi: 10.1152/ajplegacy.1938.124.2.328
20. S.Rhee, B. H.Yang, H. H. Asada, "Artifact-resistant, power-efficient design of finger-ring plethysmographic sensors", IEEE Trans. Biomed. Eng., vol. 48, no.7 pp. 795–805.2001, doi: 10.1109/10.930904.
21. J.Y. Jung, L.W. Lee, "Zigbee device access control and reliable data transmission in Zigbee based health monitoring", Proc. Int. Conf. Adv. Commun. Technol. (ICACT 2008) ,pp.795–797,2008, doi: 10.1109/ICACT.2008.4493875.
22. Y. Lee, H. Shin, J. Jo and Y. Lee, "Development of a wristwatch-type PPG array sensor module," 2011 IEEE International Conference on Consumer Electronics - Berlin , pp. 168-171, 2011, doi: 10.1109/ICCE-Berlin.2011.6031811.
23. S. Vogel, M. Hülsbusch, T. Hennig, V. Blazek, S. Leonhardt, "In-ear vital signs monitoring using a novel microoptic reflective sensor", IEEE Trans Inf Technol Biomed, vol. 13, no. 6, pp. 882-889M 2009 doi:10.1109/TITB.2009.2033268
24. K.Shin,Y. Kim, S. Bae, K. Park, S. Kim, "A novel headset with a transmissive PPG sensor for heart rate measurement", Proc. Int. Conf. Biomed. Eng. IFMBE , vol. 23, pp. 519–522, 2009, doi: 10.1007/978-3-540-92841-6_127
25. M. Poh, N. C. Swenson and R. W. Picard, "Motion-tolerant magnetic earring sensor and wireless earpiece for wearable photoplethysmography," in IEEE

Transactions on Information Technology in Biomedicine, vol. 14, no. 3, pp. 786-794, 2010, doi: 10.1109/TITB.2010.2042607

26. Y. Mendelson and C. Pujary, "Measurement site and photodetector size considerations in optimizing power consumption of a wearable reflectance pulse oximeter," Proceedings of the 25th Annual International Conference of the IEEE Engineering in Medicine and Biology Society, vol. 4, pp. 3016-3019, 2003, doi: 10.1109/IEMBS.2003.1280775
27. E. Tur, M. Tur, H. I. Maibach, R. H. Guy, "Basal perfusion of the cutaneous microcirculation: Measurements as a function of anatomic position", J. Invest. Dermatol., vol. 81, pp. 442–446, 1983.
28. J. P. deKock and L. Tarassenko, "In vitro investigation of the factors affecting pulse oximetry", J. Biomed. Eng. vol. 13, no.1, pp. 61–66, 1999, doi:10.1016/0141-5425(91)90046-a
29. T. Tigges, Z. Music, A. Pielmus, M. Klum, and A. Feldheiser, "Classification of morphologic changes in photoplethysmographic waveforms," vol. 2, no. 1, pp. 203–207, 2016, doi: 10.1515/cdbme-2016-0046.
30. T. R. Dawber, H. E.Thomas, P. M. McNamara. Characteristics of the dicrotic notch of the arterial pulse wave in coronary heart disease. Angiology, vol. 24, no. 4, pp. 244-255, 1973, doi:10.1177/000331977302400407
31. C.G. Lee, "Calculation of light penetration depth in photobioreactors", Biotechnology and Bioprocess Engineering, springer, vol. 4, pp. 78-81, 1999. doi: 10.1007/BF02931920
32. C. Sharma, S. Kumar, A. Bhargava, and S. Roy Chowdhury, "Field Programmable Gate Array Based Embedded System For Non-Invasive Estimation Of Hemoglobin In Blood Using Photoplethysmography," Int. J. Smart Sens. Intell. Syst., vol. 6, no. 3, pp. 1267–1282, 2013, doi: 10.21307/ijssis-2017-589.
33. R. McCraty and F. Shaffer, "Heart rate variability: New perspectives on physiological mechanisms, assessment of self-regulatory capacity, and health risk," Glob. Adv. Heal. Med., vol. 4, no. 1, pp. 46–61, 2015,doi:10.7453/gahmj.2014.073
34. J. L. Moraes, M. X. Rocha, G. G. Vasconcelos, F. Vasconcelos, V. Albuquerque, A.R. Alexandria, "Advances in Photopletysmography Signal Analysis for Biomedical Applications", Sensors, vol. 18, no 6, pp. 1894, 2018, doi:10.3390/s18061894

35. C. H. Lin, "Assessment of bilateral photoplethysmography for lower limb peripheral vascular occlusive disease using color relation analysis classifier", Comput. Methods Progr. Biomed., vol. 103, no.3, pp. 121–131, 2011, doi: 10.1016/j.cmpb.2010.06.014.
36. F. Fan, Y. Yan, Y. Tang, H. Zhang, "A motion-tolerant approach for monitoring SpO_2 and heart rate using photoplethysmography signal with dual frame length processing and multi-classifier fusion", Comput Biol Med. vol. 91, pp. 291-305, 2017, doi:10.1016/j.compbiomed.2017.10.017
37. D. A. Birrenkott, M. A. F. Pimentel, P. J. Watkinson and D. A. Clifton, "A Robust Fusion Model for Estimating Respiratory Rate From Photoplethysmography and Electrocardiography," in IEEE Transactions on Biomedical Engineering, vol. 65, no. 9, pp. 2033-2041, 2018, doi: 10.1109/TBME.2017.2778265.
38. F. Shaffer and J. P. Ginsberg, "An Overview of Heart Rate Variability Metrics and Norms," Front. Public Heal., vol. 5, pp. 1–17, 2017. doi:10.3389/fpubh.2017.00258
39. M. Shafique and P. A. Kyriacou, "Photoplethysmographic signals and blood oxygen saturation values during artificial hypothermia in healthy volunteers," Physiol. Meas., vol. 33, no. 12, pp. 2065–2078, 2012, doi:10.1088/0967-3334/33/12/2065
40. C. F. Pinto, J. S. Parab, M. D. Sequeira and G. M. Naik, "Development of Altera NIOS II Soft-core system to predict total Hemoglobin using Multivariate Analysis", J. Phys.: Conf. Ser. 1921 012039, 2021, doi: 10.1088/1742-6596/1921/1/012039.

Chapter 4

Hardware System Designed

4.1 Objectives

In this chapter, we discuss the objectives of the present research, problem statement, and solution. As stated earlier, the haemoglobin tests performed by a pathological laboratory are not feasible for patients who need to continually monitor their haemoglobin levels, since there is pain and discomfort associated with the blood sample withdrawal, the possibility of infection, and the recurring cost. This calls for the design and implementation of a non-invasive solution.

In the present study, our aim is to design an accurate device for the measurement of total haemoglobin through the development of a Novel Soft-core Embedded Architecture on the Altera FPGA platform. Briefly, our objectives may be stated as follows:

- To design a finger probe with multiple LEDs (5 or 6 wavelengths) and a single photodetector with high efficacy.
- To implement signal conditioning and interfacing the ADC to the FPGA.
- To design digital filters to remove noise and moving artifacts from the PPG signal.
- To develop a Multivariate regression algorithm in FPGA to detect total haemoglobin present in the blood using different wavelengths of light.
- To achieve RMSE of less than 1 g/dL.

4.2 Selection of LED wavelengths for haemoglobin estimation

Light absorbance captured by a photodetector is affected by the volume of blood, blood vessel wall movement, and the orientation of RBC [1]. Since blood absorbs more light as compared to tissue, the intensity of the absorbed light can be used to estimate a change in blood volume. Skin melanin and fat have significant responses with the shorter wavelengths of light [2]. According to research studies [3, 4], shorter wavelengths of light, such as blue and green, can only penetrate up to the capillary bed, while yellow light can

only penetrate up to the arterioles in the dermis, and further, longer wavelengths, such as red and near-infrared, can easily penetrate more deeply into the skin and reach the arteries in the tissue. According to the research findings, both haemoglobin species exhibit high absorption between 650 and 1000nm, and the oxyhemoglobin and deoxyhaemoglobin have a significant molar extinction coefficient difference. In the wavelength range from 600nm to 950nm, the wavelengths have been found to possess greater penetration power with low attenuation coefficients. According to literature [5], deoxyhemoglobin blood was absorbed more in the wavelength range of 600 to 800 nm, whereas oxyhemoglobin blood was absorbed more in the wavelength range of 820 to 1000 nm. The isosbestic point was located at 810 nm where deoxy and oxyhemoglobin absorption coefficients are the same. The experimental observation was carried out in the laboratory to obtain the spectra of blood. Here, the blood samples were diluted using double distilled water and the absorbance was measured using UV-VIS spectroscopy (Evolution 201). It was observed the spectra of the blood matched as per literature. For the present study, we chose wavelengths in such a way that one wavelength is between 900 nm and 1000 nm, with significant absorption for both oxy and deoxyhemoglobin; herein, that wavelength was 950 nm. The second wavelength was chosen at 670 nm, which is the valley of oxyhemoglobin. The third wavelength, 810 nm, was chosen as the point of interception (Isosbestic) of oxy- and deoxyhemoglobin. The other two wavelengths, 770 nm, and 850 nm were chosen on each side of the interception with a significant difference in absorption between oxyhemoglobin and deoxyhemoglobin [6]. However, depending on the availability of high-quality LED sources in this region, the wavelength selection can be slightly changed.

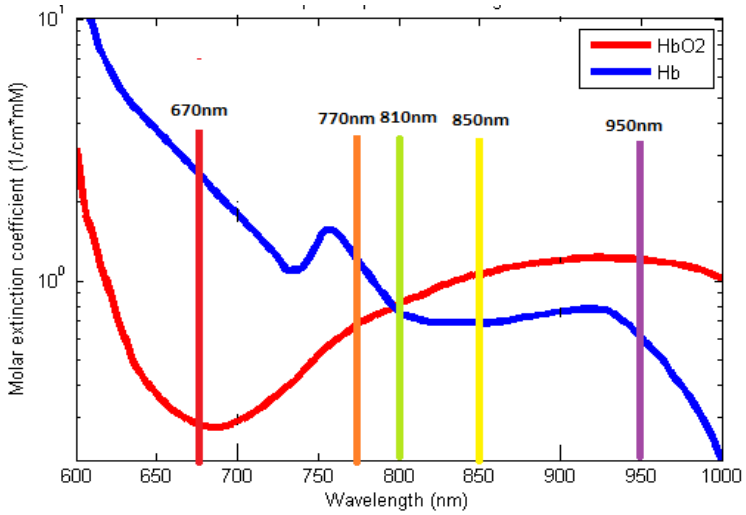

Figure 4.1: Molar extinction coefficient of haemoglobin species at five LED wavelengths.

4.3 Finger Probe Design

4.3.1 Excitation sources and detector

Sources

In this design, Multichip LEDs (MTMD6788594SMT6) and OPT101 (Photo detector with inbuilt trans-impedance amplifier) were used. The Multichip LEDs have all five sources in a small densely packaged area and the power radiated from the five LEDs is around 5 mW as shown in Table 4.1.

Table 4.1: Power of Multichip LEDs [7]

LED Wavelengths (nm)	Forward current (mA)	Forward voltage (V)	Power Output (mW)
670	20	1.8	5.2
770	20	1.65	6.3
810	20	1.50	5.2
850	20	1.45	4.7
950	20	1.25	7.6

Detector

OPT101 operates on low power single supply voltage with a dark current of 120 μA. OPT101 is an integrated combination of a photodiode and trans-impedance amplifier on a single chip as shown in Figure 4.2. This eliminates the problem of leakage current errors and noise pick up. The inbuilt trans-impedance amplifier is used to convert the photocurrent into voltage with a gain (10^6). Also, it has a high responsivity in the wavelength range from 600 nm to 1000 nm as shown in Figure 4.3.

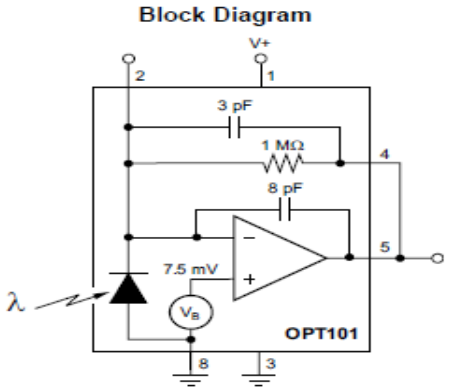

Figure 4.2: Internal Diagram of OPT101[8] .

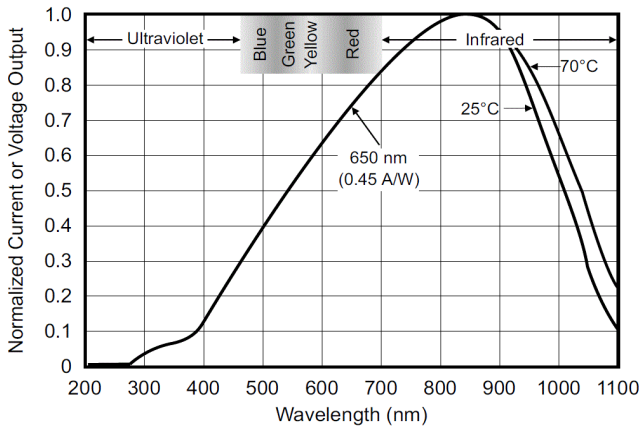

Figure 4.3: Spectral responsivity of OPT101[8].

The Multichip LEDs and OPT101 were fabricated on the PCB as shown in Figure 4.4. The two components were chosen owing to their compact size, lower space requirement, and low dark current across the OPT101 when the finger is placed inside the finger probe.

Figure 4.4: PCB fabricated with Multichip LEDs and OPT101.

In the next section, we discuss the importance of standardizing LED power and the steps involved in ensuring this.

4.4 Process of LEDs power standardization

The first step is to verify the wavelengths of the Multichip LEDs and it was done using (a) Ocean Optics USB 2000+ UV- VIS Spectrometer for the wavelengths from 670 to 850 nm and (b) Ocean NIR Quest Spectrometer for 950 nm and the Multichip LED were placed in front of the spectrometer. The USB2000 Spectrometer was connected to a laptop via a USB port and drew power it. Ocean Optics fiber optic spectrometer systems consist of low-cost, modular data acquisition components. The screenshot of Spectrasuite for Ocean Optics USB2000 is shown in Figure 4.5.

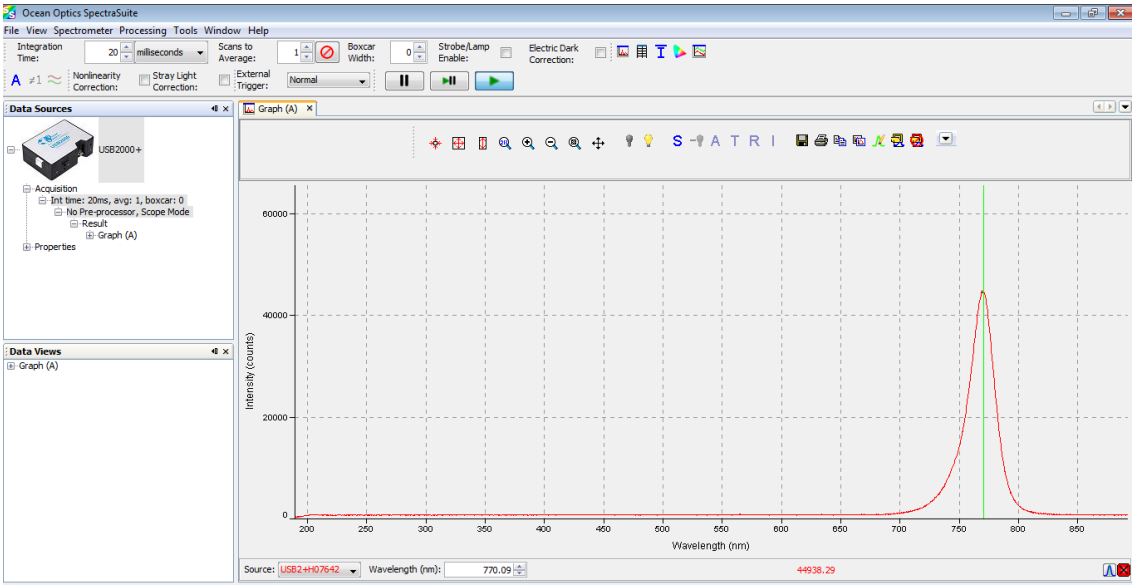

Figure 4.5: Screenshot of Spectrasuite for Ocean Optics USB2000.

The peak wavelength of all the five LEDs was observed on the Ocean Optics Spectra Suite as shown in Figure 4.6. A small variation is observed in the measured wavelengths of the Multichip LEDs as shown in Table 4.2.

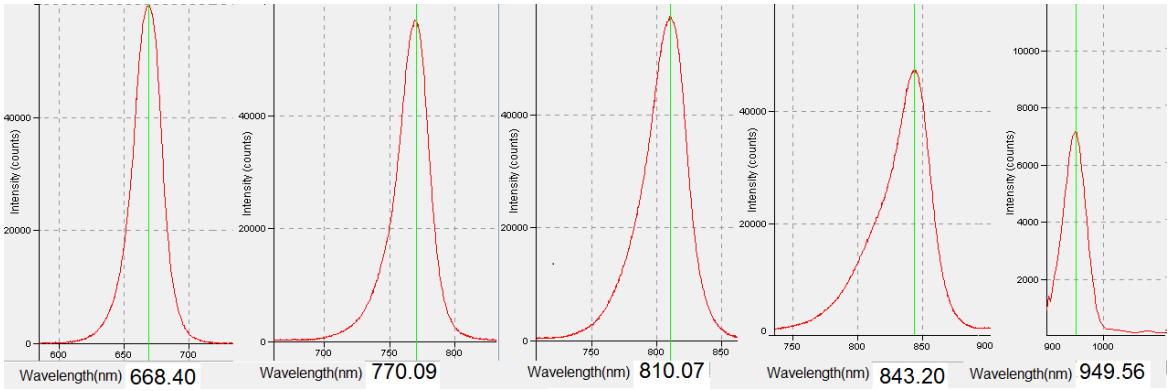

Figure 4.6: Peak wavelength of the Multichip LEDs.

Table 4.2: Wavelength of the Multichip LEDs (MTMD6788594SMT6)

Wavelength of LED (nm)	Wavelength measured (nm)	Difference (nm)
670	668.40	1.60
770	770.09	0.09
810	810.07	0.07
850	843.20	6.80
950	949.56	0.44

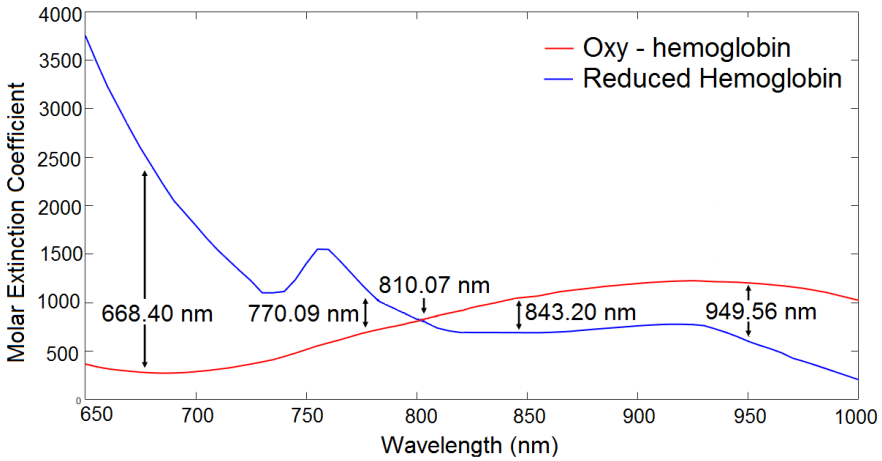

Figure 4.7: Molar extinction coefficients vs measured wavelengths of Multichip LEDs.

The measured wavelengths of the Multichip LEDs are shown in Figure 4.7. A small variation has been observed in the measured wavelengths. The power of the individual LEDs (MTMD6788594SMT6) was measured using Newport Power Meter 2936R with a Silicon Detector at a fixed distance of 1.2 cm. Initially, a fixed value of resistance (viz. 68Ω) was used and the power of the individual LEDs was measured without standardization. These outputs are listed in Table 4.3. It is observed that the power of the individual LEDs differs.

Table 4.3: Without standardized LEDs power

Wavelength of LED (nm)	LEDs power observed (mW)
670	0.65
770	0.75
810	0.67
850	0.66
950	0.96

When we recorded the PPG signal with these LEDs, we had to apply a calibration factor in the software algorithm which was resulting in a slight error in the estimation of haemoglobin. Therefore, we decided to standardize the LED power by maintaining constant power of 0.7 mW for the individual LEDs as shown in Figure 4.8. For this, we had to adjust the forward current flowing through the LEDs by varying the limiting resistance. A fixed resistance value was introduced for each individual LED to maintain

constant radiant LED power for a fixed distance. Also, the forward current (in mA) flowing through LEDs and voltage drop of each LED were measured using a multimeter. The resistors selected to obtain constant power are listed in Table 4.4.

Figure 4.8: Standardization of LEDs power using Newport power meter.

Table 4.4: Standardized LEDs power.

Wavelength of LEDs (nm)	Current flowing through the LED (mA)	Voltage drop across the LED (V_D)	Limiting resistance (Ω)
670	21.1	1.80	71
770	18.3	1.62	92
810	23.4	1.55	75
850	24.7	1.46	74
950	12.3	1.23	168

The limiting resistance for the individual LEDs is calculated using

$$R = \frac{V_S - V_D}{I} \tag{4.1}$$

where V_S is the supply voltage i.e. 3.3Vand V_D is the voltage drop of the LED, I is forward current (in mA). For 670nm with standardization, the limiting resistance was also calculated using Equation (4.1),

$$\mathrm{R} = \frac{(3.3 - 1.80)\mathrm{v}}{(21.1 * 10^{-3})\mathrm{A}} = 71\Omega$$

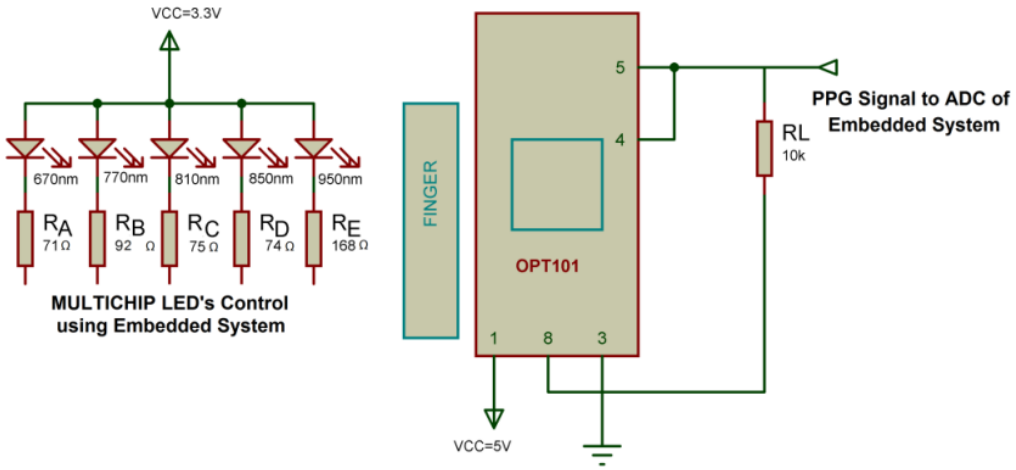

Figure 4.9: Circuit diagram of Multichip LEDs with constant power output with OPT101.

Using the circuit of Figure 4.9 (for constant LED power of 0.7 mW), the power output for each LED was calibrated by adding variable resistors and verified using a Newport power meter. The finger probe is designed with the Multichip LEDs placed on the top side of the finger probe structure and the OPT101 positioned at the bottom side of the finger probe structure as shown in Figure 4.10.

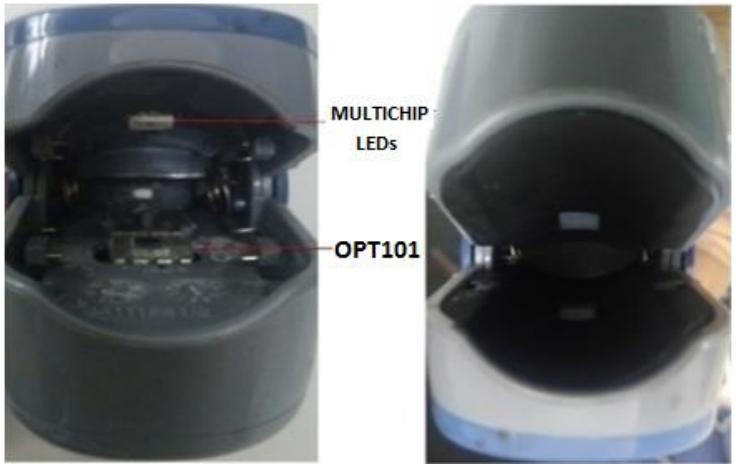

Figure 4.10: Finger Probe designed.

4.5 System design for non-invasive haemoglobin estimation

The main objective is the prediction of the total haemoglobin with the Partial Least Square Regression (PLSR) model designed using a soft-core system with five wavelength PPG signal. The block diagram of the haemoglobin meter in the FPGA platform is shown in Figure 4.11.

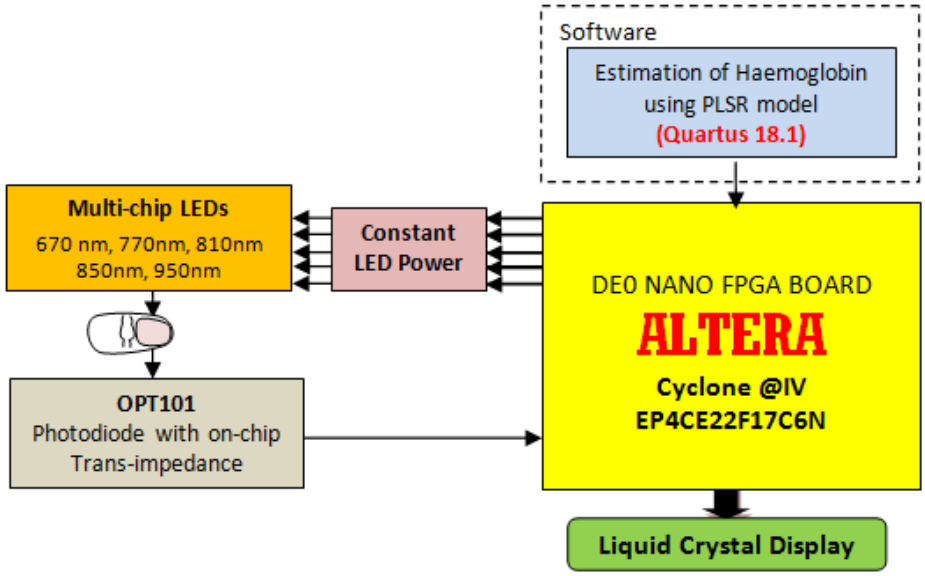

Figure 4.11: Block diagram of the non-invasive haemoglobin meter in the FPGA platform.

The heart of the designed system is the Altera NIOS II soft-core system present in the DE0 Nano FPGA Board. The finger probe consists of a light source (Multichip LED) on one side and a photodetector (OPT101) on the other side. Each individual LED from the Multichip LED was standardized with constant Power of 0.7 mW. The LED sources were controlled using the DE0 Nano FPGA Board. The light emitted from the sources travels through the fingertip and reaches the photodetector. Most of the light is absorbed by the tissues and the venous blood. The flow of blood is pulsatile due to the cardiac cycle and the transmitted light changes with time. The incoming real-time PPG signal is digitized using an in-built 12-bit A/D converter ADC128S022. The PPG signal is then pre-processed to smoothen the variations using the moving average filter. The Quality Assessment of the PPG signal is also done to extract a good quality PPG signal. The absorbance for each wavelength are then calculated from the extracted PPG signal of the subjects. These are then given as inputs to the PLSR model along with the reference

haemoglobin to calibrate the model. The PLSR model is then validated with another set of PPG signals of the subjects (i.e., Absorbances). Also, the estimated hemoglobin is calculated using the molar extinction coefficients of oxy hemoglobin and deoxy hemoglobin along with the optical densities for five different wavelengths. Finally, the total haemoglobin in blood is predicted and displayed on LCD. The entire system designed for haemoglobin estimation is shown in Figure 4.12.

Figure 4.12: The designed haemoglobin measurement system.

In the subsequent chapters, we will discuss the implementation of the Multivariate (PLSR) model and the designing of an Altera NIOS-II soft-core system for the non-invasive estimation of total haemoglobin.

References

1. A. M. Smith, M. C. Mancini, and S. Nie, "Bioimaging: second window for in vivo imaging" Nature nanotechnology, vol. 4, no. 11, pp.710, 2009.
2. D. P Jones, "Medical electro-optics: measurements in the human microcirculation", Physics in Technology, vol. 18, no. 2, pp.79, 1987.
3. R. R. Anderson, J. A. Parrish, "Optical radiation transfer in the human skin and applications in in vivo remittance spectroscopy", Bioengineering and the Skin, pp. 253–265, 1981doi:10.1007/978-94-009-7310-7_28.
4. P.A. Payne, Measurement of properties and function of skin, Clin. Phys. Physiol. Meas., vol. 12, no. 2, pp.105–129, 1991, doi:10.1088/0143-0815/12/2/001.
5. S. Prahl, Optical Absorption of Hemoglobin, https://omlc.org/spectra/hemoglobin/
6. C. Pinto, J. Parab and G. Naik, "Non-invasive hemoglobin measurement using embedded platform", Sensing and Biosensing. 29, 100373, 2020, doi:10.1016/j.sbsr.2020.100370
7. Marktech Optoelectronics Multichip Emitter, [Online] Available at https://www.digikey.in/productdetail/en/marktech-optoelectronics/MTMD6788594SMT6/1125-1253-ND/474638I.
8. OPT101, Monolithic Photodiode and Single Supply, [Online] Available at http://www/ti.com/lits/ ds/symlink/opt101.pdf.

Chapter 5

Multivariate Regression system

5.1 Multivariate Analysis

Multivariate analysis in simple terms can be defined as the simultaneous analysis of multiple variables to understand the relationship that exists between them [1]. It is a statistical process wherein the simultaneous analysis of multiple predictor variables is done with multiple independent variables with the help of matrix algebra. The main goal of multivariate analysis is to reduce a large number of data variables into a smaller number of latent variables by taking into consideration the variability existing in the data set. Thus, in multivariate data analysis, the relationship existing between the variables and the sample in the data set is captured and transformed into a new set of latent variables. The rows in the data set are termed as observations which form the sample and the columns consist of variables that represent each of the measured entities for each object. The variables are divided into X variables called predictors and Y variables called responses. Multivariate methods that are used to find the relationship between predictors and responses are called regression methods [2]. Multivariate techniques can be categorized into two types: quantitative method and classification method. The quantitative method includes multiple linear regression, principal component regression, and partial least squares regression. These techniques are useful in finding the relationship between X and Y variables. The classification method includes principal component analysis, cluster analysis, factor analysis, and discriminant analysis. These techniques are useful in situations where it is required to identify or classify the samples into groups [3]. Different multivariate calibration methods namely classical least-squares (CLS) and Inverse least-squares (ILS), multiple linear regression (MLR), principal component analysis (PCA), Principal component Regression (PCR), and Partial Least Squares Regression (PLSR) can be employed.

5.1.1 Classification methods

Discriminant Analysis

It is a method for classifying variables into groups. It uses one or more independent factors called predictor variables to predict a dependent variable called a grouping variable. Only in cases when the groups are already known before the analysis can this approach be employed [4].

Factor Analysis

It is a technique that is utilized when a large data group has to be reduced into smaller groups based on their shared variance. Factor analysis's principal objective is to explain the data's underlying composition. There are two forms of factor analysis: exploratory factor analysis, which is used to get a preliminary reduction of data, and confirmatory factor analysis, which is used to validate the presence of the components [5].

Cluster Analysis

It is a method for grouping data samples having similar values across several variables. The grouping is done so that if two samples are from the same group, they will have the highest degree of correlation and if they are from different groups, they will have the lowest degree of correlation. Cluster analysis is made up of a wide variety of techniques and approaches for grouping data. It is considered to be a great tool for exploratory data analysis [6].

Logistic Regression

Logistic Regression is one of the extensions of multiple regressions with the exception that the output Y variable is a definite variable and not a continuous one. The reason for this analysis is to classify the subject, into 1 of 2 categories using predictor variables, such that the accuracy is high. Since the output is discrete, the correlation between X and Y is nonlinear, hence the aim is to estimate the possibility, that an individual belongs to either of the groups. A probability of 0 implies that the individual is not in the main group and a probability of 1 implies that the individual is in the main group. The analysis of the logistic regression does not involve ordinary least squares, but uses a composite procedure of maximum likelihood estimation, in weighting X variables [7].

Principal component analysis (PCA

PCA is a statistical approach for characterizing spectral data variance. The causes of these variances are better understood and interpreted using PCA. The original spectra include a collection of correlated variables. PCA uses an orthogonal transformation to convert correlated variables into uncorrelated variables. The first principal components explain the maximum variance possible in the spectral data. The second principal component is chosen such that it is orthogonal to the first principal components, and explains the maximum possible remainder of variation in the data. This process is continued as long as the desired amount of variation is explained by the principal components obtained. PCA is a powerful method for reducing the dimensionality of the spectral data matrix and eliminating noise [8, 9].

$$X = TP + E \quad (5.1)$$

The orthogonal transformation decomposes the spectral data matrix X as shown in Equation 5.1. T is termed as the scores matrix, P is the principal components matrix and E is the noise matrix and contains the noise. The Singular Value Decomposition (SVD) algorithm is utilized to extract the principal components for the X matrix. In building the PCA calibration model, usually, the first k principal components are selected as the number of latent variables or factors. With a properly chosen number of factors, the necessary information for concentration modeling can be included while principal components of interferences and noise can be excluded.

5.1.2 Quantitative methods

Simple Linear Regression (SLR)

Based upon the weight of X, Y is estimated using a regression equation as shown in Equation 5.2, where X is the predictor and Y is the criterion. The slope of the regression line is the predicted Y for every sample. It is also known as weight which is the coefficient of X and for every change in X, Y changes per unit time. The line is formed which implies that the variance is maximized and the error of the sum of squares is minimized. The idea of the ordinary least squares is similar to the sum of squares (X-Mean) as the variation of scores from the mean is less [10].

$$Y_i = \beta_0 + \beta_1 X_i + e_i \quad (5.2)$$

Here, β_0 is the line's intercept and β_1 is its slope and the error e_i is assumed to have a mean value of 0.

Multiple linear regression (MLR)

MLR is a method for modeling the relationship between two or more explanatory variables and a response variable. In MLR, the relationship between Y and X is shown by the following Equation 5.3 [11].

$$Y_i = \beta_0 + \beta_1 X_{1i} + \beta_2 X_{2i} + \beta_3 X_{3i} + \cdots + \beta_p X_{pi} + e_i \quad (5.3)$$

In this way, MLR can be written as an extension of simple linear regression, and Y is considered as directly related to a linear combination of the explanatory variables.

Classical least-squares (CLS)

CLS is also called K-matrix calibration, as it originally involved the application of MLR to the expression of Beer-Lambert Law. The spectral data is modeled as a function of analyte concentration in this method.

$$\mathrm{A} = \mathrm{KC} \quad (5.4)$$

For the known samples, we start with a classical least-squares calibration using the concentration matrix C and the absorbance matrix A. We then solve for K. Each column in K contains the pure component spectra. The least-squares solution is found for Equation 5.4 i.e. it produces K that it produces the least sum of squares of error. We employ the computed K matrix to handle the prediction concentration of unknown samples. It may be calculated using the following Equation 5.5.

$$[\mathrm{K^T K}]^{-1}\mathrm{K^T A_{unkown}} = \mathrm{C_{unkown}} \quad (5.5)$$

We use $[\mathrm{K^T K}]^{-1}$which is known as the pseudo-inverse of K and $\mathrm{K^T}$ which is the transpose of K. CLS has both advantages and disadvantages. The major advantage of utilizing CLS is the estimates of true constituents are determined following the calibration procedure. However, it also requires information on the concentrations of all components present in the sample, which is sometimes impossible to obtain [12]. This may be avoided by employing augmented CLS (ACLS), which relaxes the aforementioned conditions while still allowing for robust modeling with a complex matrix.

Inverse least-squares (ILS)

The inverse expression of Beer-Lambert Law is used in this approach and this method is also called the P-matrix technique. The ILS calibration model assumes that sample concentration can be quantitatively predicted from sample spectra using Equation 5.6.

$$C = PA \tag{5.6}$$

Where concentration matrix is denoted by C and absorbance matrix by A**.** We utilize calibration samples with known concentrations, also known as the training set, to generate an inverse least square calibration [13]. We then use least squares to get the solution for the P matrix. Each wavelength will have a coefficient in each row. According to Equation 5.7, this P matrix is used to predict the concentration of unknown samples.

$$C_{unknown} = PA_{unknown} \tag{5.7}$$

The use of an ILS model eliminates the requirement for a complete understanding of the calibration set's constitution.

Principal Component Regression (PCR)

A statistical process that converts a group of correlated variables into a group of uncorrelated variables using an orthogonal transformation is called PCA. The number of Principal Components is equal to or less than the total number of variables. The transformation is described in the best possible way, so that, the 1st Principal Component has a large variance and every subsequent component has the maximum variance, under the limitation that it is perpendicular to the previous components. The remaining variables are uncorrelated. The principal components are eigenvectors of a symmetric covariance matrix and hence are orthogonal. PCA is susceptible to comparative scaling of unique variables. The independent variables are fed to a PCA and the predictors used in MLR, are scores of units. Factor variation is explained through Xscores. This gives much information in factor space, however may not be involved with the estimated surface [14].

Partial Least Square Regression

PLS is a regression technique used to analyze spectroscopy data. The PLSR technique is used to model a linear relationship between a set of predictors and a set of response variables. This relation is then used in the prediction of the value of a response variable for an unknown sample. The main aim of PLSR is to predict the responses. PLSR works in a way to extract the latent factors ‘T’ and ‘U’ to account for most of the variation in the response variables which are used for modeling the responses. T called X scores are used to predict the U called Y scores and these Y scores are used to construct predictions for the responses. PLS performs multiple linear regression to build a linear model. In PLS, it finds a linear transformation by maximizing the covariance between response variables

and predictor variables [15, 16]. PLSR links the response variable (Y), to the matrix containing predictors (X) through a latent factor, both (Y) and (X) are centered.

The Equation 5.8 represents the PLSR model is given as

$$\mathbf{Y} = \mathbf{XB} + \mathbf{E} \quad (5.8)$$

Where **Y** is **a x b** response matrix, **a** is the number of observations, and **b** is the number of variables.

X is **a x c** predictor matrix with **c** as the number of predictor variables.

B is a **c x b** regression coefficient matrix and **E** is a noise term or residual matrix which has the same dimensions as **Y**.

A **c x d** weight matrix **W** for **X** is produced in PLSR such that

T = XW where the columns of **W** are weight vectors for the **X** columns, thus producing **a x d** factor score matrix **T**.

The weights are computed in such a way that maximum covariance exists between the responses and the corresponding factor scores. The loadings for **Y** represented as **Q** are then generated using ordinary least squares procedures for regression of **Y** on **T** such that

Y = TQ + E

The prediction model is complete once **Q** is computed and **Y = XB + E** where **B = WQ**.

For the complete description of the PLSR procedure, an additional matrix **c x d** factor loading matrix is required which gives factor model

X = TP + F

where **F** represents the residual or the unexplained part of the **X** score.

To estimate the haemoglobin concentration from the absorbance signal, the signal has to be processed using multivariate techniques. The PLSR multivariate technique extracts a given number of factors from the predictor data that takes into account the variance existing in both predictors and responses. The optical densities (Absorbances) for five different wavelengths are the five predictor variables and the reference haemoglobin measured in the pathology laboratory is the response variables. Two datasets one for calibration and one for prediction are prepared. A multivariate technique is used to develop a calibration model for the above calibration dataset. PLSR technique builds a linear relationship between the set of predictors and the set of responses. This is called the calibration model. The concentration of the unknown haemoglobin is predicted by using the above model. In the next section, we discuss the various algorithms for the PLSR model.

5.2. Algorithm to implement PLSR

There are several algorithms proposed to implement PLSR, of which popular one are Non-linear Iterative Partial Least Squares (NIPALS) and Statistical Inspired Modification of PLS (SIMPLS) introduced by Wold et al.[17] and DeJong et al.[18] respectively.

5.2.1 NIPALS

The first step begins with centering and scaling matrix X and **Y** and proceeds as follows. This algorithm has found its application in chemometric and below are the steps involved to implement as given in S. Wold et. al. [19].

Step 1: A starting vector (**u)** is chosen **u** which is usually a column of **Y**. If **Y** has a single column then, **u** = **y**.

Step 2: The weights (**w)** of **X** are calculated as **w** = **X'u**/**u'u** (here **w** can be modified as $\|\boldsymbol{w}\| = 1.0$)

Step 3: The scores (**t)**, of **X,** are calculated as **t** = **Xw**

Step 4: The weights (**c)**, of Y, are calculated as **c = Y't/t't**

Step 5:Get the updated set of scores of **Y as u** = **Yc**/ **c'c**.

Step 6: The convergence test is carried to check the change in **t** by $\|t_{old} - t_{new}\| / \|t_{new}\| < \varepsilon$, here the value of ε is "small" for example 10^{-6} or 10^{-8}. If not converged, go back to step 2, otherwise continue to step 7. The process converges with one iteration if **Y** is a single variable matrix and goes on to step 7.

Step 7: The component calculated is removed from **X** and **Y** and these deflated matrices will be used to generate the next component.

p = X't/ t't X = X - tp'

Y = Y - tc'

Step 8: If the number of desired components are not found go back to step 1 to find the next components.

5.2.2 SIMPLS

In SIMPLS algorithm, we us assume the matrices X and Y are mean-centered. SIMPLS involves deflation of the X^TY covariance matrix. Below are the steps followed to implement the SIMPLS algorithm [20].

For each h =1,…, N, where N is the number of components to be found.

Step 1: Mean center the explanatory and response variable matrices, and represents them as **X** and **Y** after mean centering. Calculate the covariance matrix $\mathbf{S_h = X^T Y}$.

Step 2: The left singular vector of the matrix $\mathbf{S_h}$ is taken as $\mathbf{w_h}$.

Step 3: Normalize $\mathbf{w_h}$ using the expression $w_h = \mathbf{w_h} / \|\mathbf{w_h}\|$.

Step 4: $\mathbf{t_h}$ the h^{th}component vector is calculated as $\mathbf{t_h = Xw_h}$(when h=1, $\mathbf{t_1}$ is the first component vector)

Step 5: Normalize $\mathbf{t_h}$ as $t_h = \mathbf{t_h} / \|\mathbf{t_h}\|$.

Step 6: $\mathbf{p_h}$ the h^{th} loading vector of X is calculated as $\mathbf{p_h = X^T t_h}$(when h=1, $\mathbf{p_1}$ is the first loading vector of **X)**.

Step 7: $\mathbf{q_h}$ the h^{th} loading vector of **Y** is calculated as $\mathbf{q_h = Y^T t_h}$. (when h=1, $\mathbf{q_1}$ is the first loading vector of **Y)**.

Step 8: Deflated covariance matrix $\mathbf{S_{h+1}}$ is calculated $\mathbf{S_{h+1} = S_h - v_h(v_h^T S_h)}$, where $\mathbf{v_h = p_h}$(for h = 1)and $\mathbf{v_h = p_h - V_{h-1}(V_{h-1}^T p_h)}$ for a > 1 with $\mathbf{V_{h-1} = (v_1, v_2, \dots, v_{h-1})}$.

Steps 2 to 8 are repeated till N components are extracted.

The SIMPLS algorithm is fast as compared to NIPLAS algorithm [21]. SIMPLS does not employ a breakdown of the data sets and as such is found to be fast and easy to interpret. We have used SIMPLS in our research work due to the advantages offered by it as outlined above. A C++ code is ported to the NIOS II platform to implement the SIMPLS.

5.3 ParLeS software for preliminary analysis

ParLeS is a shareware that is developed by Raphael A. Viscarra Rossel in LabVIEW, for research and teaching in spectroscopy and chemometrics with simple Graphical User Interface (GUI) to perform many multivariate algorithms. ParLeS is used to pretreat, pre-process and transform spectra using different algorithms. It is also used to implement PLSR with cross-validation, PCA and bagging-PLSR (bootstrap aggregation-PLSR) [22]. In addition, the unique features comprise user-friendly functionality as well as the provision of several graphical output and assessment statistics. Figure 5.1 shows the ParLeS software structure.

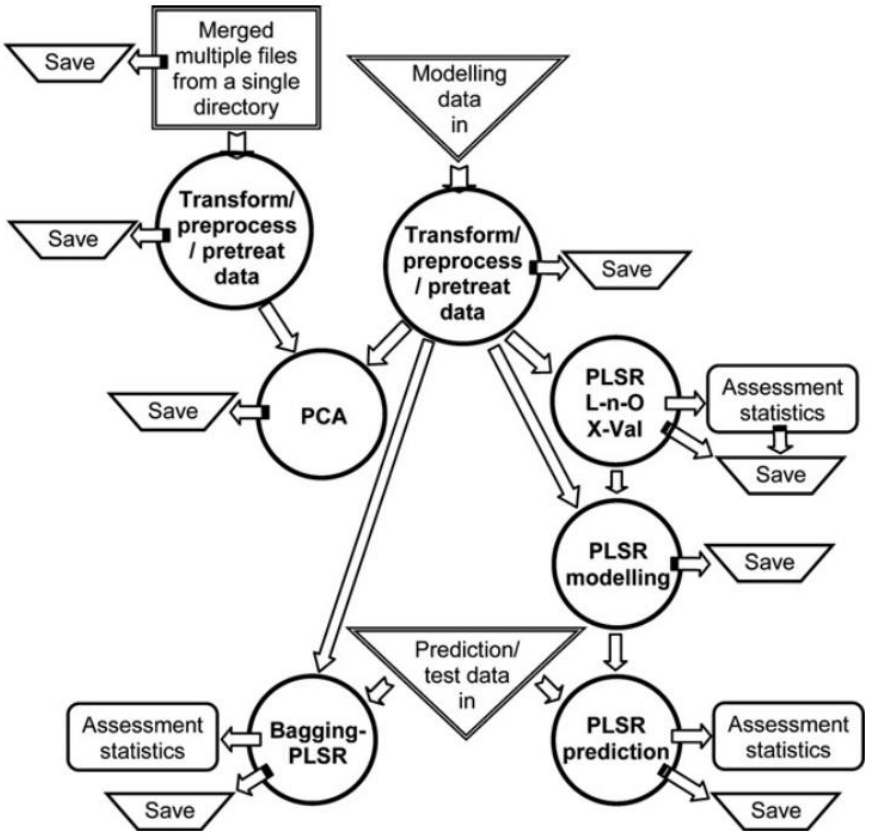

Figure 5.1: ParLes software structure [22].

5.4 Multivariate calibration model for non-invasive haemoglobin estimation

The "Import data modeling" tab is used to import the data (tab-delimited ASCII format) into the ParLeS software as shown in Figure 5.2. The path of the file must be specified in the space provided under "Get file for modeling". Next, the number of y variables present in the tab-delimited ASCII file is selected for modeling. Then the data is imported into the ParLeS software by clicking the "Import data for Modeling button".

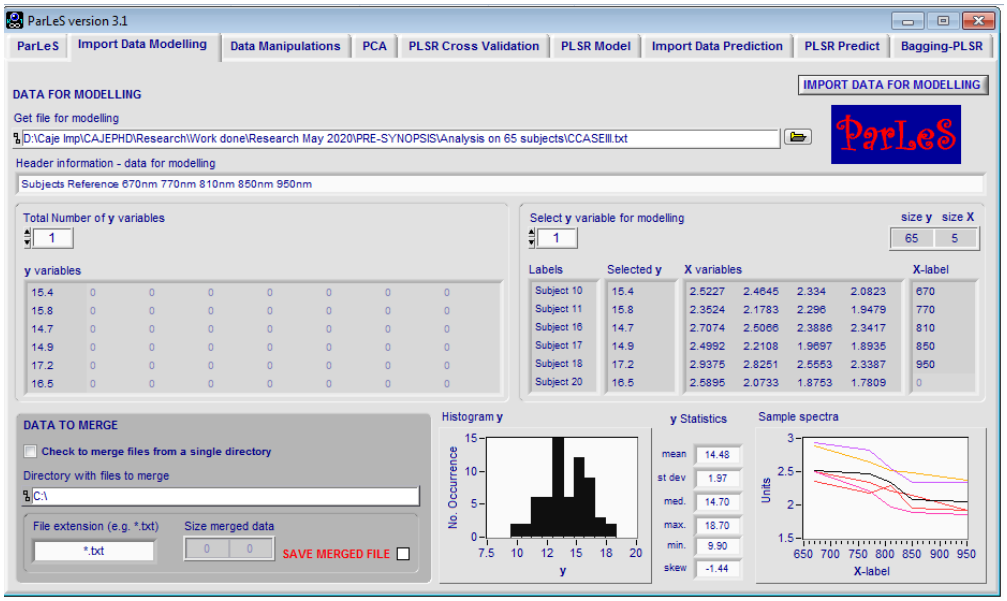

Figure 5.2: Importing of data for modeling into ParLes.

The ParLes programme (version 3.1) provides several preprocessing and transformation techniques, which may be found under the data manipulation tab. As seen in Figure 5.3, pretreatment of data such as mean centering and variance scaling is supported. Of the above options offered, we have only mean-centered out data. In order to do the Pre-Processing of data the "Run Selection" button is selected.

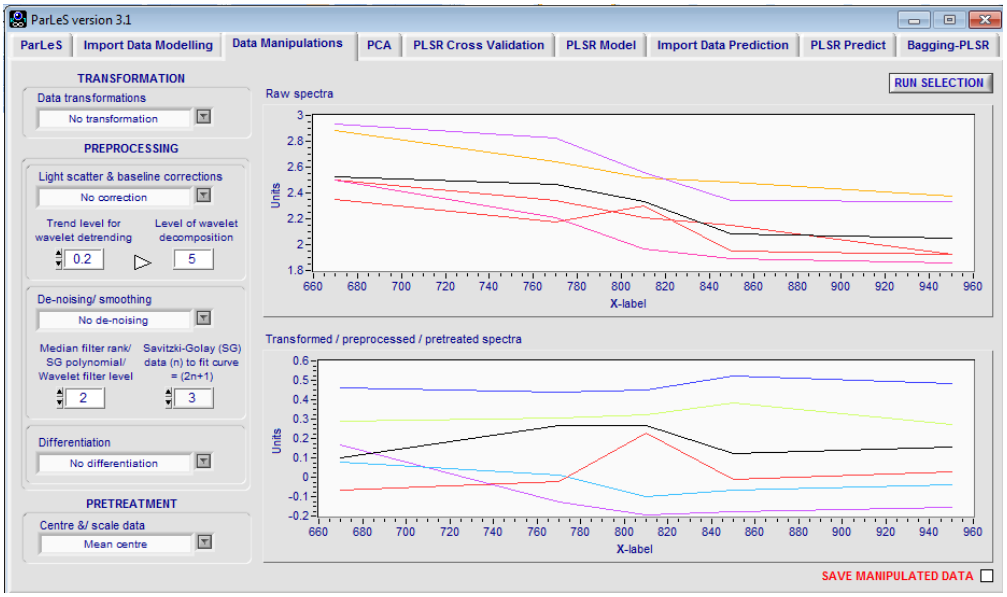

Figure 5.3: Preprocessing the datasets for calibration.

Different modeling techniques are supported by the software such as PCA, PLSR, PLSR cross-validation. Under the “PLSR Model” tab the parameters needed to build a PLSR model are specified as shown in figure 5.4. The number of factors required can be selected using the slide bar below “Select No. of factors for PLSR. The model is built using the "Run PLSR modeling" button. Once the model is created, the percentage of variation is explained by each variable in the Explained variance visualization.

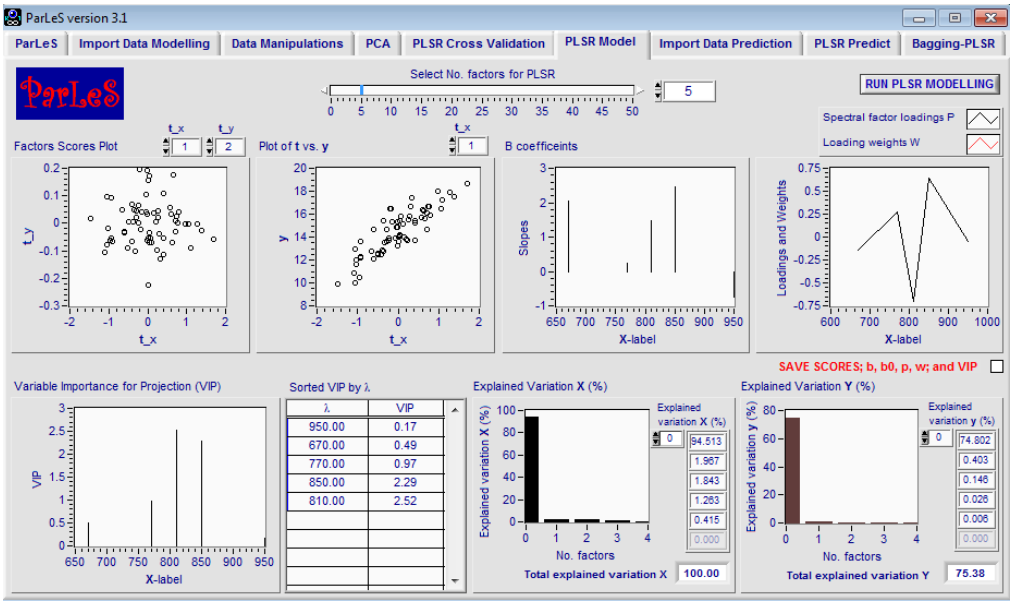

Figure 5.4: Partial Least Square Regression modeling.

The “Import Data Prediction” tab is utilized to import the data from unknown samples for prediction in tab-delimited ASCII format under "Get file for prediction" as shown in Figure 5.5 The number of y variables included in the data to be imported must be specified, and then the “Import data for prediction” button must be pressed.

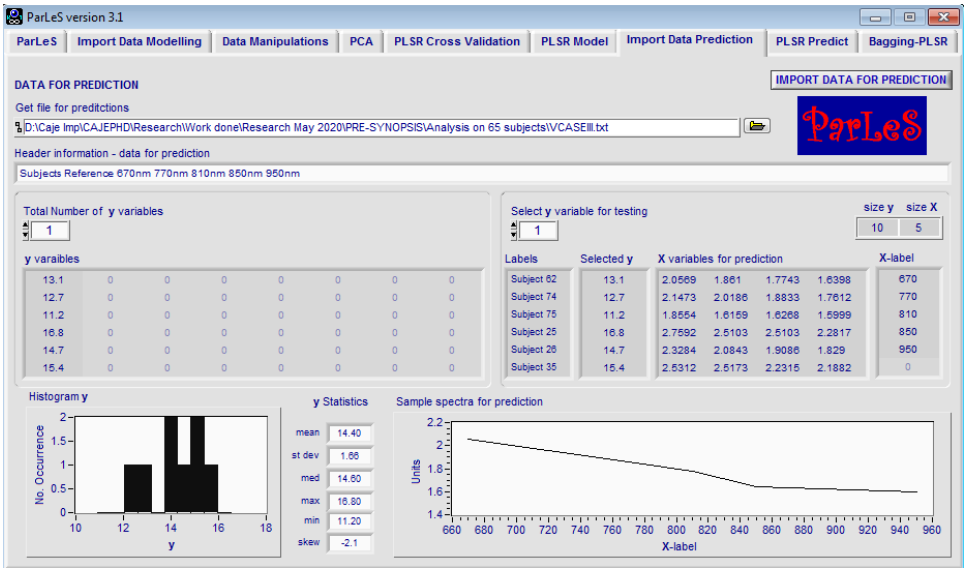

Figure 5.5: Importing of data for prediction.

Next, the “PLSR Predict” tab is used for prediction once the data has been loaded, as illustrated in Figure 5.6. The prediction is made by pressing the “Run prediction” button.

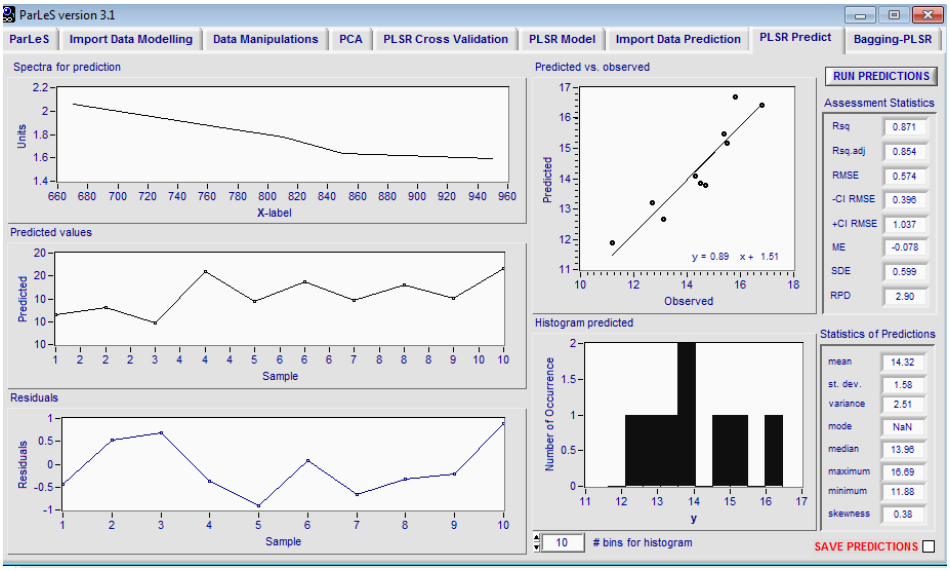

Figure 5.6: Partial Least Square Regression prediction.

Once the multivariate model was tested in ParLes Software, the PLSR algorithm was written in C++ program and ported in Altera NIOS II soft-core system to estimate non-invasive total haemoglobin which is discussed in the next chapter.

References

1. A. S. Moucheshi , E. Fasihfar, H. Hasheminasab, A. Rahmani, A. Ahmadi, "A Review on Applied Multivariate Statistical Techniques in Agriculture and Plant Science", International journal of Agronomy and Plant Production, vol.4, no. 1, pp. 127-141, 2013.
2. S. Maitra, J. Yan, "Principal Component Analysis and Partial Least squares: two Dimension reduction Technique for Regression", Casualty Actuarial Society Discussion Program, 2008.
3. M. J. Vander Werf, J. Renger, "Multivariate Data Analysis: Converting data into information", TNO,pp.1-7, 2007.
4. Discriminant Analysis, [Online] Available at https://en.wikipedia.org/wiki/Linear_discriminant_analysis
5. Factor Analysis, [Online] Available at https://en.wikipedia.org/wiki/Factor_analysis
6. Cluster Analysis, [Online] Available at https://en.wikipedia.org/wiki/Cluster_analysis
7. Logistic Regression, [Online] Available at https://en.wikipedia.org/wiki/Logistic_regression
8. S. Wold, K. Esbensen, P. Geladi, "Principal Component Analysis", Chemometrics and Intelligent Laboratory Systems, vol. 2, pp. 37-52, 1987.
9. P. Nomikos, J.F. MacGregor, "Monitoring Batch Processes Using Multiway Principal Component Analysis", AlChE Journal, vol. 40, pp.1361-1375, 1994, doi: 10.1002/aic.690400809
10. Simple Linear Regression, [Online] Available at https://en.wikipedia.org/wiki/Simple_linear_regression
11. Multiple Linear Regression, [Online] Available at http://www.stat.yale.edu/Courses/1997-98/101/linmult.htm
12. R. Kramer, "Chemometric Techniques for Quantitative Analysis", CRC Press, 1998.
13. R. G. Krutchkoff, "Classical and Inverse Regression Methods of Calibration", Technometrics, vol. 9, pp. 425-439, 1967
14. Principal Component Regression, [Online] Available at https://ncss-wpengine.netdna-ssl.com/wp-content/themes/ncss/pdf/Procedures/NCSS/Principal_Components_Regression.pdf

15. P. Geladi, and B. Kowalski, "Partial least squares regression: A tutorial", Analytica Chimica Acta, vol. 185, pp. 1-17, 1986.
16. M. J. Adams, “Chemometrics in Analytical Spectroscopy”, Royal Society of Chemistry, 2004.
17. H. Wold, “Estimation of principal components and related models by iterative least squares” in Multivariate Analysis, P. R. Krishnajah (Ed.), Academic Press, 1966, pp. 391–420, 1966.
18. S. DeJong, “SIMPLS, an alternative approach tp partial least squares regression”, Chemometrics and Intelligent Laboratory Systems, vol. 18, pp. 251–263, 1993.
19. S. Wold, M. Sjostrom, L. Eriksson, “PLS-regression: a basic tool of chemometrics”, Chemometrics and Intelligent Laboratory Systems, vol. 58, no. 2, pp.109-130, 2001.
20. Alin, C. Agostinelli, “Robust iteratively reweighted SIMPLS”, J. of Chemometrics, vol. 31, no. 3, pp. e2281,2017.
21. M. Andersson, “A comparison of nine PLS1 algorithms,” J. Chemometrics, vol. 23, no.10, pp. 518-529, 2009
22. R. A. V. Rossel, “ParLeS: Software for chemometric analysis of spectroscopic data”, Chemometrics and Intelligent Laboratory Systems, Vol. 90, no.1, pp. 72-83, 2008

Chapter 6:
Design of Soft-Core System for Haemoglobin Estimation

The Field Programmable Gate Array (FPGA) is a highly configurable logic device. The logic density is much higher than those offered by its predecessors such as Complex Programmable Logic Device (CPLD). Due to the versatility offered by FPGA, researchers and hardware designers are adopting it in their product designs. This Chapter discusses the different soft-core processors and outlines the various steps required to configure a soft-core processor on an FPGA for the purpose of haemoglobin estimation.

6.1 Field Programmable Gate Array for haemoglobin estimation

The term 'FPGA' originates from the fact that a user can deploy a gate array that is programmable on the field at any workplace [1]. FPGA consists of configurable logic blocks (CLBs) with user-programmable interconnect that enables customization, by developers,so as to realize their desired applications. This customization can be reprogrammed, if the need arises, for the accommodation of new features in the developed application. Depending on the manufacturer, the CLB may also be referred to as a logic block (LB), a logic element (LE), or a logic cell (LC). FPGAs are programmable and reconfigurable logic devices that may be utilized to create complex and large circuit designs. FPGA has three types of resources viz., input/output blocks, logic blocks and programmable interconnection. The majority of FPGAs have flip-flops and look-up tables (LUT) [2].The various families of FPGAs supplied by different manufacturers differ primarily in the number of logic modules (ranging from a few hundred to hundreds of thousand), supply voltage range, power consumption, speed, architecture, process technology, number of pins, type of packages, etc.

6.2 Soft-Core processors for embedded systems

An embedded system consists of hardware and software components working together to perform a specific application. Nowadays, embedded systems play a vital role in everyday lives. They are used in automobiles, the medical field, industrial control systems, and entertainment electronics, etc [3]. The hardware platform of the embedded system consists of a microcontroller, on-chip memory, an output device, and an input device. In the current scenario, with manufacturers pushing for increased miniaturization, the embedded system designers have to adhere to the tight constraints on area usage, size, high-performance, good power efficiency, flexibility, adaptability, reduction in product design and time-to-market deadlines [4]. Therefore, the hardware/software co-design methodology is often used in designing an embedded system to reduce the time spent on development and debugging [5]. With the increase in complexity of embedded system design, the development of every hardware component of the system from scratch has become too time-consuming and expensive for most of the designers. Therefore, the prospect of using pre-designed and pre-tested intellectual property (IP) cores in designs became an attractive alternative solution. Soft-core processors are microprocessors whose architecture and behaviour are completely specified using hardware descriptive language (HDL) and is implemented in Verilog or VHDL language. Many parallel processors can be implemented on one FPGA and can use additional FPGA resources on the same chip without being part of the processor core. The use of soft-core processors offers many advantages to the designer of an embedded system. These include a higher level of design re-use, increased design implementation options, simplified design update, lower latency between processor and FPGA components. A soft-core processor permits a designer to conveniently add or remove peripherals from the System on Peripheral Chip (SoPC). It also enables the designer to build a system to meet his/her requirements, avoiding excessive cost and reducing the time spent configuring unnecessary features. The parameters of a soft-core processor built on FPGA may be modified and reconfigured at any time merely by reprogramming the device thereby making it highly flexible. Also, it can be synthesized for any given target ASIC or FPGA technology. This grants it immunity from obsolence as compared to circuit or logic level descriptions of a processor [6]. A variety of programmes that operate on soft-core processor-based platforms have been identified. As a result, these soft-cores are increasingly becoming popular due to their reconfigurability.

6.3 A survey of soft-core processors

In this Section, we discuss the various soft-core processors which are available in the market from, both, commercial vendors and open source communities.

6.3.1 Commercial cores

NIOS II and MicroBlaze are the leading soft-core processor provided by Altera and Xilinx, respectively. Also, Cortex – M1 is the first ARM implemented for FPGA.

NIOS II

Altera Corporation, the manufacturer of NIOS II, is one of the leading vendors of CPLDs and FPGAs. NIOS II is widely used in the design of embedded systems and DSP applications. NIOS II soft-core processor is Altera's flagship IP (Intellectual Property) core processor. NIOS II is a 32-bit processor based on the popular Reduced Instruction Set Computer (RISC) processor core and uses the Harvard memory architecture. There are thirty-two 32-bit general-purpose registers in NIOS II soft-core. NIOS II processor comes in three different variants: economy, standard and fast core. Each core variant has a different number of pipeline stages, instructions, data cache memories and hardware components for different operations. Besides, each core varies in performance and size depending on the features that are selected. NIOS II/f has a six-stage pipeline and executes one instruction per cycle. It has separate Instruction and Data cache. The NIOS II also has a performance of more than 150 Dhrystone MIPS (DMIPS). The addition of the peripherals with the NIOS II processors is accomplished through the Avalon Interface Bus which contains the necessary logic for interfacing the processor with off-the-shelf IP cores or custom-made peripherals. It is feasible to build, debug andcreate an embedded system on Altera's FPGAs utilizing the associated CAD tools such as Quartus II and platform designer development tool. These tools help in building a NIOS II based system and in writing system-specific application software. The main disadvantage with NIOS II is that it can only be used in Altera FPGAs. It provides a solution to the interoperability and resource wastage by various microcontrollers and is configured by the customer or designer, as per his requirements [7]. Figure 6.1 shows the block diagram of the NIOS II soft-core system.

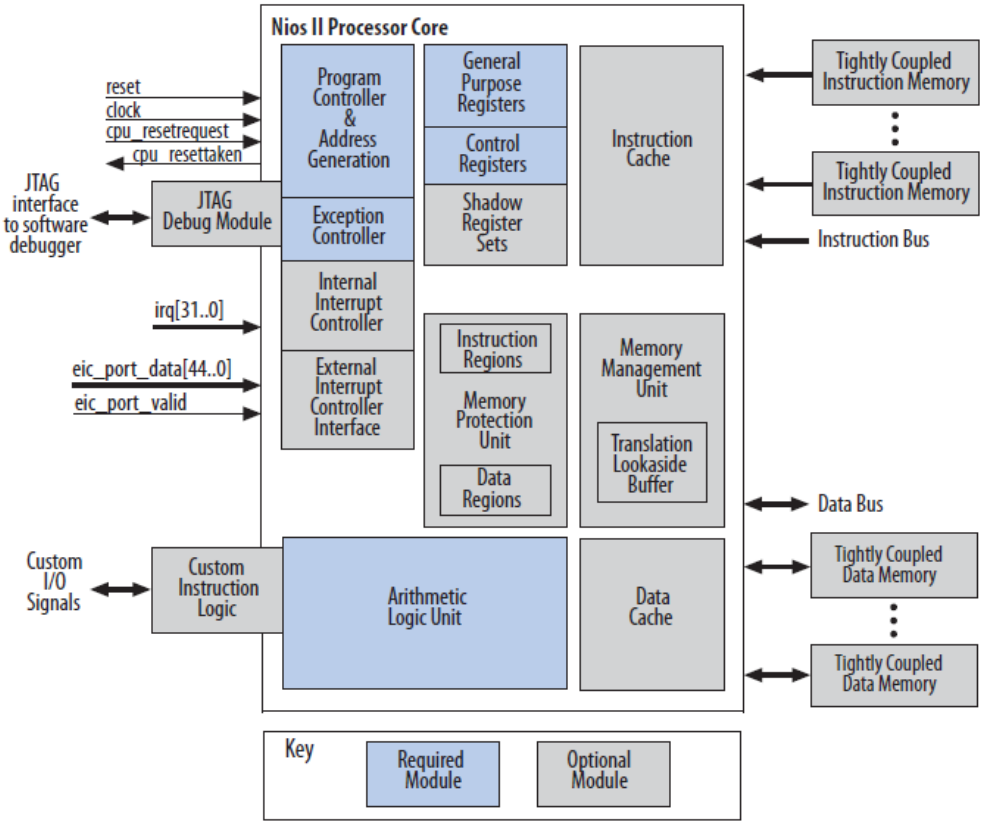

Figure 6.1: Block diagram of the NIOS II soft-core system [7].

MicroBlaze

Xilinx offers Spartan and Virtex families which are FPGA solutions. They also provide soft IP cores that target their FPGAs. MicroBlaze is a 32- bit soft-core processor that is optimized for embedded applications. It is based on Harvard architecture and can operate at up to 200MHz on a Vertex-4 FPGA chip. This processor has a three-stage pipeline with 32-bit instructions and a 32 register wide register file. The memory can reside on-chip or as an external peripheral. A general-purpose interface known as the On-chip Peripheral Bus (OPB) can be used to interface MicroBlaze with both on-chip and off-chip memories as well as other peripherals. In addition, it features a three-stage pipelining, 32-bit instructions, 32-bit general-purpose registers, two levels of interrupts, and a shift unit. Xilinx Platform Studio is available for creating a MicroBlaze-based system [8]. Figure 6.2 shows the block diagram of the Xilinx MicroBlaze core.

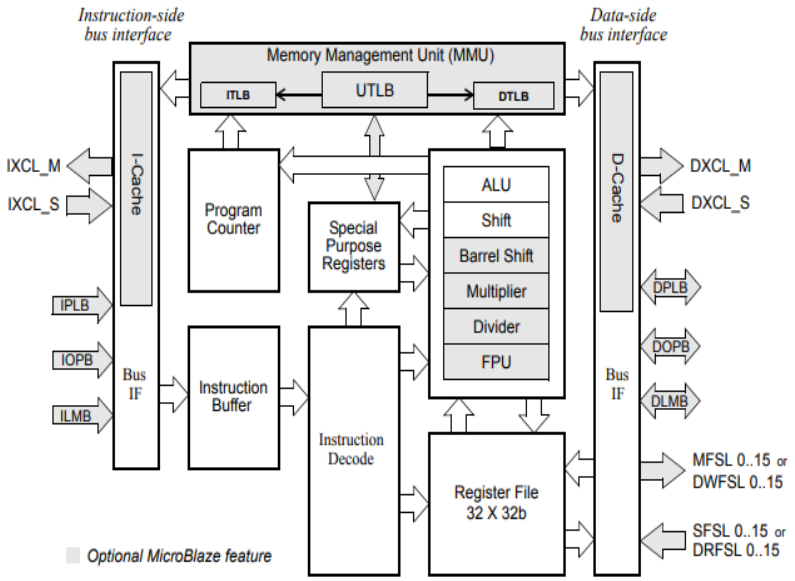

Figure 6.2: Block diagram of the MicroBlaze soft-core system [8].

Cortex – M1

The ARM Cortex™-M1 processor is the first ARM 32-bit processor designed specifically for implementation in FPGAs. The Cortex-M1 processor targets all major FPGA devices and includes support for leading FPGA synthesis tools, allowing the designer to choose the optimal implementation for each project. The main features of Cortex-M1 include a three-stage pipeline, configurable instruction and data memories (upto 1 MB), an integrated interrupt controller with support for upto 32 interrupts and has AMBA AHB-Lite 32-bit bus interface. The Cortex-M1 processor can deliver 0.8 DMIPS. It can be used with any FPGA [9]. Figure 6.3 shows the block diagram of the Cortex – M1 soft-core system.

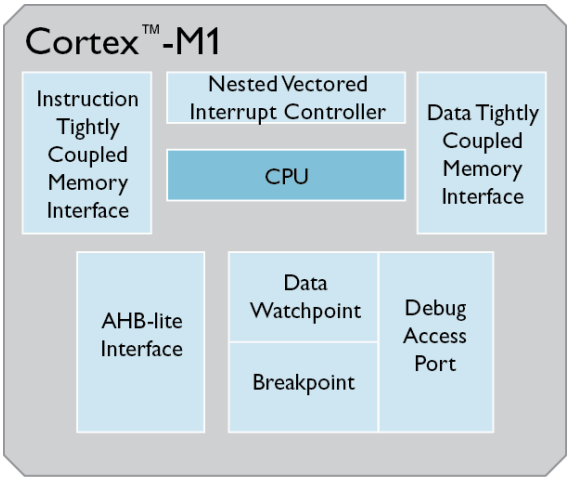

Figure 6.3: Block diagram of the Cortex – M1 soft-core system [9].

6.3.2 Open-source cores

Open-source cores are IP components that are freely available in the open-source community. Usually, these types of cores are used in academia for research as well as in the development of embedded systems. In this Section, we discuss OpenSPARC T1, LEON3, OpenRISC 1200, and LatticeMico32 soft-core processors that are available in the open-source community.

OpenSPARC T1

OpenSPARC T1 is an open-source version of the Sun Microprocessor products. It is a multi-core, 64-bit multiprocessor SPARC V9 architecture and is targeted towards commercial applications such as application and database servers. It consists of eight SPARC processor cores, with four hardware threads per core. One floating-point unit external to the core is shared by all the cores and four banks of the L2 cache. Each SPARC core has a 16 KB instruction cache, 8 KB data cache, and a fully associative instruction and data translation look-aside buffer (TLB). All the cores are connected through a 132 GB/s crossbar interconnect for on-chip communication. An on-chip J-Bus controller provides the requisite interconnect between the OpenSPARC T1 processor and I/O subsystem. [10]. Figure 6.4 shows the block diagram of the OpenSPARC T1 soft-core system.

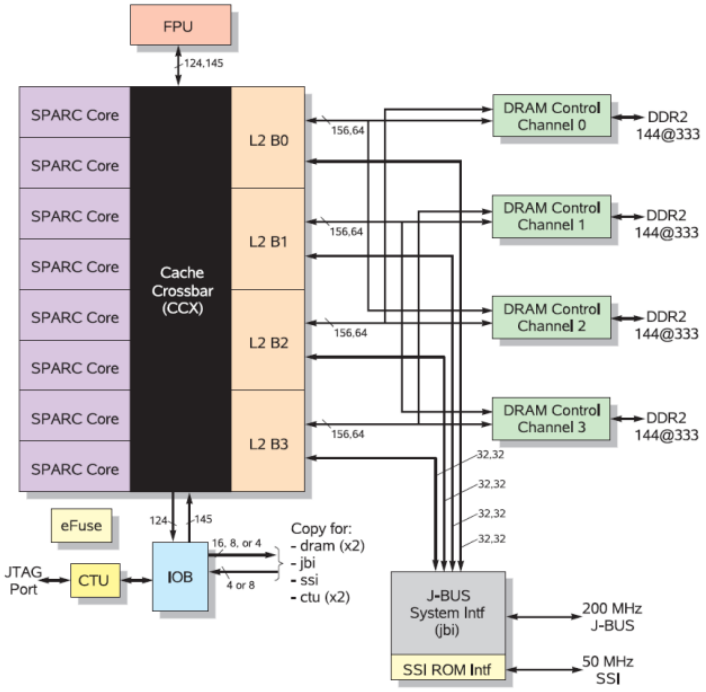

Figure 6.4: Block diagram of the OpenSPARC T1 soft-core system [10].

OpenRISC1200

OpenRISC 1200(OR1200) is one of the popular open core processors available at OpenCores.org. The OR1200 is a 32-bit scalar RISC with Harvard architecture. The main features of OR1200 include a five-stage integer pipeline, virtual memory support (MMU) and basic DSP capabilities. It has 32-bit instructions and can operate on 32-bit or 64-bit data. The Default data and instruction cache are one-way direct-mapped 8KB with 16-byte line size each. OpenRISC 1200is one of the high-performing soft-core processors with 300 Dhrystone 2.1 MIPS at 300 MHz. It supports very few FPGA development boards and its debugging solutions are complicated [11]. Figure 6.5 shows the block diagram of OpenRISC1200.

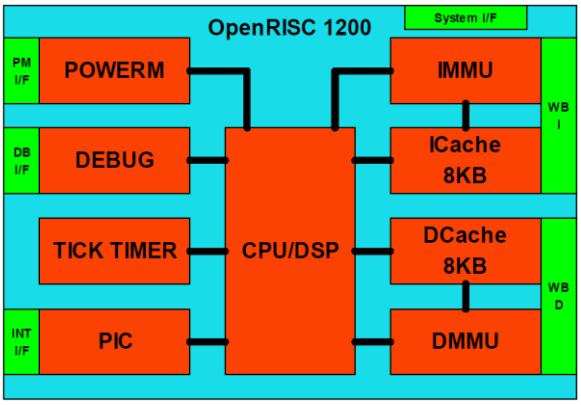

Figure 6.5: Block diagram of the OpenRISC1200 soft-core system [11].

LEON3

The LEON3 is a 32-bit processor based on the SPARC V8 architecture and is designed and maintained by Aeroflex Gaisler. The model is highly configurable for system-on-a-chip (SOC) designs. The structure of the LEON3 processor is shown in Figure6.6. It is based on Harvard architecture and uses the AMBA Advanced High-performance Bus (AHB) for all on-chip communications. Its main features include a seven-stage pipeline, separate instruction caches and data caches, a configurable number of register windows and an optional floating-point unit. The main advantage of the LEON3 processor is that it uses a structured organization of packets, folders and VHDL records. The complete source code for this processor is available for free and can be used unlimitedly for research and education activities, under the GNU GPL license. Linux and RTOS can be installed on this processor but not all FPGA development boards are supported by LEON3 [12]. Figure 6.6 shows the block diagram of the LEON 3 soft-core system.

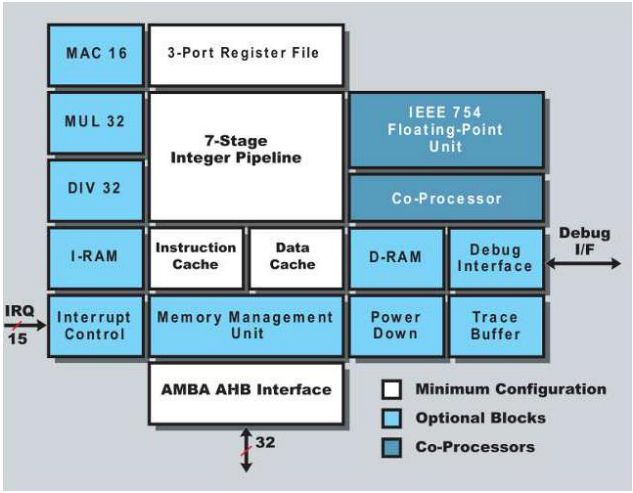

Figure 6.6: Block diagram of the LEON 3 soft-core system [12].

LatticeMico32

The LatticeMico32 is an open-source 32-bitRISC soft-core processor based on Harvard architecture from Lattice Semiconductor. LatticeMico32 provides good performance and flexibility by combining 32-bit wide instruction set with 32 general-purpose registers. Its main features include a six-stage pipeline, 32-bit instruction and data caches with capacity to handle up to 32 external interrupts. The core consumes minimal device resources while maintaining the performance required for a broad application set. It does not have a floating-point unit. To accelerate the development of microprocessor systems, several optional Wishbone-compatible peripheral components may be integrated with the LatticeMico32 [13]. Figure 6.7 shows the block diagram of the LatticeMico32 soft-core system.

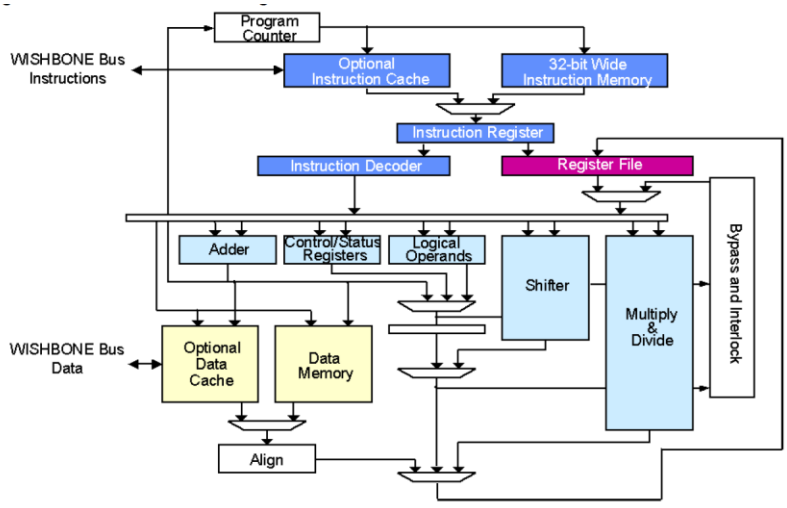

Figure 6.7: Block diagram of LatticeMico32 soft-core system [13].

6.3.3 Comparison of soft-core processors

Each processor presents a set of parameters and characteristics that throw up important challenges. The soft-core's features will also significantly influence the performance of the whole system. Table 6.1 shows a comparison of the main characteristics of available open-source and commercial soft-core processors that have been briefly described in the earlier Section. Each surveyed core has different performance characteristics and features that are suitable for specific applications. Embedded system designers should choose a processor core based on the requirements and performance constraints of their particular application. The NIOS II features an expandable instruction set with up to 256 customizable instructions whereas MicroBlaze is not provided with this kind of ability. The highest operating frequency on an FPGA can be achieved with the NIOS II and MicroBlaze. Both, the NIOS II and MicroBlaze are optimized for FPGA implementations, whereas the others are not optimized for a particular technology.

Table 6.1: Comparison of different soft-core processors.

Soft-core processor, Developing Organization	Custom Instructions	ISA	Interface Bus standard	Maximum Clock Frequency (MHz)	Pipeline Stages
Nios II (Altera)	Upto 256	32-bit RISC	Avalon	200	6-stages
MicroBlaze (Xilinx)	None	32-bit RISC	AXI, DPB, LMB	200	3-stages
Cortex M1 (ARM)	-	32-bit RISC	AMBA AHB Lite	--	3-stages
OpenSPARC T1 (Sun Microsystems)	-	32-bit RISC	JBI, SSI	200	6-stages
Open RISC 1200 (Open Cores)	Unspecified limit	32-bit RISC	Wishbone	300	5-stages
LEON3 (AeroflexGaisler)	None	32 RISC	AMBA2.0	400	7-stages
Lattice Mico 32 (Lattice Semiconductor)	-	32-bit RISC	Wishbone	85–115	6-stages

To select the best embedded platform for novel architecture, in this study, we have designed a soft-core system and implemented an algorithm on Altera NIOS II platforms to estimate non-invasive total haemoglobin.

6.4 DE0 Nano FPGA Board (selecting a hardware platform)

The DE0-Nano board provides a compact-sized FPGA development platform well-suited to prototype circuit designs for portable projects. The board is designed to be used in the simplest possible implementation, targeting the Cyclone IV family devices which contain up to 22,320 logical elements (LEs). The DE0-Nano has a set of interfaces including two external 40-pin GPIO headers and one 26-pin header to extend designs beyond the DE0-Nano board, on-board memory devices including SDRAM and EEPROM for larger data storage and frame buffering along with general user peripherals like A/D converter with LEDs, DIP switches and push-buttons. If a design needs to have mobility, portable power is a necessity; therefore, DE0 Nano board offers a two-pin external power header for battery connection [14]. The advantage of the DE0 Nano board is its size and weight, as well as its ability to be reconfigured. All the connections made through the FPGA device provide users with maximum flexibility. Thus, FPGA can be configured to implement any system design. Keeping in mind the above advantages, in the present study, we have used DE0 Nano FPGA board for the creation of the NIOS II soft-core system. The Top view and bottom view of the DE0-Nano board are shown in Figure 6.8.

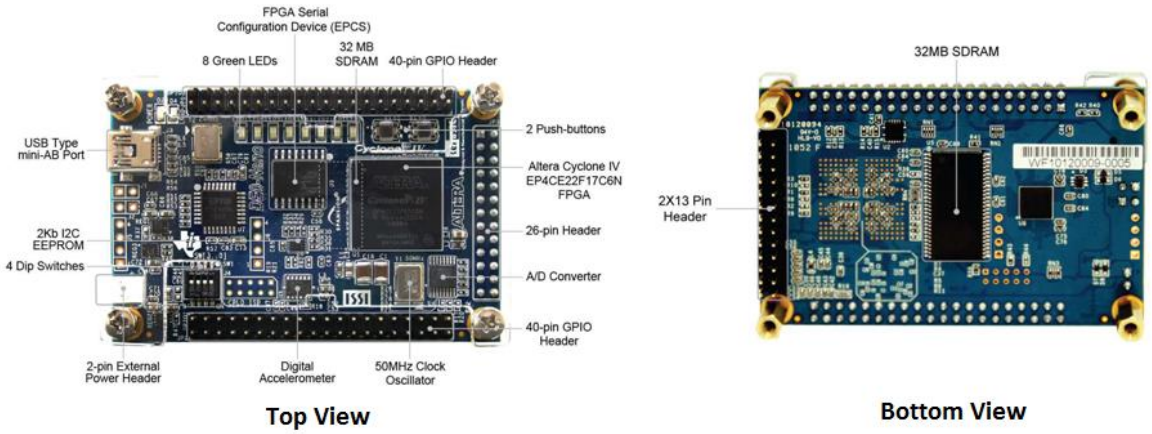

Figure 6.8: DE0 - Nano board [14].

The block diagram of DE0-Nano board is shown in Figure 6.9. The Avalon switch fabric network provides the interconnection to all the components. Appropriate interfaces and IP cores are used to access various peripherals and memories such as SDRAM, I2C EEPROM, ADC, DIP switches, etc. present on the board.

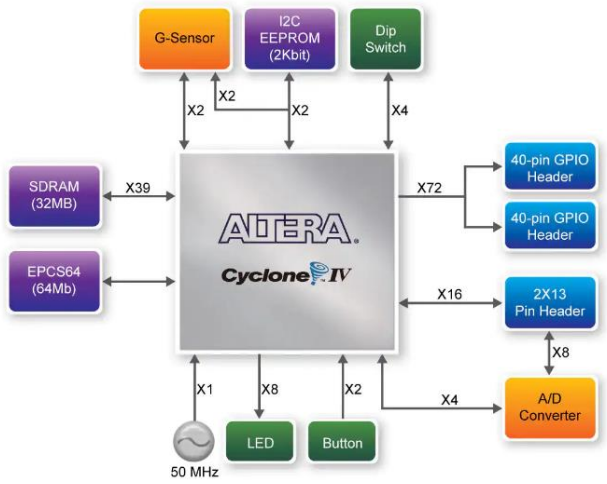

Figure 6.9: Block diagram of DE0- Nano [14].

6.5 System-on-a-Programmable-Chip for haemoglobin analysis

Platform Designer in Quartus 18.1 is a powerful system development tool. It enables one to define and generate a complete System-on-a-Programmable-Chip (SOPC) in minimal time as compared to traditional manual integration methods. To wire up the parts of the soft-core system using traditional design methods, one needs to manually write the HDL modules. Platform Designer is used to create soft-core system based on the NIOS II processor by integration of the hardware components. Using the Platform Designer, the system components are selected in a GUI and it generates the interconnect logic automatically by creating HDL files that define all system components. The custom logic can be integrated inside or outside of the Platform Designer system. In this example, the custom component within the Platform Designer system communicates with other modules through an Avalon-MM master interface. The custom logic outside the SOPC Builder system is connected to the SOPC Builder system through a PIO interface. The system interconnect fabric connects all of the SOPC Builder components using the Avalon-MM or Avalon-ST system interconnect as appropriate [15].

6.5.1 SDRAM Interface to FPGA

The DE0-Nano features a 32-MB Synchronous Dynamic Random Access Memory (SDRAM) device that uses 16-bit data lines to communicate with the FPGA. The chip uses the 3.3V LVCMOS signalling standard. The positive edge of the clock signal, DRAM CLK, is used to register all of the signals. Figure 6.10 shows the connections between the FPGA and SDRAM [16].

Figure 6.10: Connections between SDRAM and FPGA [16].

This SDRAM has a memory organisation of 4M x 16 bits x 4 banks. The SDRAM requires precise timing control. The SDRAM controller circuit IP must be included in the Platform Designer in order to access the SDRAM successfully. A connectivity network known as the Avalon switch fabric connects the NIOS II soft-core to the memory and input/output interfaces. As shown in Figure 6.11, the SDRAM controller generates all essential interface signals except the clock. The clock must be supplied separately and must meet the clock skew requirements. To ensure this, the clock signal sent to the NIOS II processor must lag the SDRAM clock by 3 ns[17]. This requirement is accomplished by a phase-locked loop circuit.

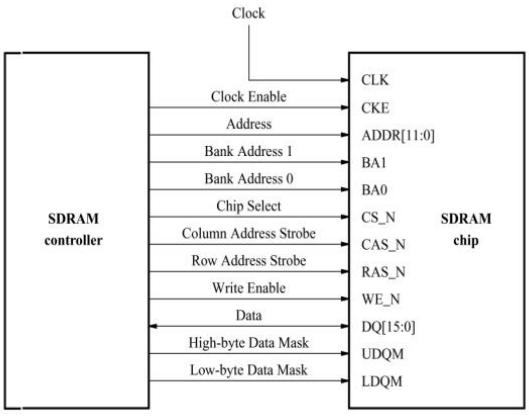

Figure 6.11: SDRAM controller interface [17].

6.5.2 ADC Interface to FPGA

The DE0-Nano has an ADC128S022 lower-power, eight-channel CMOS 12-bit analog-to-digital converter. This converter has conversion rates ranging from 50 to 200 ksps. The ADC receives an analog signal via the eight analog inputs pins IN0 through IN7. When performing a conversion, the ADC reads the signal on the channel selected and converts it into a digital signal. Figure 6.12 shows the interface between ADC128S022 with 2x13 Header [18].

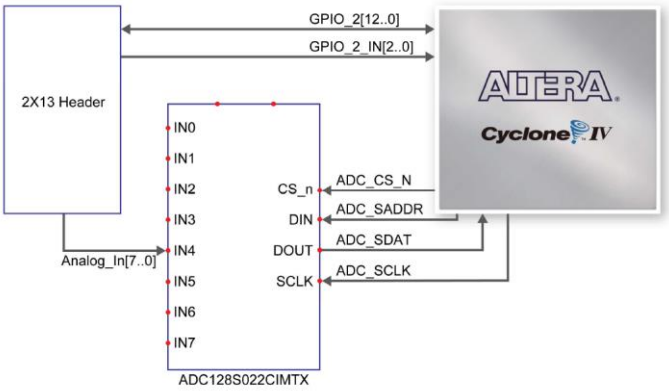

Figure 6.12: ADC128S022 with 2x13 Header [18].

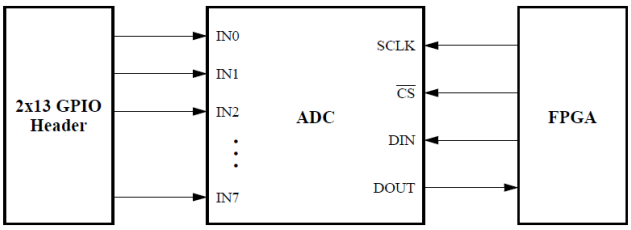

Figure 6.13: ADC128S022 interface to FPGA [18].

The ADC is connected to the FPGA by four wires, which are used to control the ADC and communicate with it, as shown in Figure 6.13. ADC uses the SCLK signal as a device clock. The ($\overline{CS}$) signal is an active low signal used to select the ADC chip. The DIN and DOUT wires are used for transferring addresses and data between two chips. The address of the next channel needed for conversion is provided by the FPGA via the DIN connection, which is mapped to the ADC_SADDR pin on the FPGA. The address is three bits long and is supplied serially to the ADC at the rate of one bit per SCLK cycle. The ADC sends digital values to the FPGA via the DOUT connector, which is mapped to the ADC_SDAT pin on the FPGA. This value is 12 bits long and is serially sent to the FPGA at 1 bit per SCLK cycle [18].

Timing and signal requirements

The user must provide the ADC with the SCLK, ($\overline{CS}$), and DIN signals, as well as capture the DOUT signal when it is being transmitted. The ADC128S002 runs on a 16-cycle operational frame as shown in Figure 6.14.

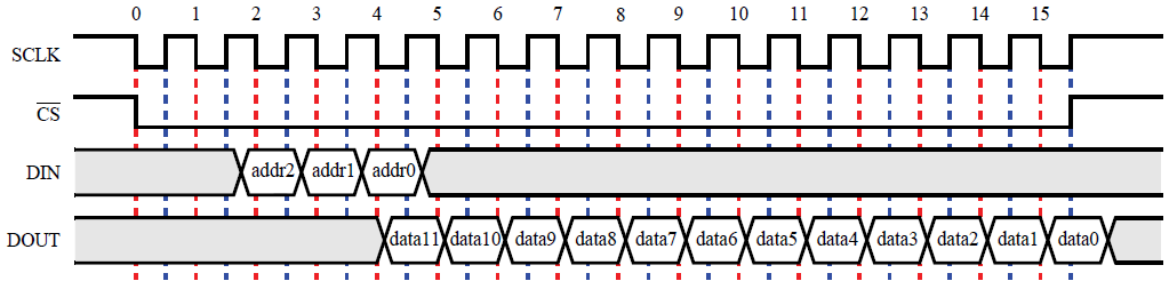

Figure 6.14: Timing requirements for the ADC.

The DOUT signal provides 12-bit converted value to the selected channel. Channel 0 is used by default when the device is turned on, and subsequent reads will use the address specified in the previous operational frame. The data bits are transmitted in descending order, with the highest-order bit arriving first. The user captures it on the rising edge of SCLK. The DIN signal is used to select the channel to be converted in the next frame. The ADC captures it on the positive edges of SCLK and delivers it in descending order. The user should generate DIN on the negative edges of SCLK to avoid any race conditions [18].

The DE0-Nano ADC Controller

The DE0-Nano ADC Controller IP Core is utilized to manage and control the signals between the ADC and the FPGA, as well as to provide the converted readings to the user [18]. The DE0-Nano ADC Controller IP core can be instantiated in a system and made part of the NIOS II system using the platform designer with its graphical user interface. It reads each of the ADC's input channels in ascending order once per update cycle and stores the acquired values locally. The updated values are accessible after the update cycle is completed. It also permits the user to customize many aspects of its operation. The number of channels used by the ADC Controller core is defined by the parameter NUM CH, which is set by the user when the core is instantiated. The SCLK frequency can also be specified via the core. In the allowable range of 0.8 to 3.2 MHz, the user can enter the desired value. The value is placed in the registers upon the completion of the conversion.

6.6 Altera NIOS II soft-core for non-invasive haemoglobin estimation

In our design using Platform Designer in Quartus 18.1, the SOPC components selected were 32-bit NIOS II CPU, On-chip memory, SDRAM, RS232 UART, Interval Timer, Parallel Ports, ADC, and LCD. This has been accomplished with the help of SOPC builder in Quartus II where one needs to merely select the required components from the available IP list.

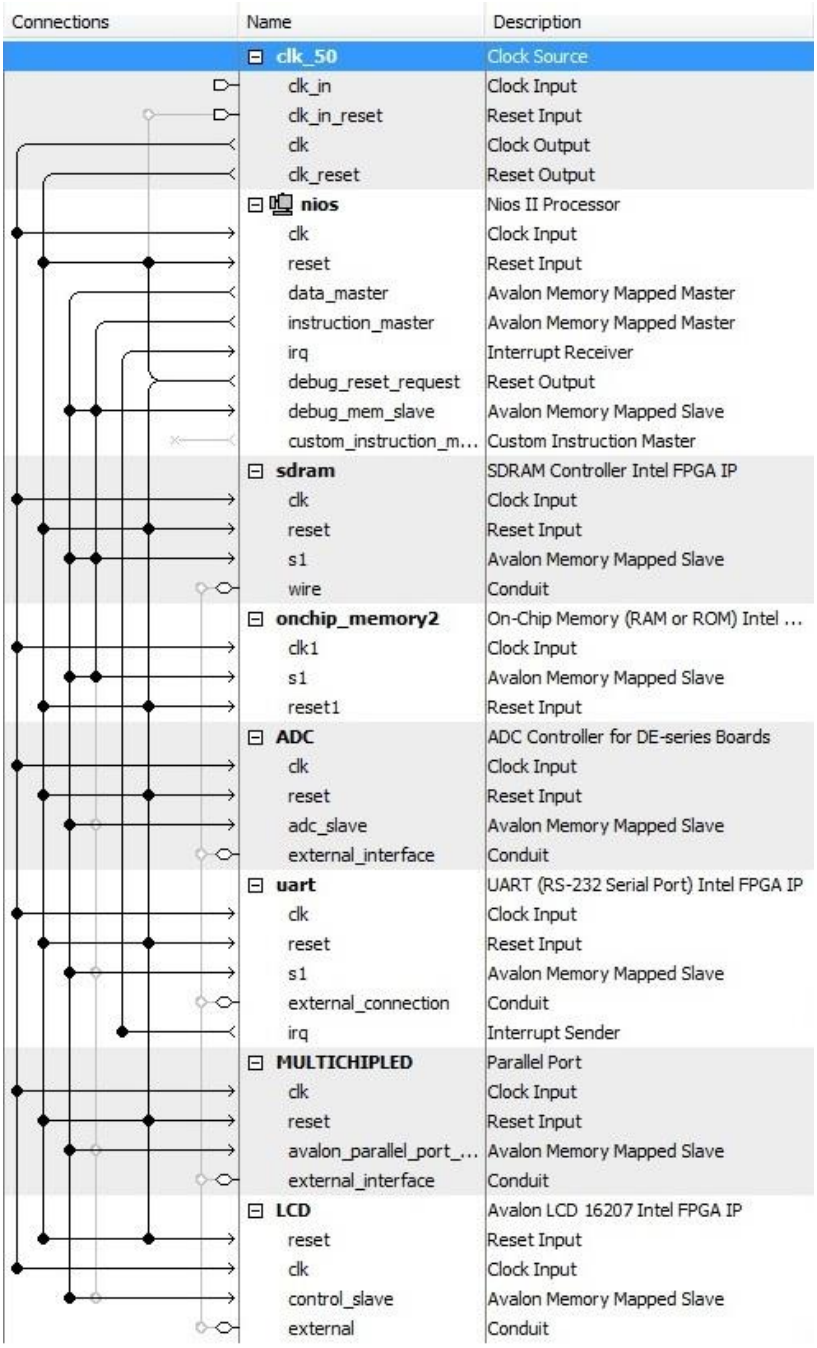

Figure 6.15: Selected SOPC components to build the system.

After selecting the SOPC components, the hardware descriptive language (HDL) files are generated. This generated system is then brought to the Quartus Block diagram file window and the pin mapping is done as shown in Figure 6.16.

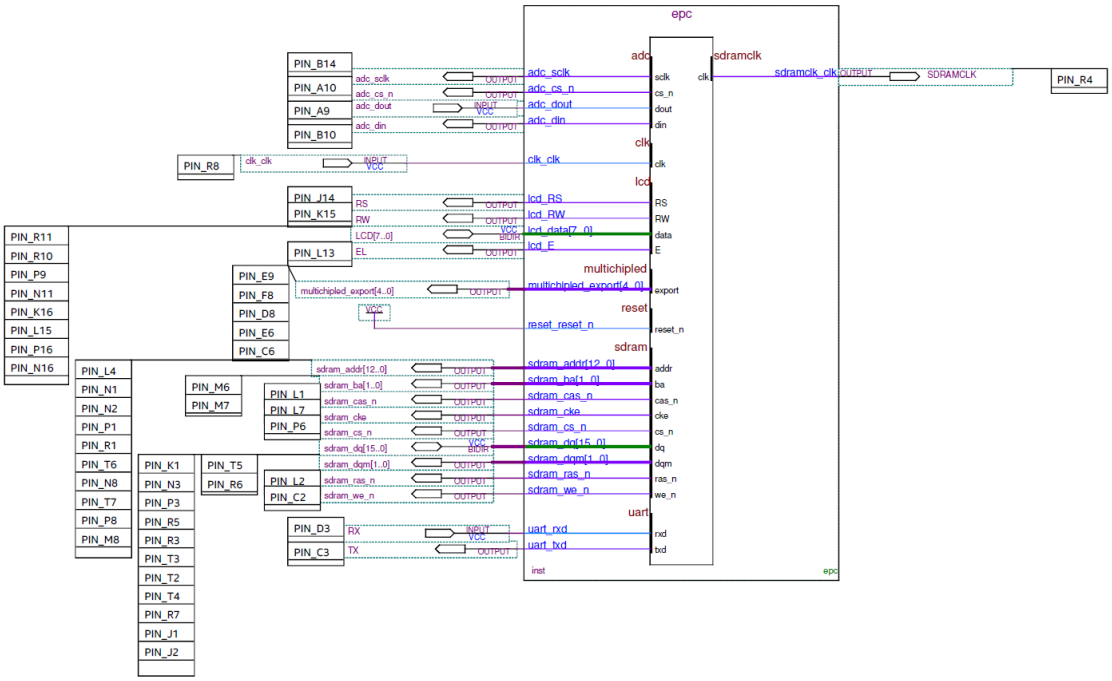

Figure 6.16: The NIOS II instance generated in Quartus II software.

After compiling the entire design, it displays the number of logic elements, registers, pins and memory bits being utilized, as shown in Figure 6.17.

Flow Status	Successful - Wed Aug 12 00:38:18 2020
Quartus Prime Version	18.1.0 Build 625 09/12/2018 SJ Standard Edition
Revision Name	epc
Top-level Entity Name	TOP
Family	Cyclone IV E
Device	EP4CE22F17C6
Timing Models	Final
Total logic elements	4,672 / 22,320 (21 %)
Total registers	2981
Total pins	63 / 154 (41 %)
Total virtual pins	0
Total memory bits	386,048 / 608,256 (63 %)
Embedded Multiplier 9-bit elements	6 / 132 (5 %)
Total PLLs	1 / 4 (25 %)

Figure 6.17: Resources used for system design.

The completed SOPC design is then downloaded with SRAM Object file (.sof) on Cyclone IV on the DE0 Nano FPGA board using a USB blaster. Once downloaded, the application program to estimate total haemoglobin is written and compiled using the NIOS II Software Build Tools (SBT) for Eclipse.

6.6.1 Programming the NIOS II soft-core

NIOS II Software Build Tools (SBT) is a collection of utilities targeted to build embedded C/C++ applications for the soft-core. The C/C++ programming is accomplished using the Eclipse graphical user interface [19]. It provides identical support for both C and C++ development. It also provides editing, building, and debugging for software development tasks. Next, the code is loaded into the SDRAM of the DE0 Nano FPGA Board. Figure 6.18 shows the graphical user interface of NIOS II SBT.

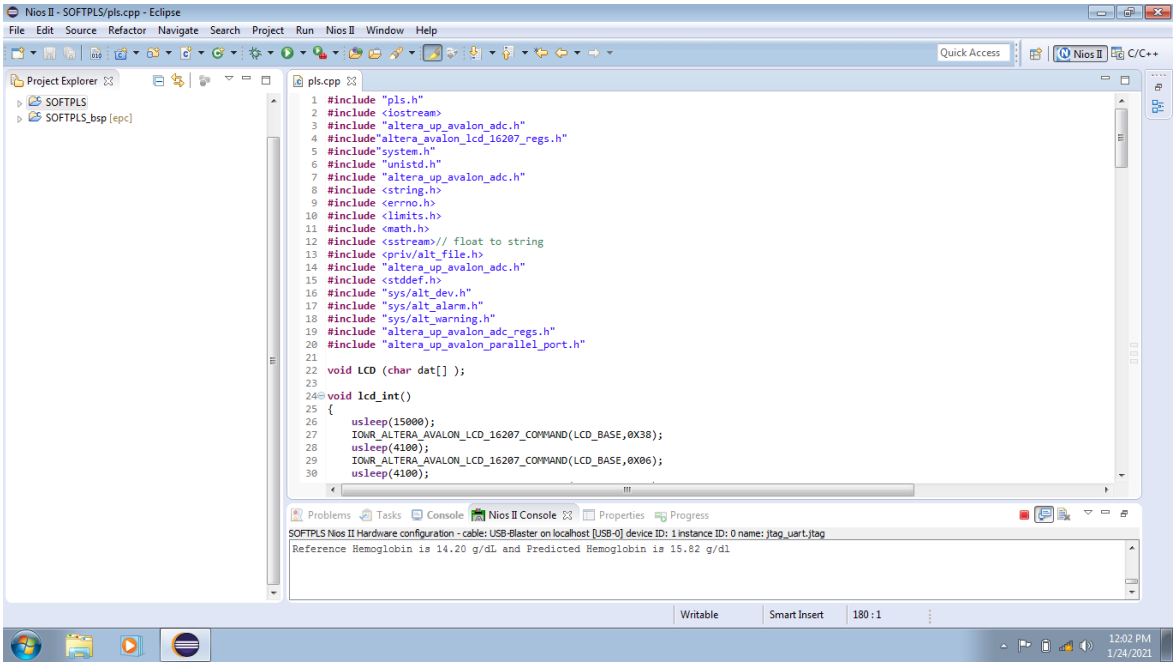

Figure 6.18: Graphical user interface of NIOS II SBT.

To test the usability of multivariate analysis, we executed for various matrix manipulations like curve fitting, matrix transpose, finding determinant, multiplication and inverse operations before actual implementation of SIMPLS algorithm using the designed NIOS II soft-core system. To estimate haemoglobin concentration, we need to build a calibration model using PLS multivariate technique. The acquired data is processed using the PLS algorithm in 'C++ language' for computing the unknown concentration of the haemoglobin. The designed system was tested for multivariate analysis by running SIMPLS algorithm in C++ to estimate the haemoglobin level of blood in humans. The flowchart followed is depicted in Figure 6.19.

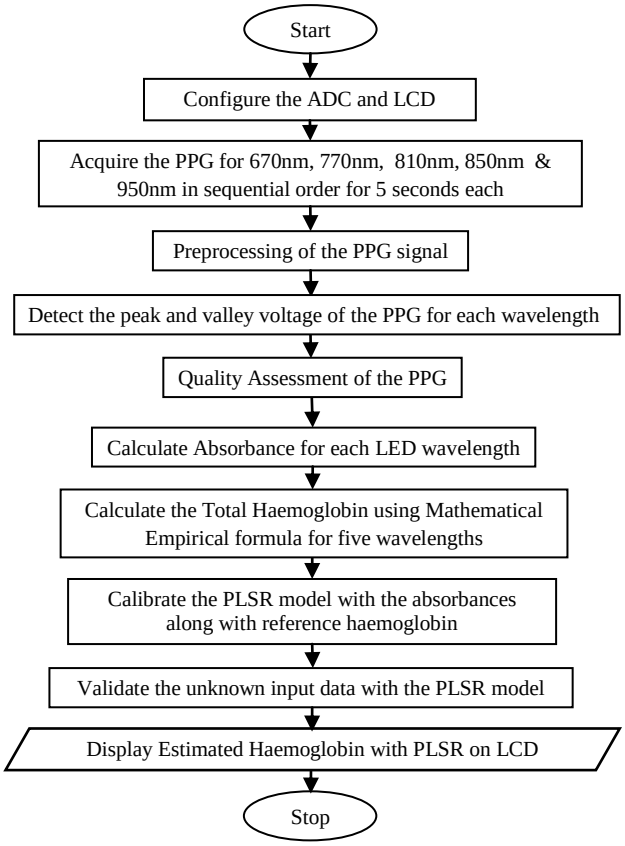

Figure 6.19: System flowchart for estimating haemoglobin.

First, the ADC and LCD are configured. The PPG signal is recorded for five different wavelengths of LEDs in sequential order (viz., 670 nm, 770 nm, 810 nm, 850 nm, and 950 nm) respectively for 5 seconds each. Next, the PPG signal is filtered by using a moving average filter. Then, the peak and valley voltage of the PPG signal is extracted for each LED wavelength. Then, the Quality Assessment for the PPG signal is done for each PPG signal, where the mean of peaks and the mean of valley voltage of the PPG signal are calculated. If the peak and valley voltages are closer to the mean peak and mean valley, the values are then saved; else, they are discarded duringthe computation. Next, the AC component (Peak Voltage - Valley Voltage) and DC component (Valley Voltage) for each PPG LED wavelength are calculated to obtain the absorbance for each PPG signal. This is followed by the estimation of the total haemoglobin of the subject using the mathematical empirical formula for the five wavelengths. The PLSR model is calibrated with the absorbance at the five different wavelengths along with the reference haemoglobin. Next, the PLSR model is validated with the unknown values i.e. Absorbance of the PPG signal at five LED wavelengths. Finally, the haemoglobin concentration is predicted using the PLSR model and displayed on the LCD.

PPG Signal Preprocessing

The performance of the biosignal processing for the non-invasive diagnosis of diseases andthe calculation of physiological parameters arevery important factors. The distinctive features of the filtered PPG signal are thepeaks and valleys of the PPG signals. These parameters are used for the calculation of Heart rate, HRV, SPO_2, and Total Haemoglobin. Also, other features like dicrotic notch, rise time from valley to peak, and fall time from peak to the valley are used for the estimation of blood pressure and diagnosis of cardiovascular disease. The PPG signal can be corrupted due to motion artifacts and respiration rate. Reliable peak detection from the corrupted PPG signal is very important for processing the signal. This involves a robust algorithm for peak and valley detection in a noisy PPG signal.Figure 6.20(a) shows the acquired PPG signal of a subject at five different LED wavelengths. Figure 6.20(b) shows the scaled PPG signal for 810 nm which consists of DC and AC components of the PPG signal. The PPG signal consists of noise which is removed by using a moving-average filter to smoothen the signal by reducing the variations between the samples. as shown in figure 6.21(a). It was observed that if the haemoglobin concentration in blood is low, more light is transmitted thereby producing a larger PPG signal and vice versa.

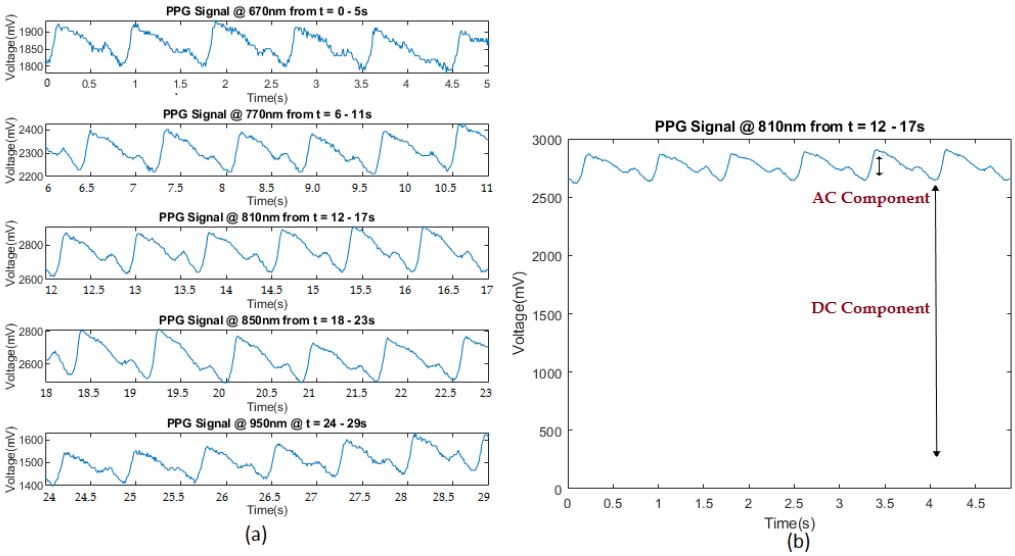

Figure 6.20: PPG signal before filtering.

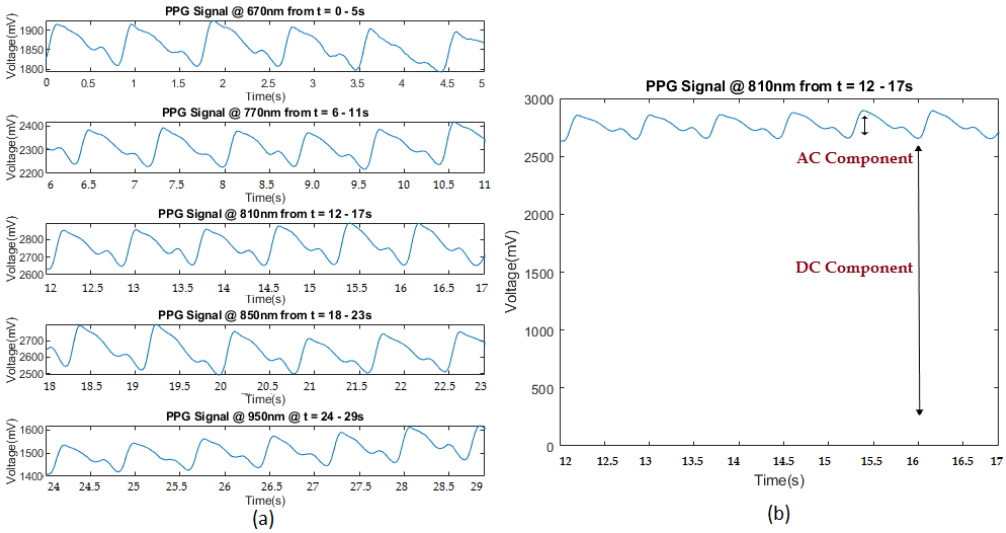

Figure 6.21: PPG signal after filtering.

Once the entire system is designed on Altera NIOS II, the C++ code is downloaded into the DE0- NANO FPGA board and the finger probe is connected to the selected GPIO pins of the FPGA. Each individual LED is sequentially turned on for a duration of 5 seconds for acquiring the PPG signal. All the five PPG signals are recorded and the main features are extracted from the PPG signal e.g. Systolic Peak and Valley for each PPG signal. Based on the above features, optical densities (absorbances) are calculated for each PPG signal and the algorithm is utilized to estimate the total haemoglobin using the empirical formula. Also, the total haemoglobin is estimated using Multivariate (PLSR) model to estimate the total haemoglobin in blood. The results obtained are briefly discussed in the next Chapter.

References

1. H. Amano. "Principles and Structure of FPGAs ", Springer Singapore, 2018.
2. R. P. Jain, “Modern Digital Electronics”, Tata McGraw-Hill Education Pvt. Ltd., 2009.
3. P. Mishra, N. Dutt, “Architectural description languages for programmable embedded systems”, IEE Proc. of Computers and Digital Techniques, vol. 152, pp. 285–297, 2005.
4. M. Chiodo, P. Giusto, A. Jurecska, H. C. Hsieh, et al. “Hardware-software codesign of embedded systems”, *IEEE Micro*, vol. 14, pp. 26-36,1994.
5. R. Ernst, “Codesign of Embedded Systems: status and trends”, Proc. of IEEE Design and Test, pp. 45–54, 1998.
6. D. Arbinger, J. Erdmann, “Designing with an embedded soft-core processor”, [Online] Available at https://www.embedded.com/designing-with-an-embedded-soft-core-processor/
7. NIOS II Processor Reference Guide, [Online] Available at: https://www.intel.com/content/dam/www/programmable/us/en/pdfs/literature/hb/nios2/n2cpu-nii5v1gen2.pdf
8. MicroBlaze Processor Reference Guide, [Online] Available at: https://www.xilinx.com/support/ documentation/sw_manuals/xilinx11/mb_ref_guide.pdf
9. CORTEX-M1, [Online] Available at: https://community.arm.com/developer/ip-products/processors/b/processors-ip-blog/posts/armv6-m-vs-armv7-m---unpacking-the-microcontrollers
10. OpenSPARC T1 Microarchitecture Specification, [Online] Available at: https://www.oracle.com/ technetwork/systems/opensparc/t1-01-opensparct1-micro-arch-1538959.html
11. OpenRISC [Online] Available at: https://opencores.org/projects/or1k_old/openrisc%201200
12. LEON3, [Online] Available at:http://www.actel.com/ipdocs/leon3_ds.pdf
13. LatticeMico32 Open,Free 32 bit Soft Processor [Online] Available at: http://www.latticesemi.com/en/Products/DesignSoftwareAndIP/IntellectualProperty/IPCore/IPCores02/LatticeMico32.aspx
14. DE0 Nano User Manual, [Online] Available at: https://www.ti.com/lit/ug/tidu737/tidu737.pdf

15. Introduction to the Platform Designer Tool, [Online] Available at: ftp://ftp.intel.fr/Pub/fpgaup/pub/Intel_Material/17.1/Tutorials/Introduction_to_the_Qsys_Tool.pdf
16. Using SDRAM on Altera's DE0 Board with Verilog Designs, [Online]Available at: ftp://ftp.intel.com Pub /fpgaup/pub/Intel_Material/14.1/Tutorials/Verilog/DE0-Nano/Using_the_ SDRAM.pdf
17. Using SDRAM on Altera's DE0 Board with VHDL Designs, [Online] Available at: ftp://ftp.intel.com / Pub/fpgaup/pub/Intel_Material/11.1/Tutorials/VHDL/DE0-Nano/Using_the_SDRAM.pdf
18. Using the DE0-Nano ADC Controller, [Online] Available at: ftp://ftp.intel.com/Pub/fpgaup/pub/Intel_Material/16.1/Tutorials/Using_DE_Series_ADC.pdf
19. Nios II Software Build Tools, [Online] Available at: https://www.intel.com/content/dam/www/programmable/us/en/pdfs/literature/hb/nios2/n2sw_nii52015.pdf

Chapter 7

Results and Discussions

In this study, the finger probe was designed with a Multichip LED with five wavelengths and a single silicon photodetector with an on-chip trans-impedance amplifier. The entire experimental setup was designed to estimate non-invasive haemoglobin levels with five LED wavelengths (670 nm, 770 nm, 810 nm, 850 nm, and 950 nm). It was safe because the radiated LED power was standardized at 0.7 mW and the fingertip was exposed to LED wavelengths for less than 30 seconds. To carry out this experiment we have taken the Institutional Human Ethical Clearance (IHEC). Before acquiring the data, the subjects were explained about the procedure involved in the research work and then formal consent was obtained from the subjects. The PPG signals were recorded at five different LED wavelengths, while the subjects were in the seated rest position. The pathological measurement of haemoglobin was also done at Manda's clinic using 5 part Hematology Analyzer (Mindray company BC 5150) at the same time to validate the estimated result obtained from our designed system. The total haemoglobin was estimated with empirical formula with three and five LED wavelengths and comparison was done between them. To further improve the prediction accuracy, total haemoglobin was estimated with multivariate (PLSR) model and is also discussed in the next section briefly.

To present our result and the performance of our model, we calculated the goodness of fit (R^2), correlation coefficient (r), Root mean square error (RMSE), and the Bland-Altman plot, in this research work and have discussed as follows.

Root mean square error

RMSE is the square root of the mean of the square of all errors represented in Equation 7.1.

$$RMSE = \sqrt{\frac{\sum_{i=1}^{N}(x-y)^2}{N}} \tag{7.1}$$

where x = estimated haemoglobin, y = reference haemoglobin, N is the number of subjects.

Accuracy of Prediction

The accuracy of our system is calculated using Equation 7.2.

$$A = 1 - \left(\sqrt{\frac{\sum_{i=1}^{N} (x - y)/x}{N}} \right) x100 \tag{7.2}$$

Correlation coefficient

The correlation coefficient (r) shows how strongly two measurement methods are linearly related. r is computed as the ratio of covariance between the variables to the product of their standard deviations. The value of r is between -1.0 and +1.0. The formula for Pearson's correlation is represented in Equation 7.3,

$$r = \frac{\sum_i (x_i - \bar{x})(y_i - \bar{y})}{\sqrt{\sum_i (x_i - \bar{x})^2} \sqrt{\sum_i (y_i - \bar{y})^2}} \tag{7.3}$$

where n is the sample size, x_i, y_i are the individual sample points and $\bar{x}, \bar{y}$ are the mean values. Although a correlation coefficient gives us an indication of the strength of linear relationship between the two estimation methods, we need to assess the agreement between two measurement methods. So, we used the Bland-Altman plot to assess the agreement between two measurements.

Bland-Altman plot and analysis

To establish the overall degree of agreement in healthcare research, it is essential to compare two techniques of measurement. Traditional correlational studies can be replaced with the Bland–Altman plot. The Bland–Altman plot depicts agreement graphically by using the mean and standard deviation of the differences between two measurements to create statistical limits of agreement. The difference (Measurement Method #1 vs. Measurement Method #2) is shown on the vertical axis, while the mean ([Measurement Method #1 + Measurement Method #2]/2) is shown on the horizontal. The bias between the two tests is measured by the mean of differences between reference and estimated values. One can discover bias between the mean differences of two measures and estimate an agreement interval using Figure 7.1. Within this interval, 95 % of the data points should fall within ± 2 standard deviations of the mean difference. Therefore, the agreement interval allows one to evaluate the range of variability between the two methods, and it must be chosen before the plot is constructed depending on clinical objectives. When analysing a Bland–Altman plot, there are a few things to keep in mind. Firstly, determine where the mean difference falls, as this indicates whether one method of measurement tends to overestimate (i.e., the mean difference is greater than zero) or underestimate (i.e.,

the mean difference is less than zero). The closer the mean difference is to zero, the better is the agreement between the two measurements. To determine the precision of this result, 95 % confidence interval (CI) of the mean difference is calculated. If the line representing zero falls beyond the 95 % CI, there is a significant difference between the two measurements, indicating that one technique overestimates or underestimates the other. Secondly, the spread of the limits of agreement must be determined since the standard deviation of the differences between the two measurements reveals random variation around the mean. The wider limits of agreement shows less precision while narrower limits shows less precision which indicates that the two methods are comparable.

The bias between the two tests is measured by the mean of differences between reference and estimated values.

$$\text{Bias } (\bar{d}) = \frac{1}{n}\sum_{a=1}^{n} d_a \qquad (7.4)$$

where d_a= Estimated value -Reference value, n = the number of subjects

$$\text{Standard deviation}(SD) = \sqrt{\frac{1}{n-1}\sum_{a=1}^{n}\left(d_a - \bar{d}\right)^2} \qquad (7.5)$$

Limits of agreement between the two tests are defined by a 95% prediction interval of a particular value of the difference.

$$\text{limits of agreement} = \text{Bias} \pm 1.96\ S_d \qquad (7.6)$$

The limits of agreements are defined as ± 1.96 times the SD from the mean of differences. The limits of agreement are represented by the outer red coloured dotted lines, and bias is represented by the middle blue coloured line as shown in Figure 7.1.

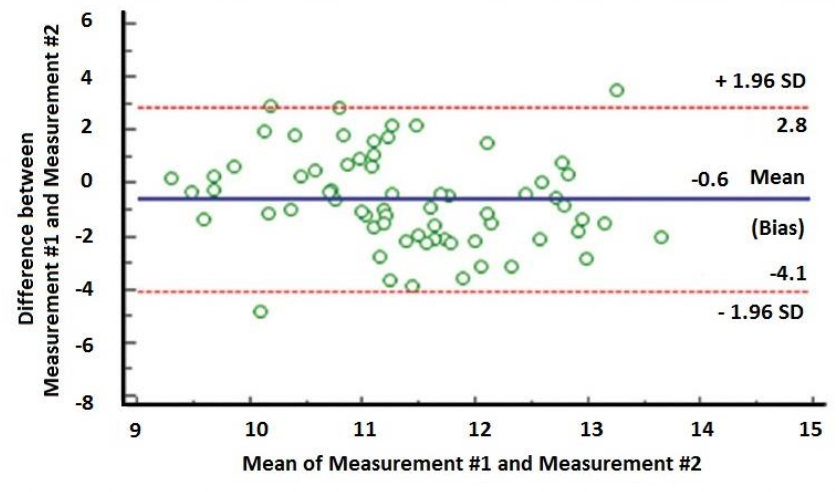

Figure 7.1: Bland- Altman plot.

7.1 Analysis of haemoglobin estimation with three and five LED wavelengths (Case I)

In Case I, fifteen subjects were enrolled in the preliminary study. The age range of participating subjects was 18 to 35 years with less variations with respect to age and skin. The non-invasive total haemoglobin was estimated with three and five LED wavelengths using mathematical empirical formula and the reference haemoglobin was measured in the pathology laboratory.

Table 7.1: Haemoglobin estimation for 15 Subjects (Case I).

	Estimated total haemoglobin with the designed system (Non-invasive method)		Total haemoglobin measured in	Error in total haemoglobin measured	
Subject No	Three LED wavelengths (g/dL)	Five LED wavelengths (g/dL)	pathology laboratory (g/dL)	Three LED wavelengths (g/dL)	Five LED wavelengths (g/dL)
Sub.1	16.87	17.02	17.50	-0.63	-0.48
Sub.2	16.56	17.13	17.00	-0.44	0.13
Sub.3	11.53	11.87	11.20	0.33	0.67
Sub.4	15.42	16.34	16.20	-0.78	0.14
Sub.5	13.15	13.98	14.00	-0.85	-0.02
Sub.6	12.80	12.97	12.50	0.3	0.47
Sub.7	15.03	15.83	15.70	-0.67	0.13
Sub.8	16.36	16.55	16.00	0.36	0.55
Sub.9	16.12	16.62	16.80	-0.68	-0.18
Sub.10	11.89	12.07	12.20	-0.31	-0.13
Sub.11	14.12	14.69	14.90	-0.78	-0.21
Sub.12	12.34	13.11	12.90	-0.56	0.21
Sub.13	15.16	15.49	16.10	-0.94	-0.61
Sub.14	13.45	14.49	14.20	-0.75	0.29
Sub.15	11.32	11.64	12.00	-0.68	-0.36
			RMSE	0.64 g/dL	0.36 g/dL

The result of Table 7.1, shows non-invasive measurement of total haemoglobin using three and five LED wavelengths (non-invasive method). Also, a comparative study was made with the haemoglobin measured using the invasive method in the pathology laboratory. The blue and red bar graph indicates estimated haemoglobin with three LED wavelengths and with five LED wavelengths and the green bar graph indicates the reference hemoglobin measured in the pathology laboratory as shown in Figure 7.2.

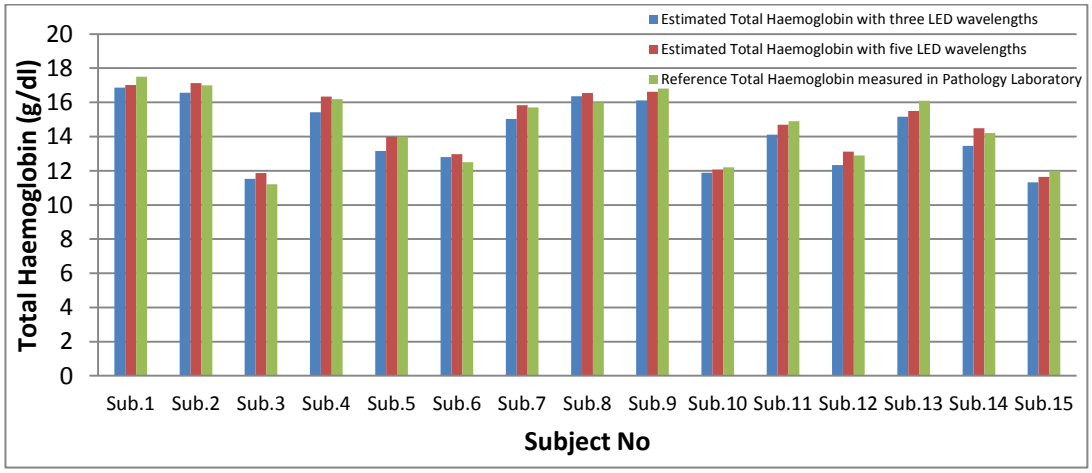

Figure 7.2: Total haemoglobin for 15 subjects (Case I).

Figure 7.3 shows the regression analysis for estimated total haemoglobin v/s reference haemoglobin for three and five LED wavelengths.

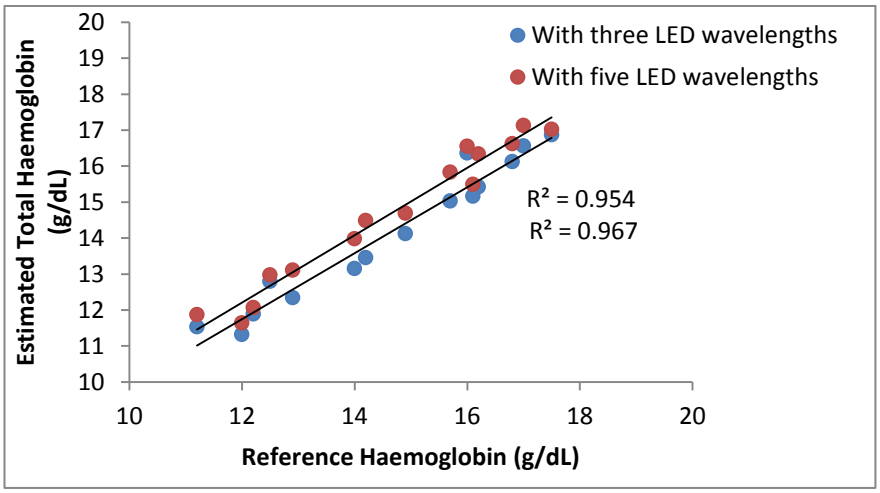

Figure 7.3: Regression analysis for estimated total haemoglobin v/s reference haemoglobin (Case I).

Initially, total haemoglobin was estimated with three wavelengths (λ_1=670nm, λ_2=810nm and λ_3=950nm) using mathematical empirical formula and the RMSE was 0.64 g/dL with the Regression Coefficient of R^2=0.954, but our aim was to further improve the prediction accuracy. Hence we selected another two wavelengths, 770nm and 850nm to get more information about oxyhaemoglobin and deoxyhaemoglobin. By adding these two wavelengths, the RMSE significantly improved to 0.36 g/dL and the Regression Coefficient (R^2=0.967) which is good. For this reason, the five wavelengths PPG is an excellent choice for the measurement of non-invasive blood haemoglobin and we continued our further research work with five LED wavelengths.

7.1.1 Multivariate calibration (PLSR) model in NIOS II soft-core system for non-invasive haemoglobin estimation with five LED wavelengths

Initially, multivariate PLSR model was implemented using ParLeS 3.1 software for the analysis. For the PLSR model, 12 Subjects' PPG signals was used as the calibration set, and 3 Subjects' PPG signal was used for validating the PLSR model. Also, the PLSR algorithm was implemented using C++ and ported on the designed NIOS II soft-core system in DE0 Nano FPGA Board to predict the total haemoglobin concentration in blood.

Table 7.2: Estimated total haemoglobin with five LED wavelengths.

Subject No	Reference haemoglobin	Estimated total haemoglobin	
		With empirical formula	With PLSR model
Sub. 1	16.10	15.49	15.89
Sub. 2	14.20	14.49	14.17
Sub. 3	12.00	11.64	11.98
	RMSE	0.44	0.12
	r	0.97	0.99
	Accuracy	97.05%	99.44%

Table 7.2 shows the estimated total haemoglobin with empirical formula and with PLSR model for five LED wavelengths. The estimated total haemoglobin with mathematical empirical formula gave a RMSE of 0.44 g/dL and with PLSR model gave a

RMSE of 0.12 g/dL for the validation data with three subjects. The accuracy and correlation was also improved with the PLSR model. Also, the system was validated with Bland-Altman plot as shown in Figure 7.4 (a) and (b), it was observed that the upper and lower limit of 95% confidence interval agreement for estimating total haemoglobin with empirical formula was 0.68 and -1.1 respectively and with PLSR model it was 0.12 and -0.30. Also, the bias was -0.23 g/dL and -0.09 g/dL for estimating total haemoglobin with empirical formula and the PLSR model respectively. The result showed that with multivariate PLSR model, the estimation of total haemoglobin was very precise and showed good agreement between the two measurements.

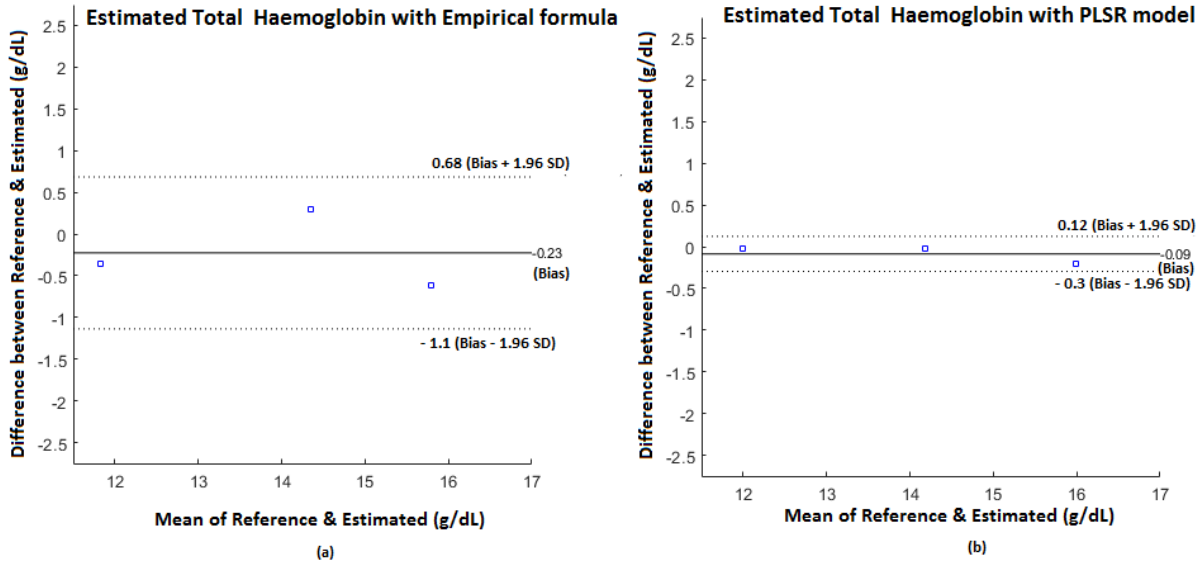

Figure 7.4: Bland-Altman plot (Case I).

7.2 Analysis of haemoglobin estimation with five LED wavelengths (Case II)

In Case II, seventy five subjects were enrolled in this study. The age range of participating subjects was 18 to 60 years with an average of 29 years that included 28 females and 47 males. In this study, the subjects were chosen with diverse variations such as age and skin. The non-invasive total haemoglobin was estimated with five LED wavelengths using mathematical empirical formula and also multivariate (PLSR) model. The results were compared with each other and is discussed as follows.

Table 7.3: Haemoglobin estimation with empirical formula for 25 Subjects (Typical) with five LED wavelengths (Case II).

Subjects	Age	Gender	Height	Weight	BMI	Reference haemoglobin	Estimated haemoglobin	Error
Sub.1	35	M	165	62	22.8	17.5	18.05	0.55
Sub.2	29	M	167	58	20.1	18.7	19.27	0.57
Sub.3	37	M	165	82	30.1	15.1	14.53	-0.57
Sub.4	20	M	165	65	23.8	16.7	16.34	-0.36
Sub.5	32	M	167	90	32.3	16.8	16.5	-0.30
Sub.6	21	M	174	60	19.8	15.5	14.83	-0.67
Sub.7	28	M	172	75	25.4	14.3	13.53	-0.77
Sub.8	23	M	176	92	29.7	15.7	15.81	0.11
Sub.9	28	M	180	82	25.3	16.3	15.94	-0.36
Sub.10	26	M	183	61	18.2	10.5	11.25	0.75
Sub.11	27	M	176	74	23.9	9.9	9.53	-0.37
Sub.12	38	F	152	62	26.8	12.5	12.93	0.43
Sub.13	37	F	143	46	22.5	10.0	10.84	0.84
Sub.14	21	F	152	49	21.2	13.5	13.17	-0.33
Sub.15	27	F	160	54	21.0	13.8	14.67	0.87
Sub.16	38	M	178	86	27.1	18.0	16.98	-1.02
Sub.17	22	F	164	55	20.4	12.8	11.94	-0.86
Sub.18	40	F	158	80	32.0	13.6	13.91	0.31
Sub.19	56	M	165	80	29.3	15.2	15.31	0.11
Sub.20	26	F	170	63	21.8	14.0	14.16	0.16
Sub.21	37	F	152	56	24.2	12.2	11.34	-0.86
Sub.22	37	F	163	67	25.2	11.2	11.18	-0.02
Sub.23	50	M	157	80	32.4	13.7	13.50	-0.20
Sub.24	57	F	170	78	27.0	13.9	13.26	-0.64
Sub.25	45	F	154	60	25.3	13.6	13.21	-0.39

Table 7.3 shows the observation of typical 25 subjects estimation of haemoglobin with five LED wavelengths. The database included age, gender, height, weight and Body Mass Index (BMI). The RMSE between the reference haemoglobin and the estimated total

haemoglobin with mathematical empirical formula for five LED wavelengths was 1.09 g/dL for 75 subjects in the age group of 18 to 60 with different skin texture.

7.2.1 Multivariate calibration (PLSR) model in Altera NIOS II soft-core system for non-invasive haemoglobin estimation with five LED wavelengths

Cross-validation is a technique used to find out how accurately a predictive model will perform in practical scenario. Here, we divided the datasets manually to cross-validate our model. For the PLSR model, 65 Subjects' PPG signals were used for calibrating the model, and 10 Subjects' PPG signals for validating the model for three different cross-validation scenarios having 10 subjects selected randomly for validation.

With cross-validation Set I

Table 7.4: Estimation of total haemoglobin with cross-validation Set I.

Subject	Reference haemoglobin	Estimated total haemoglobin	
		With Empirical formula	With PLSR model
Sub. 1	13.60	11.05	12.16
Sub. 2	17.50	18.05	18.09
Sub. 3	16.70	14.82	15.19
Sub. 4	18.70	19.27	18.89
Sub. 5	13.70	15.06	15.02
Sub. 6	15.90	16.29	16.56
Sub. 7	16.70	16.52	16.49
Sub. 8	12.30	11.35	12.07
Sub. 9	10.90	10.86	11.54
Sub. 10	14.20	14.24	14.48
	RMSE	1.17	0.87
	R	0.91	0.93
	Accuracy	94.19%	95.12 %

Table 7.4 shows the estimated results with the mathematical empirical formula and PLSR model for cross-validation Set I. The RMSE, correlation coefficient (r), and

accuracy for estimated total haemoglobin with empirical formula was 1.17 g/dL, 0.91, and 94.19 % respectively and with PLSR model was 0.87 g/dL, 0.93, and 95.12 % respectively. Figure 7.5 shows the regression analysis for estimated total haemoglobin v/s reference haemoglobin for cross-validation Set I. The coefficient of determination for estimation of total haemoglobin with empirical formula was R^2=0.839 and with PLSR model was R^2=0.872.

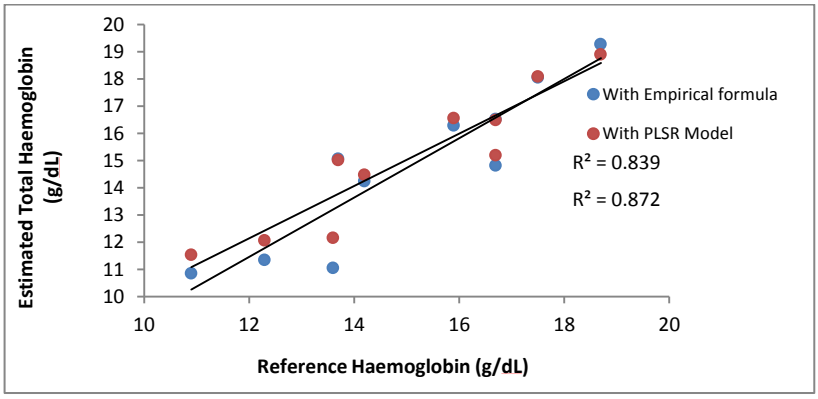

Figure 7.5: Regression analysis for estimated total haemoglobin v/s reference haemoglobin for cross-validation Set I.

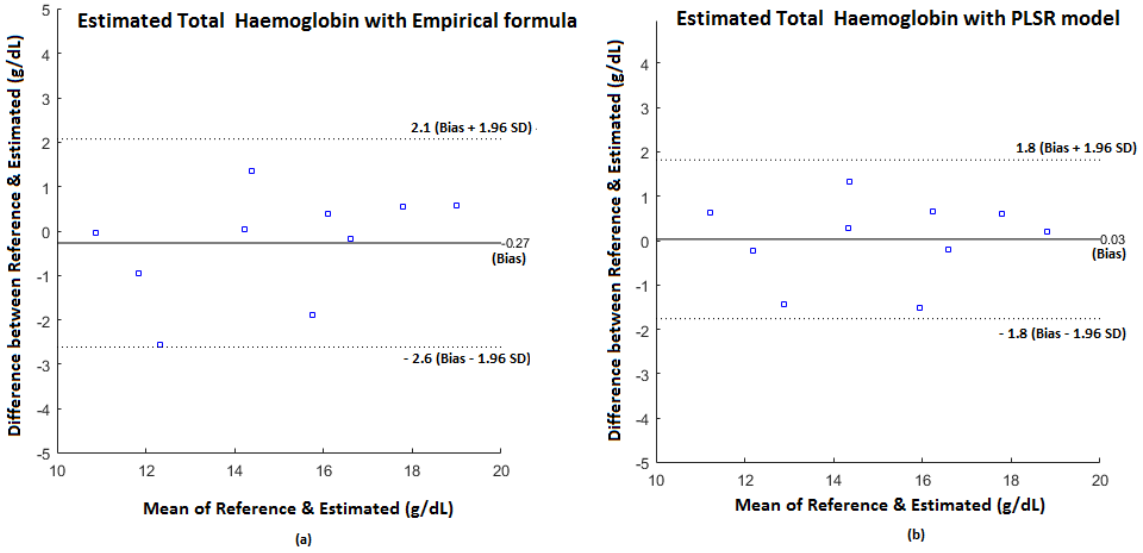

Figure 7.6: Bland-Altman analysis for cross-validation Set I.

From Figure 7.6 (a), it is observed that the bias was -0.27 g/dL, SD of 1.19 g/dL, and limits of agreement from -2.6 to 2.1 g/dL for estimating total haemoglobin with empirical formula. For Figure 7.6 (b), the bias, SD, and limits of agreement was 0.03 g/dL, 0.91 g/dL, and -1.8 to 1.8 g/dL respectively for estimating total haemoglobin with the PLSR model.

With cross-validation Set II

Table 7.5: Estimation of total haemoglobin with cross-validation Set II.

Subject No	Reference haemoglobin	Estimated haemoglobin	
		With Empirical formula	With PLSR model
Sub. 1	13.10	11.88	12.65
Sub. 2	12.70	12.79	13.22
Sub. 3	11.20	11.18	11.88
Sub. 4	16.80	16.5	16.42
Sub. 5	14.70	13.16	13.79
Sub. 6	15.40	15.41	15.47
Sub. 7	14.50	13.28	13.84
Sub. 8	15.50	14.83	15.17
Sub. 9	14.30	13.53	14.08
Sub. 10	15.80	16.46	16.69
	RMSE	0.83	0.57
	r	0.92	0.93
	Accuracy	95.52%	96.36%

Table 7.5 shows the estimated results with the mathematical empirical formula and PLSR model for cross-validation Set II. The RMSE, r, and accuracy were 0.83 g/dL, 0.92 and 95.52% with empirical formula and 0.57 g/dL, 0.93, and 96.36 % with the PLSR model. The coefficient of determination for estimation of total haemoglobin with empirical formula was R^2=0.853 and with PLSR model was R^2=0.870 as shown in Figure 7.7.

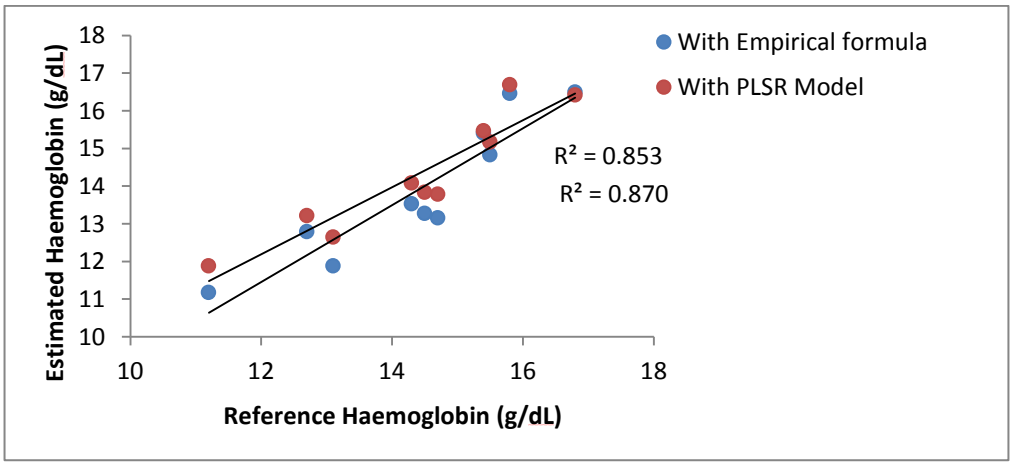

Figure 7.7: Regression analysis for estimated total haemoglobin v/s reference haemoglobin for cross-validation Set II.

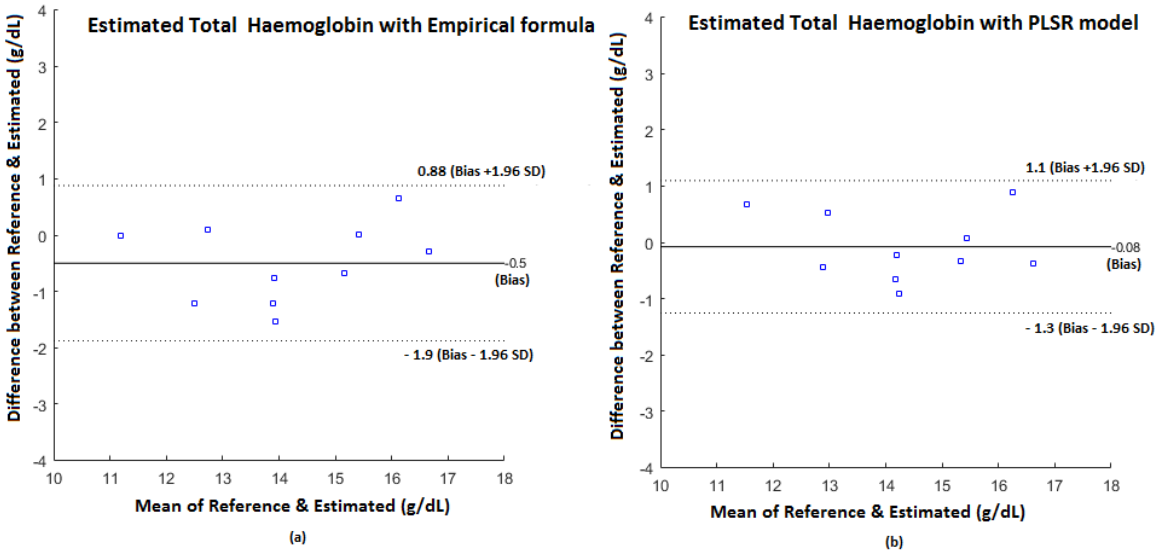

Figure 7.8: Bland-Altman analysis for cross-validation Set II.

From Figure 7.8 (a), the bias was -0.50 g/dL, SD of 0.70 g/dL, and limits of agreement from -1.9 to 0.88 g/dL with empirical formula. From Figure 7.8 (b), the bias, SD, and limits of agreement were 0.08 g/dL, 0.60 g/dL, and -1.3 to 1.1 g/dL respectively with the PLSR model.

With cross-validation Set III

Table 7.6. Estimation of total haemoglobin with Cross-validation Set III

	Reference	Estimated haemoglobin	
Subject No	haemoglobin	With Empirical formula	With PLSR model
Sub. 1	15.40	15.52	15.39
Sub. 2	15.80	14.84	15.18
Sub. 3	14.70	13.02	13.83
Sub. 4	16.70	16.34	16.33
Sub. 5	15.10	14.53	14.68
Sub. 6	12.90	12.77	13.58
Sub. 7	12.80	11.94	12.95
Sub. 8	15.30	13.86	14.51
Sub. 9	13.20	14.06	14.33
Sub. 10	12.50	12.93	13.40
	RMSE	0.89	0.68
	r	0.84	0.89
	Accuracy	94.80%	95.77%

Table 7.6 shows the estimated results with the mathematical empirical formula and PLSR model for cross-validation Set III. The RMSE, r, and accuracy with empirical formula was 0.89 g/dL, 0.84, and 94.87% respectively and with PLSR model, it was 0.68 g/dL, 0.89, and 95.77 % respectively. Figure 7.9 shows the regression analysis for estimated haemoglobin v/s reference haemoglobin for cross-validation Set III. The coefficient of determination for estimation haemoglobin with empirical formula was R^2=0.706 and with PLSR model was R^2=0.80.

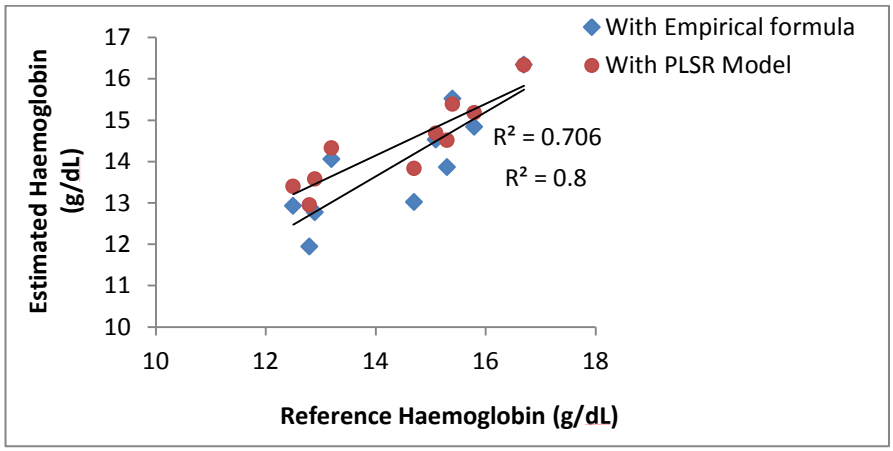

Figure 7.9: Regression analysis for estimated haemoglobin v/s reference haemoglobin for cross-validation Set III .

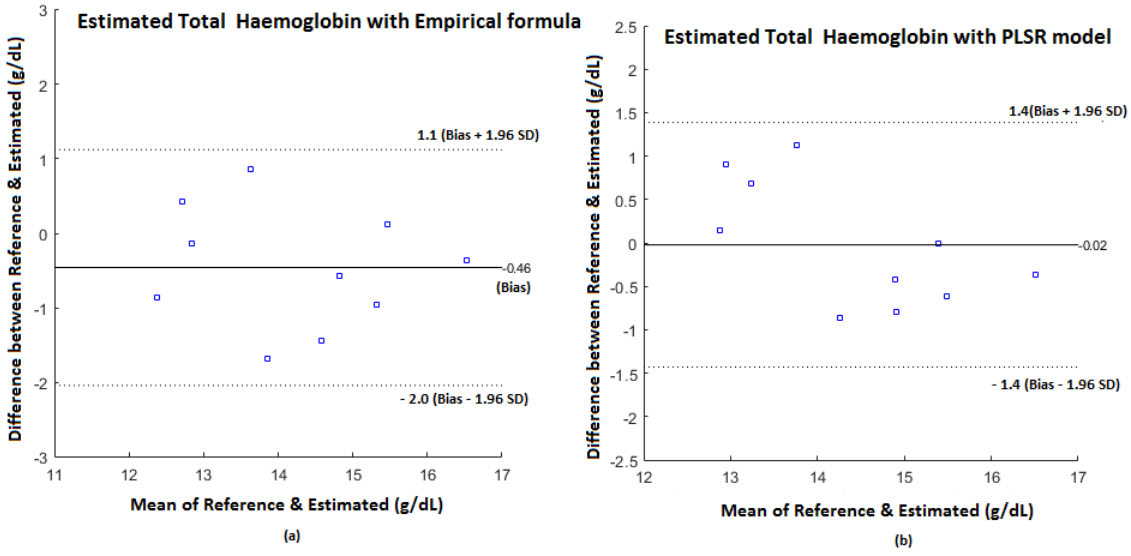

Figure 7.10: Bland-Altman analysis for cross-validation Set III.

From Figure 7.10 (a), it is observed that the bias was -0.46 g/dL, SD of 0.81 g/dL, and limits of agreement from -2.0 to 1.1 g/dL for estimating haemoglobin with empirical formula. From Figure 7.10 (b), the bias, SD, and limits of agreement were -0.02 g/dL, 0.72 g/dL, and -1.4 to 1.4 g/dL respectively for estimating haemoglobin with the PLSR model. In all three Bland-Altman plot and analysis for different cross-validation sets, the data points were less spread with less bias, which clearly shows that haemoglobin estimation with the multivariate PLSR model is more precise.

The main objective of this research work was to design a portable system for predicting total haemoglobin with an error of less than 1g/dl which was achieved by using five LED wavelengths to acquire the PPG signal and by applying the PLSR multivariate technique.

7.3 CONCLUSIONS

A low-cost, portable, non-invasive total haemoglobin meter has been designed using fixed LED sources (Multichip LEDs) with a wavelength ranging from 670 to 950 nm along with Silicon detector OPT101 for PPG signal acquisition. The entire soft-core system was designed and the PLSR algorithm was implemented in the NIOS II on Altera Nano DE0 Board to estimate total haemoglobin in the blood. The filtering and Quality Assessment for the PPG signals were implemented to smoothen the PPG signal and to extract good quality peaks. The result of this study showed a good significant correlation between haemoglobin concentration and characteristics of the PPG signal.

In Case I: Analysis with empirical formula was done with 15 subjects in the age group of 18 to 35 years with less variations such as age and skin. It was observed that total haemoglobin estimation with three wavelengths gave RMSE of 0.64 g/dL and 0.36 g/dLwith five wavelengths which was much better. With the PLSR model implemented in the FPGA Board, the system accuracy improved by estimating total haemoglobin with RMSE of 0.12 g/dL with prediction accuracy of 99.43% for 3 subjects in the validation set for five wavelengths.

In Case II (5 wavelengths): Analysis was done with 75 subjects in the age group of 18 to 60 years with skin variations. With the PLSR model, the RMSE was reduced for

Cross-Validation I: 0.87 g/dL

Cross-Validation II: 0.57 g/dL

Cross-Validation III: 0.68 g/dL

The system was also validated with Bland-Altman Analysis and it was observed that the PLSR model showed better agreement in estimating total haemoglobin precisely with less bias. It was observed that RMSE with 75 subjects was slightly on the higher side as we have considered the diverse population with variation in skin color and age.

ANNEXURE I

Program for LCD

```
#include"altera_avalon_lcd_16207_regs.h"
void lcd_int()
{
usleep(15000);
IOWR_ALTERA_AVALON_LCD_16207_COMMAND(LCD_BASE,0X38);
usleep(4000);
IOWR_ALTERA_AVALON_LCD_16207_COMMAND(LCD_BASE,0X06);
usleep(4000);
IOWR_ALTERA_AVALON_LCD_16207_COMMAND(LCD_BASE,0X0E);
usleep(4000);
IOWR_ALTERA_AVALON_LCD_16207_COMMAND(LCD_BASE,0X01);
usleep(2000);
}

int main()
{
int i;
char j[16] ="   NON-INVASIVE  ";
char k[16]="    HAEMOGLOBIN  ";
lcd_int();

while(1){
        IOWR_ALTERA_AVALON_LCD_16207_COMMAND(LCD_BASE,0X80);
        usleep(2000);
        for(i=0;i<16;i++){
        IOWR_ALTERA_AVALON_LCD_16207_DATA(LCD_BASE,j[i]);
        usleep (30000);
        }
        IOWR_ALTERA_AVALON_LCD_16207_COMMAND(LCD_BASE,0XC0);
        usleep(2000);
        for(i=0;i<16;i++){
        IOWR_ALTERA_AVALON_LCD_16207_DATA(LCD_BASE,k[i]);
        usleep (30000);
        }
        }
        return 0;
        }
```

ANNEXURE II

Program for ADC and LCD

```
#include "altera_up_avalon_adc.h"
#include"altera_avalon_lcd_16207_regs.h"

void lcd_int()
{
usleep(15000);
IOWR_ALTERA_AVALON_LCD_16207_COMMAND(LCD_BASE,0X38);
usleep(4000);
IOWR_ALTERA_AVALON_LCD_16207_COMMAND(LCD_BASE,0X06);
usleep(4000);
IOWR_ALTERA_AVALON_LCD_16207_COMMAND(LCD_BASE,0X0E);
usleep(4000);
IOWR_ALTERA_AVALON_LCD_16207_COMMAND(LCD_BASE,0X01);
usleep(2000);
}

int main()
{
int i;
alt_up_adc_dev *adc;
unsigned int thousand, hundred, ten, unit;
int count;
int data;
int channel;
char j[16]="  NON-INVASIVE ";
char k[16]="  HAEMOGLOBIN  ";
lcd_int();

while(1){
        IOWR_ALTERA_AVALON_LCD_16207_COMMAND(LCD_BASE,0X80);
        usleep(2000);
        for(i=0;i<16;i++){
        IOWR_ALTERA_AVALON_LCD_16207_DATA(LCD_BASE,j[i]);
        usleep (30000);
        }
        IOWR_ALTERA_AVALON_LCD_16207_COMMAND(LCD_BASE,0XC0);
        usleep(2000);
        for(i=0;i<16;i++){
        IOWR_ALTERA_AVALON_LCD_16207_DATA(LCD_BASE,k[i]);
        usleep (30000);
```

```
        }

data = 0;
channel = 0;
adc = alt_up_adc_open_dev ("/dev/ADC");
while (adc!=NULL){
        alt_up_adc_update (adc);
        count += 1;
        data = alt_up_adc_read (adc, channel);
        data=((data*3300)/4095);
        thousand=(data/1000)+48;
        hundred=((data/100)%10)+48;
        ten=((data/10)%10)+48;
        unit=(data%10)+48;

        IOWR_ALTERA_AVALON_LCD_16207_COMMAND(LCD_BASE,0XC0);
        usleep(2000);
        IOWR_ALTERA_AVALON_LCD_16207_DATA(LCD_BASE,thousand);
        usleep (30000);
        IOWR_ALTERA_AVALON_LCD_16207_DATA(LCD_BASE,hundred);
        usleep (30000);
        IOWR_ALTERA_AVALON_LCD_16207_DATA(LCD_BASE,ten);
        usleep (30000);
        IOWR_ALTERA_AVALON_LCD_16207_DATA(LCD_BASE,unit);
        usleep (30000);
        IOWR_ALTERA_AVALON_LCD_16207_DATA(LCD_BASE,'g');
        usleep (30000);
        IOWR_ALTERA_AVALON_LCD_16207_DATA(LCD_BASE,'m');
        usleep (30000);
        IOWR_ALTERA_AVALON_LCD_16207_DATA(LCD_BASE,'/');
        usleep (30000);
        IOWR_ALTERA_AVALON_LCD_16207_DATA(LCD_BASE,'d');
        usleep (30000);
        IOWR_ALTERA_AVALON_LCD_16207_DATA(LCD_BASE,'L');
        usleep (30000);
}
}
return 0;
}
```

ANNEXURE III

Program for PLSR Algorithm

```
#include "pls.h"
#include <iostream>
#include "altera_up_avalon_adc.h"
#include"altera_avalon_lcd_16207_regs.h"
#include"system.h"
#include "unistd.h"
#include <string.h>
#include <math.h>
#include "altera_up_avalon_adc.h"
#include <stddef.h>
#include "sys/alt_dev.h"
#include "sys/alt_alarm.h"
#include "sys/alt_warning.h"

void LCD (char dat[] );
void lcd_int()
{
        usleep(15000);
        IOWR_ALTERA_AVALON_LCD_16207_COMMAND(LCD_BASE,0X38);
        usleep(4000);
        IOWR_ALTERA_AVALON_LCD_16207_COMMAND(LCD_BASE,0X06);
        usleep(4000);
        IOWR_ALTERA_AVALON_LCD_16207_COMMAND(LCD_BASE,0X0E);
        usleep(4000);
        IOWR_ALTERA_AVALON_LCD_16207_COMMAND(LCD_BASE,0X01);
        usleep(2000);
        }

void LCD(char dat[]){
  int index = 0;
       while(dat[index]!='\0'){
      IOWR_ALTERA_AVALON_LCD_16207_DATA(LCD_BASE,dat[index]);
      usleep (30000);
      index++;
      }
}
```

```
float rounding(float var)
{
        float value = (int)(var * 100 + .5);
           return (float)value / 100;
}

int main(int argc, char ** h, char** b)
{
        int index=0;
        char string[] =  "NIOS II HB meter";
        char string1[] = "using PLSR model";
        lcd_int();
        IOWR_ALTERA_AVALON_LCD_16207_COMMAND(LCD_BASE,0X01);
        usleep(2000);
        IOWR_ALTERA_AVALON_LCD_16207_COMMAND(LCD_BASE,0X80);
        usleep(2000);
        LCD(string);
        IOWR_ALTERA_AVALON_LCD_16207_COMMAND(LCD_BASE,0XC0);
        usleep(2000);
         LCD(string1);
        usleep (3000000);

   char text1[] = "Refer.:";
   char text2[] = "Pred. :";
   char text3[] = "g/dL";

        Mat2D X_orig(65, 5);
             X_orig << 2.9376,    2.5676,    2.4566,    2.2564,    2.2053,
                       2.3631,    2.0895,    1.9365,    1.8144,    1.8104,
                       2.5227,    2.4645,    2.334,     2.0823,    2.0489,
                       2.3524,    2.1783,    2.296,     1.9479,    1.921,
                       2.7318,    2.3192,    2.1971,    2.1369,    2.0726,
                       2.3816,    2.2443,    1.923,     1.8293,    1.7529,
                       2.7074,    2.5066,    2.3886,    2.3417,    2.164,
                       2.4992,    2.2108,    1.9697,    1.8935,    1.8556,
                       2.9375,    2.8251,    2.5553,    2.3387,    2.3347,
                       2.5895,    2.0733,    1.8753,    1.7809,    1.7368,
                       2.8824,    2.6388,    2.5194,    2.4807,    2.3776,
                       2.2573,    2.0136,    1.8761,    1.8014,    1.7662,
                       2.7592,    2.5103,    2.5103,    2.2817,    2.2489,
                       2.3284,    2.0843,    1.9086,    1.829,     1.7717,
                       1.8517,    1.7257,    1.9759,    1.9592,    1.7124,
                       2.6643,    2.29,      2.1602,    1.9976,    1.9648,
                       2.375,     2.1793,    2.0109,    1.8475,    1.7989,
```

2.5037, 2.3385, 2.2092, 2.1462, 1.9245,
2.5334, 2.2443, 2.1044, 2.0458, 1.9743,
2.7536, 2.3943, 2.2928, 2.2186, 2.1788,
2.4349, 2.1261, 1.9254, 1.8826, 1.8634,
2.5312, 2.5173, 2.2315, 2.1882, 2.0412,
2.3479, 2.3212, 2.3153, 2.2249, 2.1003,
2.5924, 2.0409, 2.0144 , 1.9453 , 1.892,
2.7164, 2.5352, 2.4298 , 2.2533 , 2.1736,
2.638, 2.5809, 2.4831 , 2.2008 , 2.0503,
2.4098, 2.2952, 2.0128 , 1.9757 , 1.9295,
2.7501, 2.4623, 2.2866 , 2.2486 , 2.1732,
1.9407, 1.7504, 1.5471 , 1.5542 , 1.612,
2.7323, 2.4577, 2.4276 , 2.4243 , 1.9463,
2.2617, 2.0414, 1.992 , 1.8705 , 1.7417,
2.9807, 2.7331, 2.6502 , 2.5687 , 2.4598,
1.7306, 1.5082, 1.4418 , 1.3008 , 1.2504,
2.2042, 2.0915, 1.8566 , 1.7411 , 1.7164,
1.874, 1.778, 1.6524 , 1.4401 , 1.4378,
2.402, 2.0792, 1.9394 , 1.8304 , 1.7795,
2.395, 2.2868, 2.2132 , 1.8545 , 1.7946,
2.1848, 2.0977, 1.8561 , 1.8477 , 1.8283,
1.8554, 1.6159, 1.6268 , 1.5999 , 1.5798,
2.6541, 2.1362, 2.0063 , 1.9145 , 1.893,
2.2417, 2.0286, 1.9855 , 1.9514 , 1.8286,
2.087, 1.9994, 1.8848 , 1.7418 , 1.7072,
2.0517, 1.6963, 1.5352 , 1.4714 , 1.434,
2.1933, 1.9613, 1.8185 , 1.7727 , 1.7211,
2.5634, 2.1618, 2.0338 , 1.8265 , 1.8175,
2.1209, 1.9592, 1.7362 , 1.7109 , 1.6569,
1.8554, 1.6159, 1.6268 , 1.5999 , 1.5798,
2.5702, 2.4149, 2.2528 , 2.1292 , 2.0808,
2.5086, 2.2628, 1.9887 , 1.8942 , 1.8302,
2.3534, 2.0618, 1.9399 , 1.6983 , 1.6714,
2.2388, 2.3585, 2.1442 , 1.9058 , 1.9019,
1.9582, 1.7553, 1.6122 , 1.5489 , 1.6084,
2.1473, 2.0186, 1.8833 , 1.7612 , 1.7494,
1.8554, 1.6159, 1.6268 , 1.5999 , 1.5798,
2.867, 2.6278, 2.5712 , 2.3531 , 2.283,
2.61, 2.3078, 2.1428 , 2.0805 , 2.0138,
2.3676, 2.0992, 1.8886 , 1.7915 , 1.729,
2.7504, 2.4971, 2.3623 , 2.3557 , 2.2174,
2.381, 2.2598, 2.1227 , 2.0543 , 1.9846,
2.3199, 2.0032, 1.8316 , 1.7857 , 1.7159,
2.1932, 1.9248, 1.7069 , 1.6553 , 1.5879,

```
                2.5969,     2.132,     1.971  ,     1.96  ,     1.8849,
                2.3567,     2.2114,    2.0379 ,     1.965 ,     1.9273,
                2.5552,     2.286,     2.112  ,     2.0373 ,    2.0198,
                2.0569,     1.861,     1.7743 ,     1.6398,     1.5952;

Mat2D Y_orig(65, 1);

    Y_orig << 15.8,
              14.5,
              15.4,
              15.8,
              13.7,
              16.5,
              14.7,
              14.9,
              17.2,
              16.5,
              16.5,
              15.4,
              16.8,
              14.7,
              14.7,
              15.5,
              14.3,
              15.5,
              14,
              15.7,
              15.3,
              15.4,
              17.4,
              15.3,
              16.1,
              16.3,
              15.4,
              16.4,
              10.5,
              15.6,
              13.6,
              17.9,
              9.9,
              12.5,
              10,
              13.9,
              13.6,
```

```
                13.5,
                11.6,
                14.1,
                13.7,
                12.6,
                13,
                12.5,
                13.9,
                12.1,
                12,
                15.2,
                14.9,
                12.8,
                14,
                12.2,
                12.7,
                11.2,
                18,
                15.8,
                14.7,
                16.7,
                15.1,
                12.9,
                12.8,
                13.6,
                13.2,
                13.8,
                13.1;

Mat2D X_pred(10, 5);
        X_pred << 2.0864,   1.7443,   1.647,    1.5015,   1.4513,
                  3.0626,   2.9608,   2.7724,   2.4952,   2.3067,
                  2.5808,   2.457,    2.1991,   2.0228,   1.9394,
                  3.1313,   3.0273,   2.8775,   2.7402,   2.5642,
                  2.4048,   2.2908,   2.2658,   2.0594,   2.0385,
                  2.8708,   2.6025,   2.4245,   2.2464,   2.1535,
                  2.7574,   2.4977,   2.3892,   2.3567,   2.2821,
                  1.8992,   1.758,    1.7,      1.577,    1.5674,
                  1.8003,   1.7279,   1.5925,   1.4919,   1.49,
                  2.4384,   2.2322,   2.0104,   1.9896,   1.9781;
```

```
Mat2D Y_actual(10, 1);
                    Y_actual << 13.6,
                                17.5,
                                16.7,
                                18.7,
                                13.7,
                                15.9,
                                16.7,
                                12.3,
                                10.9,
                                14.2;

   Mat2D X = X_orig ;
   Mat2D Y = Y_orig ;

   PLS_Model plsm;
   int npred = X_orig.cols();
   int nresp = Y_orig.cols();
   int ncomp = 5;
   plsm.initialize(npred, nresp, ncomp);

while (1){
   plsm.plsr(xmat,ymat, KERNEL_TYPE1);

  for(int h = 0; h<= 0; h++){
      IOWR_ALTERA_AVALON_LCD_16207_COMMAND(LCD_BASE,0X01);
     usleep(2000);
     IOWR_ALTERA_AVALON_LCD_16207_COMMAND(LCD_BASE,0X80);
      usleep(2000);
     LCD(text1);
     index =0;
          while(display[h][index]!='\0'){

IOWR_ALTERA_AVALON_LCD_16207_DATA(LCD_BASE,display[h][index]);
                    usleep (30000);
                    index++;
                    }
 IOWR_ALTERA_AVALON_LCD_16207_COMMAND(LCD_BASE,0XC0);
         usleep(2000);
         LCD(text2);

  float dat;
  dat=  *(meansy.data()) + *(plsm.fitted_values(xmatp).data() + h);
  dat = rounding(dat);
```

```
   std::ostringstream ss;
   ss << dat;
   std::string s(ss.str());
   index = 0;
  while(s[index]!='\0'){
   IOWR_ALTERA_AVALON_LCD_16207_DATA(LCD_BASE,s[index]);
   usleep (30000);
   index++;
   }
   IOWR_ALTERA_AVALON_LCD_16207_COMMAND(LCD_BASE,0XCC);
   usleep(2000);
   LCD(text3);
   usleep(5000000);
   }   }
return 0;
}
```